Technology Development and Field Monitoring in nZEB

US Country report IEA HPT Annex 49 Task 3

Authors
Van D. Baxter, PE, baxtervd@ornl.gov
Ahmad Abuheiba, abuheibaag@ornl.gov
Oak Ridge National Laboratory

W. Vance Payne, Ph.D., vance.payne@nist.gov
Brian Dougherty
National Institute of Standards and Technology

Prof. Reinhard Radermacher, Ph.D., raderm@umd.edu
Jiazhen Ling, Ph.D., jiazhen@umd.edu
Center of Environmental Energy Engineering, University of Maryland
Prof. Jelena Srebric, Ph.D., jsrebric@umd.edu
Center for Sustainability in the Built Environment (City@UMD), University of Maryland

Annex 49 Report Task 3 Field Monitoring

Draft July 2020

International Energy Agency
Heat Pumping Technologies

Imprint

IEA HPT Annex 49 "Design and integration of Heat pump for nearly Zero Energy Buildings"

The work presented here is a contribution to the Annex 49 in the Heat Pumping Technologies (HPT) Technical Collaboration Programme (TCP) of the International Energy Agency (IEA)

Operating Agent (Switzerland):
IET Institute of Energy Technologies, HSR University of Applied Sciences Rapperswil
Prof. Carsten Wemhöner, carsten.wemhoener@hsr.ch, Lukas Rominger, lukas.rominger@hsr.ch

Austria:
Unit for energy efficient building UIBK, University of Innsbruck, Austria
Dr. Fabian Ochs Fabian.Ochs@uibk.ac.at, Mara Magni Mara.Magni@uibk.ac.at
IWT Institute of Thermal Engineering, Graz Technical University, Austria:
DI Dr. tech. Andreas Heinz andreas.heinz@tugraz.at
AIT Austrian Insitute of Technology
Philip Horn, Philip.Horn@ait.ac.at

Belgium:
Institute of Aero, Free University of Brussels, Brussels, Belgium
Prof. Dr. Patrick Hendrick, patrick.hendrick@ulb.ac.be

Estonia:
Technical University of Tallinn
Prof. Dr. Jarek Kurnitski, jarek.kurnitski@taltech.ee, Jevgeni Fadejev, jevgeni.fadajev@taltech.ee

Germany:
Technical University Georg-Simon Ohm, Nuremberg
Prof. Dr. Arno Dentel, Arno.Dentel@th-nuernberg.de,
Christina Betzold, Christina.Betzold@th-nuernberg.de
Institute of Building Services and Energy Design IGS, Unversity of Braunschweig
Franziska Bockelmann, bockelmann@igs.tu-bs.de
TEB GmbH, Vaihingen/Enz
Dr. Thomas Dippel, dippel@teb-online.de

Norway:
SINTEF Community, Trondheim, Norway
Øystein Rønneseth, oystein.ronneseth@sintef.no, Maria Justo Alonso, maria.j.alonso@ntnu.no
NTNU
Prof. Dr. Laurent Georges, laurent.georges@ntnu.no, Dr. John Clauß, John.Clauss@sintef.no
COWI AS
Dr. Ing. Jørn Stene, jost@cowi.no

Sweden:
SP Technical Research Institute of Sweden, Borås
Ola Gustafsson, ola.gustafsson@ri.se

United Kingdom:
Renewable Energy, Glen Dimplex, UK
Martin Betz, martin.betz@glendimplex.co.uk

USA:
Oak Ridge National Laboratory, Oak Ridge, Tennessee, USA
Van D. Baxter, baxtervd@ornl.gov, Ahmad Abuheiba, abuheibaag@ornl.gov
National institute of Standards and Technology (NIST), Gaithersburg, Maryland, USA
Vance Payne, Ph.D., vance.payne@nist.gov, Brian Dougherty, brian.dougherty@nist.gov
Centre of Environmental Energy Engineering (CEEE), University of Maryland
Prof. Reinhard Radermacher, Ph.D., raderm@umd.edu, Jiazhen Ling, Ph.D., jiazhen@umd.edu
Center for Sustainability in the Built Environment (City@UMD), University of Maryland, College Park, Maryland, USA Prof. Jelena Srebric, Ph.D., jsrebric@umd.edu

Abstract

The International Energy Agency (IEA) Heat Pumping Technologies (HPT) Annex 49, “Design and Integration of Heat Pumps for Nearly Zero Energy Buildings,” deals with the application of heat pumps (HPs) as a core component of the HVAC system for nearly or net-zero energy buildings. This report covers the Task 3 activities of the US team.

Three institutions are involved on the US team and have worked on the following projects.

- Oak Ridge National Laboratory (ORNL) summarized development activities since the conclusion of IEA HPT Annex 40 for several integrated HP (IHP) systems—electric ground-source IHP and air-source IHP versions and engine-driven AS-IHP version.
- The University of Maryland partnered with ORNL and Blue Bear Management to develop a personal cooling device called RoCo that can provide personalized conditioned air to occupants in inadequately or unconditioned environments. With RoCo, building facility management can elevate the HVAC thermostat settings without compromising occupants’ thermal comfort. Researchers have found that a 4°F increase in thermostat settings can save 12–30% energy savings. Therefore, RoCo is a promising technology that can help reduce building energy consumption and facilitate achievement of net-zero energy building performance.
- The National Institute of Standards and Technology (NIST) is working on a field study effort on the NIST Net-Zero Energy Residential Test Facility. Two air-source split-system HPs were installed in a residential, net-zero energy home that was constructed as a laboratory on the NIST campus in Gaithersburg, Maryland. The first HP was a two-stage, 7 kW (2 ton), 15.8 seasonal energy efficiency ratio (SEER), 9.05 heating seasonal performance factor (HSPF) conventionally ducted system; the second HP was a variable-speed, 10.6 kW (3 ton), 14 SEER, 8.35 HSPF, high-velocity ducted system. These two systems operated side by side, using separate supply ducts and a common return duct, on a weekly alternating schedule to condition the home that was operated with very consistent simulated thermal loads. The team wanted to determine whether the high-velocity system could provide comparable energy-use efficiency to the conventional system. The results of this study showed that it did meet the required loads and had slightly greater efficiency; the average cooling coefficient of performance (COP) was (0.40 ± 0.11) higher, and the average heating COP was statistically equal. A new firmware was provided at the end of the heating season that greatly improved the performance of the high-velocity system; its average heating COP went from (1.8 ± 0.9) to (2.5 ± 1.1) at a 95% confidence level. The new firmware heating COP averaged (1.05 ± 0.23) higher than the old firmware over the same outdoor temperatures. The defrost performance is very different for these two systems, yet they consumed equivalent energy per HDD. The conventional system uses a timed-initiate, temperature-terminate algorithm with auxiliary electric resistive heating, whereas the high-velocity system uses calculated evaporator parameters with a hot-gas bypass before a full reverse-cycle defrost with no supplementary resistive heat.

Contents

List of Figures

List of Tables

1 Overview of US Contributions in Annex 49

1.1 Background of nZEB and Developments in the United States

As documented in the Annex 49 Task 1 report [1], the United States is committed to reducing energy consumption in new and existing buildings and has set aggressive goals for doing so. In its 2015 report, “A Common Definition for Zero Energy Buildings,” the US Department of Energy (DOE) sought to establish a commonly agreed upon definition of zero-energy buildings (ZEBs) (alternatively known as *net-zero energy buildings [nZEBs]* and *zero net energy [ZNE] buildings*), including supporting nomenclature and measurement guidelines [2].

Broadly, the document defines ZEB as “an energy-efficient building where, on a source energy basis, the actual annual delivered energy is less than or equal to the on-site renewable exported energy.” Extending the ZEB concept, the document includes definitions for *zero-energy campuses*, *zero-energy communities*, and *zero-energy portfolios*, each with the same criteria as ZEBs but applied to campuses, communities, and portfolios, respectively.

The site boundary should include the point-of-utility interface. Figure 1.1 [2] shows the site boundary for ZEB energy accounting based on building energy use, on-site renewable energy production, delivered energy, and exported energy. For a single building on a single property, the site boundary is typically the property boundary.

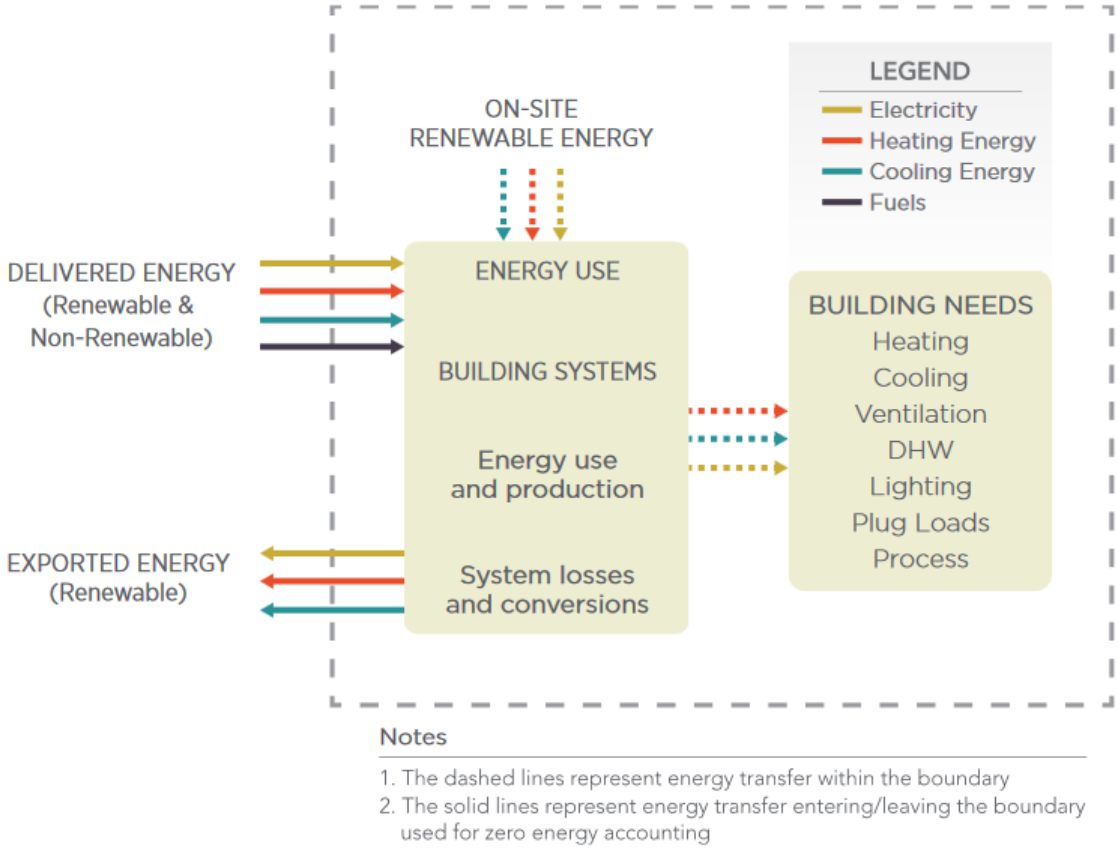

Figure 1.1. Site boundary of energy transfer for zero-energy accounting [2].

Government-sponsored programs and non-profit organizations, such as ENERGY STAR and Leadership in Energy and Environmental Design, have played were crucial to developing US certifications and rating systems that help homeowners and contractors build and retrofit low-

energy, high-performance buildings. As demand for nZEBs continues to grow, guidance from the programs, especially in regard to individual components and appliances incorporated into the building, will likely increase.

1.1.1 Market Status of nZEB in the United States

Commercial Buildings

As part of a 2016 research report published by New Buildings Institute, the number and location of existing commercial ZEBs were examined. Of the 395 buildings identified in the United States, 53 were ZEB (Figure 1.2), 279 were ZEBs under construction or had limited data to verify zero-energy performance, and 62 were classified as “ultralow energy verified buildings,” meaning they could be zero energy if final steps were taken to implement on-site renewable generation. The assessment also concluded that the location of commercial ZEBs was very diversified across climate zones [3].

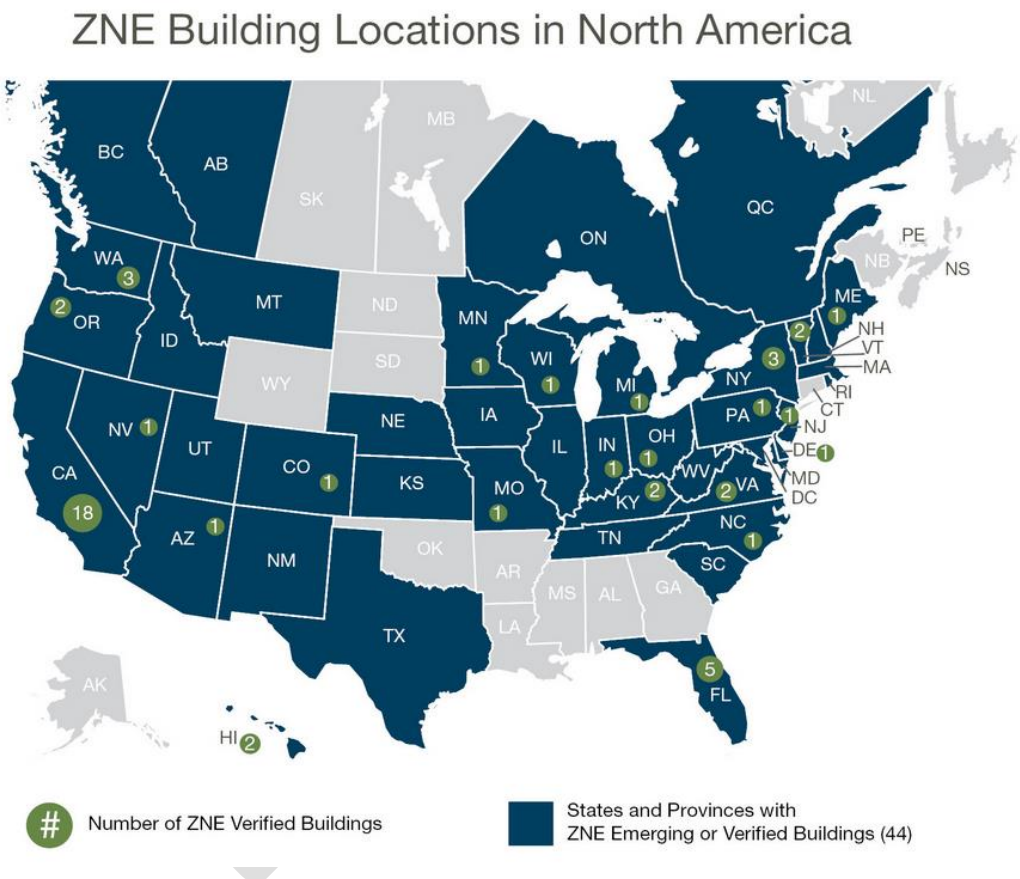

Figure 1.2. Geographic distribution of ZNE building locations as tracked by New Buildings Institute [3].

Although most existing commercial ZEBs are relatively small (>930 m^2 [10,000 ft^2]), projects are expanding in size and building type, including office buildings and K–12 schools. This conclusion is supported by combining the New Buildings Institute study ZEBs with the verified and emerging ZNEs for 332 total projects and by observing the breakdown of building types shown in Figure 1.3 [3].

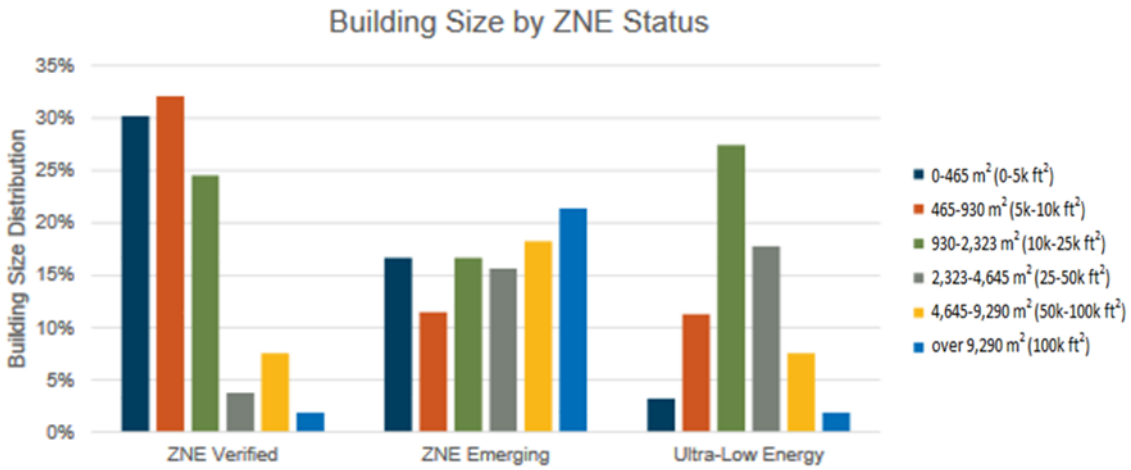

Figure 1.3. Breakdown of building types in New Buildings Institute study [3].

Residential Buildings

In the United States, the most recognizable high-efficiency home market indicator is the ENERGY STAR program[1] for new homes [4]. Maximizing the energy efficiency of a home or building is important to facilitate reaching the nZEB performance level. Recent estimates of cost and energy savings for the Version 3 ENERGY STAR home criteria indicate that monthly energy cost savings can exceed investment costs by 5–65% depending on the US location [5]. To date, over 1,700,000 ENERGY STAR-certified homes have been built, with estimates for 2016 ranging from about 72,000 to more than 92,000 [6, 7]. According to ENERGY STAR, savings from the construction of these homes are the equivalent of [7]:

- Eliminating the emissions from over 22,000 passenger vehicles
- The carbon sequestered by nearly 3,000,000 tree seedlings over 10 years
- Saving the environment 105,000 metric tons of CO_2

The national market share in the new homes sector of ENERGY STAR-certified homes reached 10% in 2016. This figure was exceeded in nine states during the same year, with Arizona topping the list at 53% of new homes being certified. Figure 1.4 displays ENERGY STAR market shares for all states within the continental United States [7].

[1]http://www.energystar.gov/

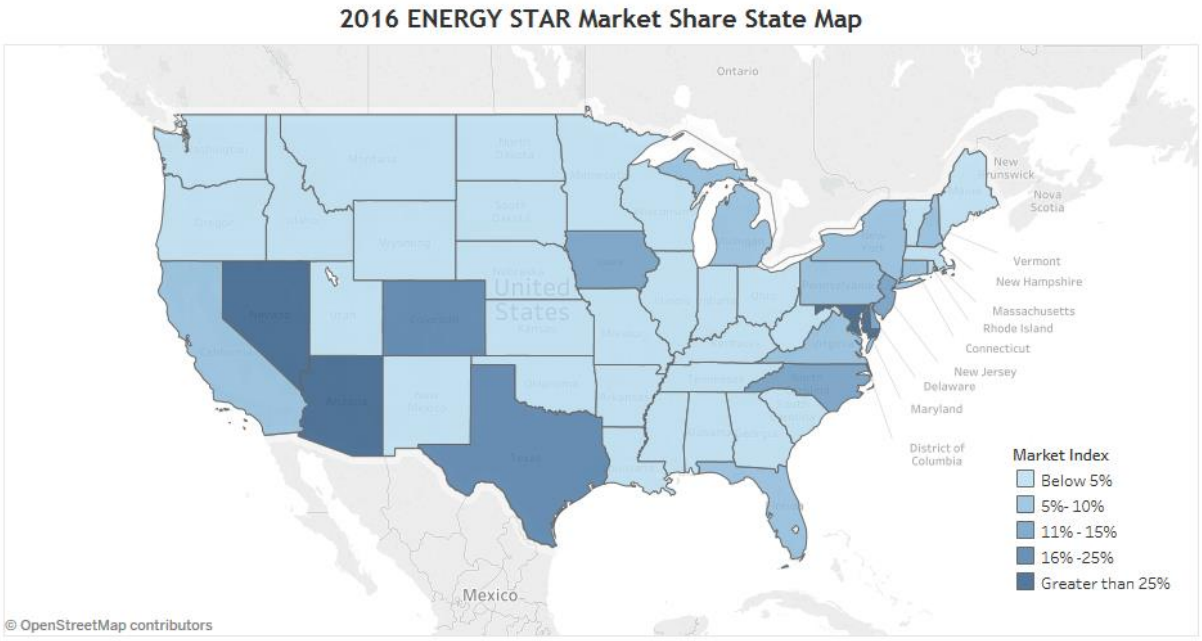

Figure 1.4. 2016 ENERGY STAR market share state map [7].

Individual states have developed specific goals and accompanying plans to achieve certain levels of nearly and net-zero energy. For example, the California Public Utilities Commission has adopted the Big Bold Energy Efficiency Strategies that identifies near-term, mid-term, and long-term milestones to move the state toward the following [8]:

- All new residential construction in California will be ZNE by 2020.
- All new commercial construction in California will be ZNE by 2030.
- HVAC will be transformed to ensure its energy performance is optimal for California‘s climate.
- All eligible low-income customers will be given the opportunity to participate in the low-income energy-efficiency program by 2020.

1.2 Overview of US Contributions

The US contributions to the Annex work are primarily to Task 3. Detailed summaries of the contributions are presented in the following three sections.

- Professor Reinhard Radermacher leads a team at the University of Maryland that has been developing a personal cooling system called RoCo. In section 2, details of the development along with evaluation of its energy and thermal comfort performance are summarized.
- Van Baxter, a team from Oak Ridge National Laboratory (ORNL), and several manufacturing and other private sector partner companies have been developing integrated heat pump (IHP) concepts. An electric-driven ground-source (GS)-IHP has entered the market. Results of field performance demonstrations in two commercial/institutional buildings are summarized. Field test results for two prototype electric air-source (AS)-IHPs are presented. A project to reduce the production cost of a prototype gas–engine-driven AS-IHP system is also discussed.
- Vance Payne and a team from NIST have investigated the field performance of two air source heat pumps (ASHP) each having a different air-distribution system at the Net-Zero Energy Residential Test Facility (NZERTF) on the NIST campus. The first heat pump (HP) was a two-stage, 7 kW (2 ton) system having a rated 15.8 seasonal energy efficiency ratio

(SEER), and a rated 9.05 heating seasonal performance factor (HSPF). This ASHP utilized a conventional central air-duct system for distribution of conditioned air. The second HP was a variable-speed, 10.6 kW (3 ton) system with rated 14 SEER and 8.35 HSPF. This ASHP used a smaller size, high velocity central air-ducted distribution. These two systems operated side-by-side, using separate supply ducts and a common return duct, on a weekly alternating schedule. Section 4 of the report provides a detailed summary of the study results.

2 Energy and Thermal Comfort Evaluation of a Personal Cooling Device

2.1 Introduction

RoCo (Roving Comforter) is a personal-sized HP that cools indoor air to maintain occupants' thermal comfort. The latest version of RoCo has a stylish appearance, is 30 in. tall, and weighs ~40 lb., Figure 2.1 [9]. The top of RoCo is an intelligent air nozzle that automatically locks onto its user and directs the airflow to the desired parts of the body. RoCo can operate for up to 8 hours due to the onboard state-of-the-art phase-change material that stores the waste heat. The novel phase change material (PCM) regeneration process requires only a "one-click" switch and ensures the thermal battery can be recharged in less than 40% of its operating time. Initial experimental work shows that RoCo's cooling capacity, which is around 150 W, successfully provides thermal comfort without rejecting waste heat or requiring wires and ducts during operation. This cooling capacity sets RoCo apart from other conditioning devices (e.g., fans, ice coolers) that are currently on the market. Therefore, RoCo was designed with the vision of opening the market for new technology in the space conditioning and thermal comfort field.

Figure 2.1. Latest version of RoCo.

RoCo is equipped with unmatched comfort technology. Some of its features are described as follows.

Intelligent nozzles: RoCo's intelligent nozzle(s) deliver conditioned air to the parts of the body that need it most. Thermal comfort studies reveal that various parts of the body have different sensitivity levels for thermal sensation. RoCo ensures that users receive most of the cooling/heating where it is most needed through flexible nozzles that adjust air supply locations and supply air conditions (temperature, RH, etc.). The high-end module saves personal preference data, such as air temperature and velocity, for different human metabolic rates. RoCo knows users' thermal requirements better than anyone else.

Highly efficient thermal management module: The primary feature of this personal cooling/heating device is the next-generation miniature HP system with built-in PCM storage. Benefiting from linear mini-compressor and next-generation air-to-refrigerant heat exchangers, the system delivers cooling and heating at minimum power consumption without releasing waste heat. With the help of RoCo, building operators and homeowners can extend HVAC

setpoints and achieve considerable energy savings without compromising occupants' thermal comfort.

Through the project, the University of Maryland team developed three generations of RoCo, creating a total of seven devices. RoCo reaches an overall coefficients of performance (COP) of 3.54 (project goal of vapor compression cycle (VCC) coefficient of performance (COP) is ≥3.0) with a measured evaporator capacity of 150 W. The overall cycle COP with the total power consumption from cooling and PCM recharging is 1.6. Forty human subject (HS) tests were conducted to measure RoCo's thermal comfort. Overall, all participants in the experiment reported comfortable and very comfortable comfort levels while using RoCo, which are correlated to target predicted percent dissatisfied (PPD) values (<10%). The effective cooling range attributed to RoCo is 2 to 13 W, which—although short of Advanced Research Projects Agency–Energy goals of 23 W—is a sufficient cooling rate for HS to accomplish savings in energy consumption for overall building cooling. The difference between cooling delivered from RoCo (in the range of 100 W) and effective cooling represents the fact that, even for a localized thermal management device, a majority of generated cooling is used to condition air that is directly circulated to provide personal cooling. However, this difference is one order of magnitude smaller than traditional air conditioners.

2.2 Potential Energy Savings with RoCo for Different Climate Conditions

(Additional authors/contributors: Mohammad Heidarinejad, Daniel Alejandro Dalgo, Nicholas W. Mattise, Jelena Srebric)

This study assesses the potential energy savings for personalized cooling with RoCo for a time period typically requiring central cooling in the US office buildings. This study considered different climate types, and the selected time period includes May 15–September 15. This investigation used EnergyPlus to simulate the building located in seven different cities across the United States, as shown in Figure 2.2 and Table 2.1. Selected cities and climates [9].

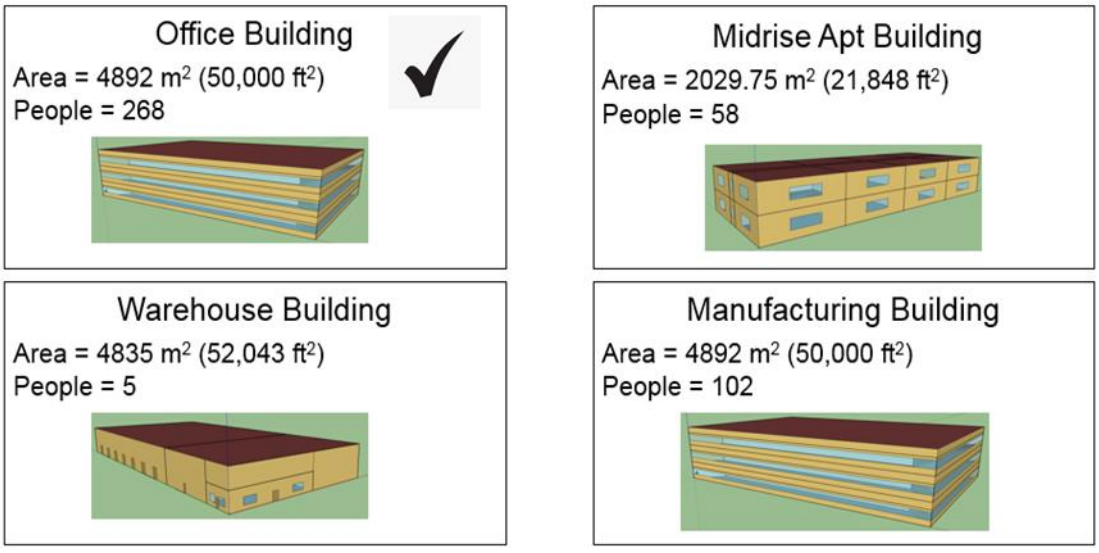

Figure 2.2. Common building types in the United States.

Table 2.1. Selected cities and climates [9].

	City	Climate
1	Austin, Texas	Climate zone 2A: hot/humid (**CDD 18ºC = 441)**
2	Chicago, Illinois	Climate zone 5A: cool/humid (**CDD 18ºC = 199)**
3	Honolulu, Hawaii	Climate zone 1A: very hot/humid (**CDD 18ºC = 408)**
4	Minneapolis, Minnesota	Climate zone 6A: cold/humid (**CDD 18ºC = 185)**
5	New York City, New York	Climate zone 4A: mixed/humid (**CDD 18ºC = 243)**
6	Phoenix, Arizona	Climate zone 2B: dry (**CDD 18ºC = 744)**
7	San Francisco, California	Climate zone 3C: warm/marine (**CDD 18ºC = 30)**

To evaluate the impacts of building construction materials and new building equipment performance when using RoCo for personalized cooling, this study deployed two sets of building energy models covering both the old building and existing building code compliances suggested by the DOE Commercial Reference Buildings [9]. According to the Commercial Building Energy Consumption Survey, office buildings account for 18.8% of all building spaces in the United States. Consequently, this study aimed to assess the impacts of various scenarios in which RoCo operates in distinct building space types located in different geographic locations.

The energy simulation inputs for old building models follow pre-1980 DOE standards, as specified in DOE Commercial Reference Buildings [10]. The input parameters for existing buildings comply with ASHRAE Std. 90.1 [11]. The selected cities represent a variety of climate zones in the United States, according to ASHRAE Std. 169-2006 [12]. The main objective of this study was to evaluate the impact of introducing RoCo in different climate zones in the United States (Table 2.2). This assessment used the computer simulation results to summarize the potential savings for adopting RoCo nationwide.

Table 2.2. Commercial electricity prices [13].

City	Off-peak	Mid-peak	Peak
Austin, Texas	0.067	3.91	6.54
Chicago, Illinois	6.24	N/A	6.24
Honolulu, Hawaii	16	16.9	16.9
Minneapolis, Minnesota	3.02	N/A	15.13
New York City, New York	1.34	N/A	18.99
Phoenix, Arizona*	5.48/5.15	10.5/10.7	15.41/16.48
San Francisco, California	20.7	23.4	25.8

*Phoenix summer/Phoenix summer peak

2.2.1 General descriptions

This study uses DOE Commercial Reference Buildings as the baseline models (Figure 2.2) for the office. For each city, the first simulation represents the current building performance, which serves as the baseline for comparing the potential energy savings associated with RoCo. Additionally, the baseline provides the necessary inputs for the HVAC system—such as system capacity, airflow rate, and duct sizing—which are later used in the simulation models that represent extended setpoint temperatures and RoCo. Specifying these inputs prevents

EnergyPlus from downgrading/upgrading the building's HVAC system for the cases with extended temperatures and allows all studied cases to be accurately and fairly compared.

After the baseline models, this study explored the potential energy savings associated with the extended temperature setpoints in each building space. These results led to the potential savings associated with the central temperature setpoint. Furthermore, the results of these simulations provide understanding and later quantify the energy impact associated with RoCo. All distributed heat-rejection systems, such as RoCo, must account for the energy penalties associated with internal equipment and heat-rejection methods, which include infiltration at dedicated openings for heat rejection, a building's HVAC fan power, and space constraints for each RoCo. The building model is fully described in the following section with an example of the energy effects associated with the current RoCo. The current operational characteristics of RoCo include the following [12]:

- operates 4 hours
- removes 165 W from the space
- consumes 70 W electric load to recharge electric battery
- electrical battery recharges from 22:00 to 4:00 (6 hours)
- requires 10 W fan power to recharge PCM
- PCM recharges from 22:00 to 2:00 (4 hours)
- rejects PCM heat outside the building space
- rejects PCM heat inside the building space

An important aspect of using RoCo for cooling is the potential cost savings due to the peak energy demand shifting. RoCo reduces cooling electricity consumption during the day when electricity costs are the highest based on a local time-of-use program. Many cities across the United States offer time-of-use programs for commercial and residential buildings to regulate energy consumption during high-demand periods. The time-of-use program entails off-peak, mid-peak, and peak hours with associated electricity rates. The most expensive times are the peak hours, followed by the mid-peak hours, and lastly the off-peak hours. Table 2.2 and 2.3 provide the electricity rates for commercial and residential buildings. The electricity price for the residential sector is more expensive than the commercial sector. The electric company serving Chicago was only able to provide the flat rate price for commercial and residential sectors according to their policy. Table 2.4 shows the peak and off-peak hours for each city. Commonly, during the weekends and holidays, the electricity rate falls into the off-peak price for all cities.

Table 2.3. Residential electricity price, cents/kWh [13].

City	Off-peak	Mid-peak	Peak
Austin, Texas	6.16	9.51	14.98
Chicago, Illinois	6.24	N/A	6.24
Honolulu, Hawaii	18.2	23.7	26.7
Minneapolis, Minnesota	3.02	N/A	20
New York City, New York	13.97	N/A	41.65
Phoenix, Arizona	6.11	N/A	24.47
San Francisco, California	32	N/A	40

Table 2.4. Peak and off-peak hours for each city [13].

City	Off-peak hours	Mid-peak hours	Peak hours
Austin, Texas	22:00 –6:00	06:00–14:00 20:00–22:00 06:00–22:00	14:00–20:00
Minneapolis, Minnesota	21:00–09:00	N/A	09:00–21:00
Honolulu, Hawaii	21:00–07:00	07:00–17:00	17:00–21:00
New York City, New York	00:00–08:00	N/A	08:00–24:00
Chicago, Illinois	N/A	N/A	N/A
San Francisco, California	21:30–08:30	08:30–12:00 18:00–21:30	12:00–18:00
Phoenix, Arizona	19:00 –24:00	N/A	12:00–19:00

The potential costs savings associated with extended setpoints and RoCo are a combination of electricity prices and cooling degree-days (CDD) 18°C. This study normalizes the electricity price of each city as a ratio between the off-peak to peak price, as shown in Eq. (1). This normalization reveals potential profitable markets for RoCo. In Eq. (1), unity is subtracted to sort each city into an ascending order (Figure 2.3). This study proposes that cities with electricity price ratios higher than 0.3 and a CDD 18°C higher than 400 could be the highest profitable markets for RoCo. Cities such as Austin, Minneapolis, New York, and Phoenix have high CDDs and a high electricity price ratio between off-peak and peak, making them a suitable market for systems such as RoCo (Figure 2.3). On the other hand, cities such as Chicago and San Francisco have low cooling requirements and a low price ratio, which prevents potential cash savings associated with extending temperature setpoints and RoCo. Similarly, Honolulu might not be a potential market due to the small price ratio for the electricity rate.

$$Price\ Ratio\ deff = 1 - \frac{off\ peak\ price}{on\ peak\ price}. \quad (1)$$

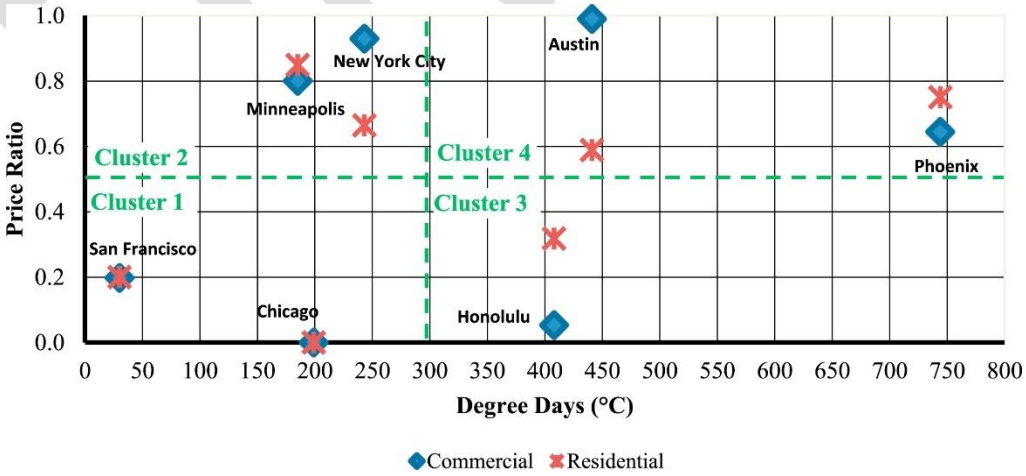

Figure 2.3. CDDs vs. price ratio [13].

2.2.2 Model Description and Results

The baseline model for this building space assumes a gross floor area of 4,892 m^2 (50,000 ft^2) and 268 occupants. The energy simulation estimates that the cooling season expands from May 15 to September 15 for the old and new office models. The main differences between the

old and new office models are construction materials and HVAC systems. Specifically, the new office model has variable air volume, whereas the old office model has a constant air volume. This study considered three different temperature schedules (Figure 2.4) for each model to compare the building energy consumption. The first temperature schedule is the baseline in which room temperature is 24°C (75.2°F) from 6:00 to 22:00 and 26.7°C (80.6°F) from 22:00 to 6:00 of the following day.

The second temperature schedule (Max80) follows the extended setpoint temperature required by the DELTA program in which room temperature is 26.7°C (80.6°F) (Max80) throughout the day. The third temperature schedule is a combination of the baseline and Max80 schedules in which the temperature setpoint is 24°C (75.2°F) from 6:00 to 13:00 and 26.7°C (80.6°F) from 13:00 to 6:00 of the following day. This study assumes that RoCo operates between 13:00 to 17:00 hours every day to provide cooling during the extended setpoint. According to preliminary results, increasing the daytime (6:00–22:00) temperature more than 26.7°C (80.6°F) increases the fan energy consumption. Additionally, based on experience, building managers would not operate buildings at temperatures higher than 26.7°C (80.6°F) to avoid occupant discomfort. The building's fan increases the energy consumption to satisfy the temperature changes in the space.

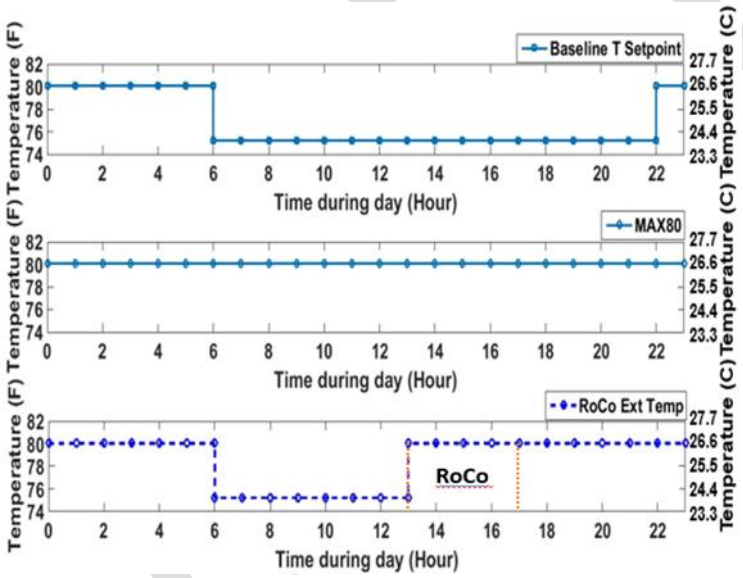

Figure 2.4. Temperature schedules for office buildings [13].

The simulation results demonstrate that by extending the temperature setpoint to 26°C (80°F), the energy required to cool the building reduces from approximately 20 to 38% for old office models and 7 to 11% for new office models (Figure 2.5). San Francisco and Chicago are associated with low CDDs in which cooling is a minor portion of the building's total energy. Therefore, the extended temperature setpoint to 26.7°C (80.6°F) in old offices significantly reduces cooling energy by 38% in Chicago and 64% in San Francisco, but it does not affect the building's total energy consumption. The results indicate an increase in the fan energy consumption in the old offices, which limits the total energy savings to 4–5% since fan energy represents approximately 17% [14] of the total energy in the building.

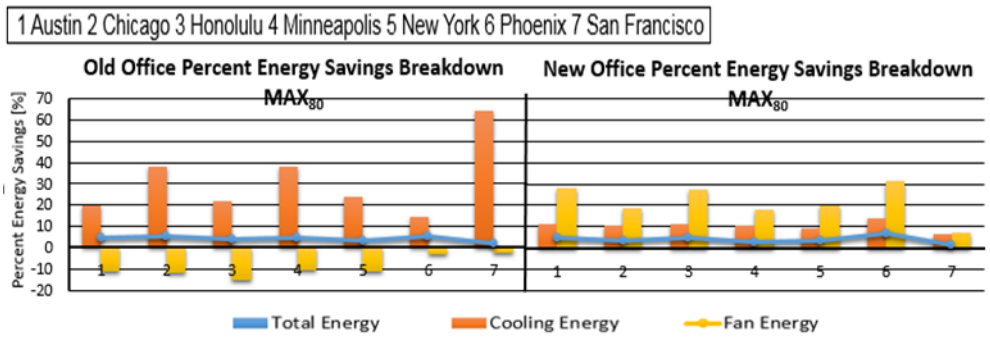

Figure 2.5. Max80 energy savings for office buildings.

The energy increase is a characteristic of constant volume systems in which the fan operates for longer periods to benefit from free cooling and maintain the desired temperature setpoint of 26.7°C (80°F). In contrast, the results for new offices buildings indicate potential savings in the fan energy ranging from 7 to 32%; however, the fan energy is only 3% of the total energy in the building, which has a negligible impact on the building's overall energy consumption. The simulation results indicate that the potential savings for cooling energy using the extended setpoint temperature of 26.7°C (80.6°F) are approximately 10%, which represent—depending on the city—approximately 1 to 3% of the building's total energy. For both models, the internal equipment is the same since no additional equipment have been added to the space. An important difference between the old and new building models is the internal equipment energy, which represents 22 and 38%, respectively, of the total energy in the buildings.

Introducing RoCo to the building environment increases the internal equipment energy by 9%. On the other hand, operating RoCo in old offices enables savings in cooling energy that range from 11 (Phoenix) to 51% (San Francisco) (Figure 2.6). However, as with the previous case, the fan energy in old offices indicates an increase of approximately 8%, which—combined with the internal equipment energy—limit the total energy savings to 2% (Figure 2.6). The results for the new office models show that cooling energy savings range from 11 (Phoenix) to 5% (San Francisco). Additionally, the results indicate potential savings for the fan energy; however, as explained in the previous section, fan energy does not contribute much to the building's total energy use. For this building model, the total energy does not change compared with the baseline model since the increase in interior equipment energy counterbalances the savings in cooling energy (Figure 2.6).

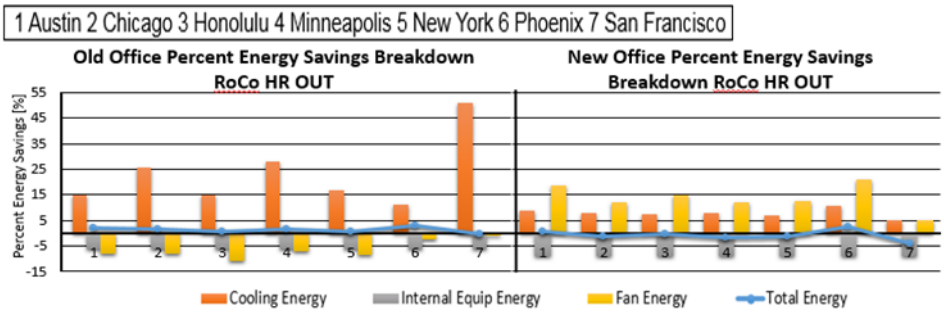

Figure 2.6. Extended temperature RoCo energy savings in office buildings.

To demonstrate the effect of rejecting RoCo's heat inside a building, this study compares the cooling energy and fan energy for heat rejection outside and inside. Figure 2.7 shows the cooling energy and fan energy for both cases. The results indicate that the cooling energy savings reduce by ~3% when rejecting heat inside for old and new buildings. Likewise, in the old buildings, the fan energy increases by 7% since it must remove more heat from the space

during RoCo's heat rejection process. The fan energy for new office buildings is a small part of the total energy; therefore, its change is negligible. The cooling energy for San Francisco stays the same for both heat rejection processes. The overall energy savings in the building reduces by ~2% when heat is rejected inside.

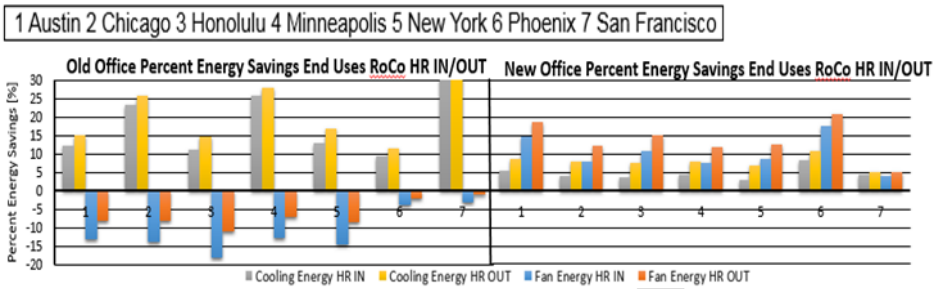

Figure 2.7. Heat rejection in/out comparison in office buildings.

2.2.3 Cost Analysis

The cost analysis of office buildings reveals higher potential cash savings in the old building compared with the new buildings. Figure 2.8 shows the cost savings breakdown for each city and each case. Phoenix has the most savings associated with Max80, RoCo (heat rejection outside), and RoCo (heat rejection inside), which escalate up to $3,200. As predicted by Figure 2.5, Chicago, Honolulu, and San Francisco have limited cash savings potential due to the combination of low price ratio and low CDDs. The cash savings for new office buildings are lower than the old office due to the high internal energy, which offsets the cash savings associated with cooling energy. By rejecting heat inside, the cash savings are limited due to a slight increase in cooling energy added by this process.

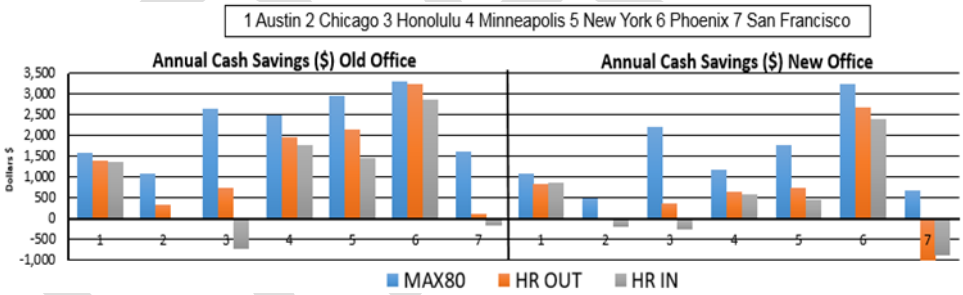

Figure 2.8. Office buildings cash savings.

2.3 PCM Material Development and PCHX Design

This section discusses the development of one of RoCo's most important components: the PCM heat exchanger (HX). The graphite enhanced PCM was an enabling technology for this project. To efficiently store the heat extracted by the HP for multiple hours without releasing waste heat, a high-energy density system capable of accepting the thermal power levels generated was required. To reduce costs, a simple phase change heat exchanger (PCHX) design was needed that must be optimized for integration with the RoCo HP. The compressed expanded natural graphite (CENG)-PCM composite material provided an ideal solution to this challenge, providing high values for the effective thermal conductivity and latent heat.

The selection of the graphite bulk density influences several PCHX design parameters, as shown in the Figure 2.9 for one of the prototype PCHXs. A bulk density of 50 kg/m^3 was chosen

since it minimizes the PCHX mass and volume while requiring a lower limit of refrigerant tubing and charge.

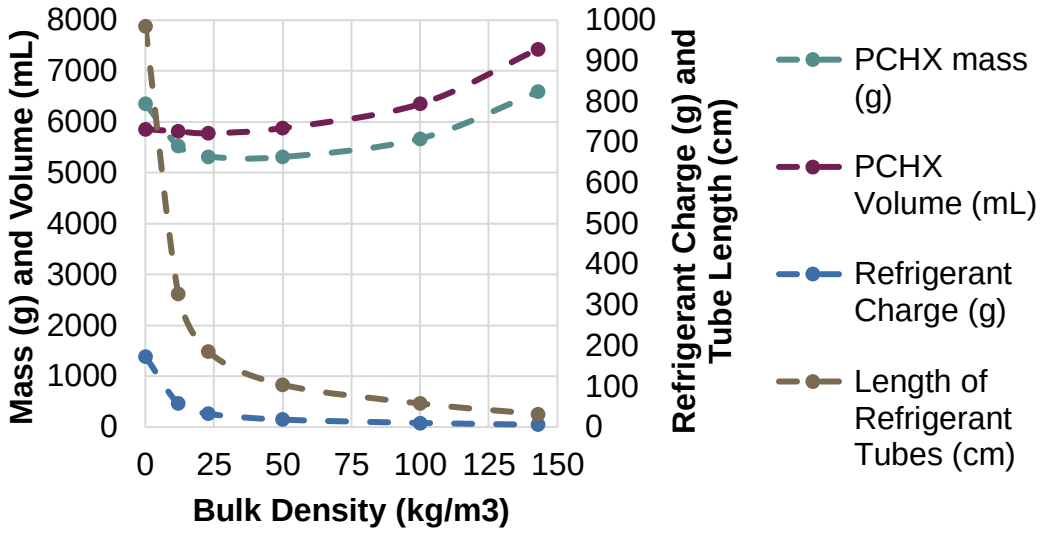

Figure 2.9. Summary of the impact of graphite foam bulk density on PCHX design parameters.

The PCM-CENG composite material employed for the project used an organic material for the PCM called PureTemp PT37, which has a melting point of 37°C. Composite samples were prepared by different methods, but melting the PCM in a vacuum furnace while maintaining contact with the CENG provided a way to almost completely saturate the CENG with PCM so that void volume was minimal. Percent void was less than 1% using this method. This led to the intimate contact of the PCM with the graphite, yielding optimal heat transfer despite the CENG's low material density and maximizing the system's PCM mass, thus providing the greatest possible latent heat storage capacity. A thermal conductivity of nearly 5 W/m-K was achieved for the composite, and the PCHX volumetric and gravimetric energy densities were measured at 75.3 Wh/L and 72.9 Wh/kg, respectively. This significantly exceeds the project's target values of 65 Wh/L and 64 Wh/kg for the PCHX.

For the PCHX fabrication approach described previously using sheets of CENG, inserting the refrigerant tubing in the PCHX must be completed after producing the CENG-PCM composite. This requires drilling holes into the composite, inserting tubes, and brazing the required fittings, which is a complicated, time-consuming process. To fabricate the PCHX with this method, small blocks of the CENG-PCM composite material—produced using the same technique as full-sized discs—were poured into a mould in which the fully assembled copper heat exchange tubing network is located, and additional PCM was added to fill the voids. An optimal distribution of the block sizes can be used to minimize the void space between CENG blocks in the final product. Figure 2.10 shows a schematic of this concept, including an approach intended to minimize the contact resistance from the tubing to the PCM.

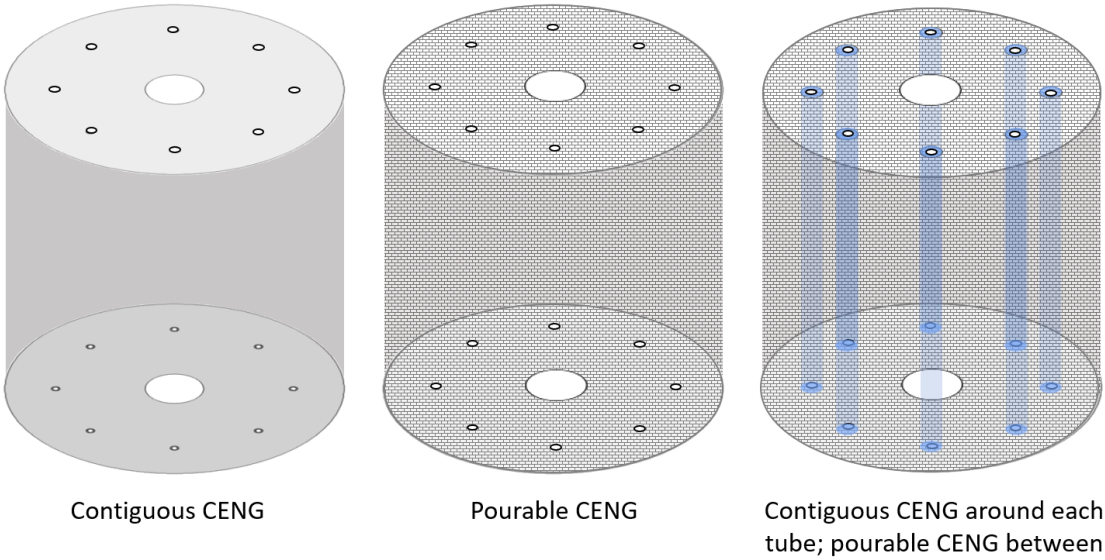

Figure 2.10. PCM condenser design.

Lower cost PCM material development was also pursued as part of the research. Salt hydrates offer the potential for high thermal energy storage capacity at a significantly lower cost than other PCMs. However, salt hydrates have issues with material stability under repeated thermal cycling due to incongruent melting and with the material supercooling before freezing begins. The team conducted a feasibility study of salt hydrate-graphite composites, specifically addressing methods to stabilize salt hydrates by nucleating on expanded graphite and then compressing them into a porous composite. It was demonstrated that incorporating a salt hydrate within a CENG structure can improve the material stability by reducing incongruent melting, thereby improving the cycling performance of the material. A new method for preparing a CENG-salt hydrate PCM composite was developed using a sodium sulphate decahydrate that shows promise as a low-cost PCM material. The data in Figure 2.11 shows the measured latent heat from a sample of the CENG-salt hydrate material for five freeze-melt cycles. Considering that this sample did not contain any stabilizing agents except CENG (it was only CENG and sodium sulphate decahydrate), this is a promising result. Pure sodium sulphate decahydrate typically begins to degrade after only the first cycle. Future research is planned to understand the mechanisms at work and improve the stability of CENG-salt hydrate composites for thermal energy storage.

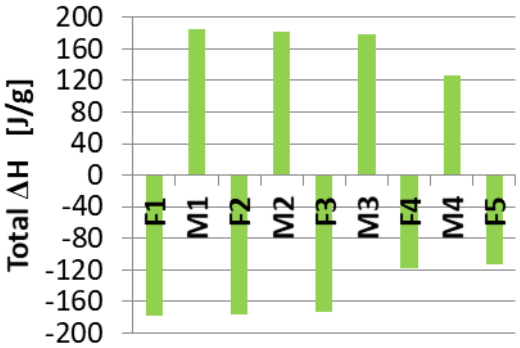

Figure 2.11. CENG-salt hydrate latent heat.

Several factors contributed to the success of this project. Developing the CENG-PCM composite material resulted in a latent heat storage material with relatively high thermal conductivity without significantly reducing thermal storage capacity. The team repeatedly used

a combination of thermal modeling and experimentation to improve and validate understanding. Examples include identifying optimal material parameters for the final design through modeling, measuring performances at component and system levels and comparing with model predictions, and validating assumptions such as the magnitude of thermal contact resistance between tubing and the CENG-PCM composite. These proven approaches all contributed significantly to the positive results achieved.

2.4 RoCo Power Consumption Measurement

The team also evaluated RoCo power consumption. Table 2.5 provides the RoCo steady-state power consumption performance. Two cyclic tests were conducted, and the results justify the use of a low-cost PCM material: fatty alcohol. Figure 2.12 shows the cyclic test results.

Table 2.5. RoCo steady-state power consumption performance.

System performances	Unit	Results	Uncertainty
Suction pressure	kPa	563.1	1.7
Discharge pressure	kPa	1,188.3	1.7
Evaporating temperature	°C	19.8	--
Condensing temperature	°C	45.9	--
Superheat	K	5.0	0.5
Subcooling	K	1.0	0.5
Refrigerant mass flow rate (MFR)	g/s	0.98	0.001
Evaporator capacity (ref. side)	W	149.9	~0.8
COP	-	3.54 (Y3 goal is >3.0)	0.04
Air inlet temperature	°C	26.0	0.25
Air outlet temperature	°C	21.3	0.25
Evaporator capacity (air side)	W	159.9	~15

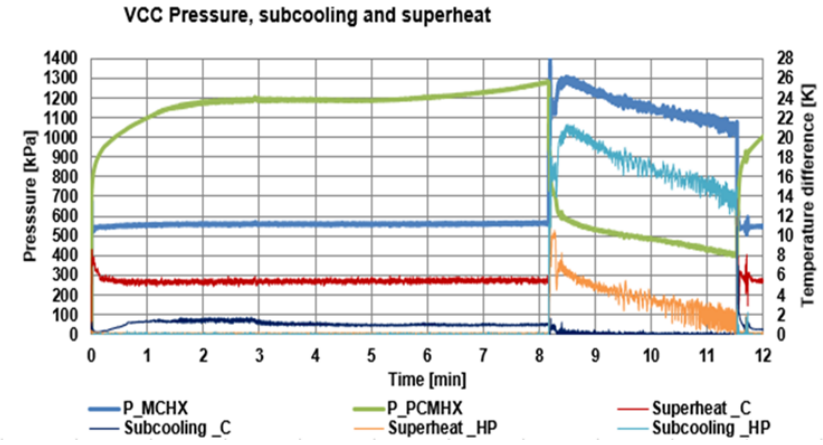

Figure 2.12. Pressure profile of RoCo under cyclic operation .

2.5 RoCo Thermal Comfort Testing

(Additional authors/contributors: Shengwei Zhu, Daniel Dalgo, Jelena Srebric, Shinsuke Kato)

Another important goal for designing RoCo is to achieve good thermal comfort. According to the approved experiment's protocol, the room temperature changes from 27 ± 1°C during the

first hour to 29 ± 1°C during the second hour, as shown in Figure 2.13. During the experiment, HS reported their thermal sensation and comfort level based on a seven-point scale and wore a smart bracelet that monitored their heart rate, skin temperature, and galvanic response. Similarly, during the last two rounds of experiments, heat flux sensors and temperature sensors were included in the experiment. Each HS had the option to request, deny, or stop using RoCo at any point during the experiment. Most of the HS chose to position the RoCo to their side (left or right) at approximately 3 ± 0.5 ft. Similarly, the position of the nozzle was consistently maintained toward their upper body, specifically their torso and face. The results indicate that most of the HS request RoCo during the second hour of the experiment when the room temperature reaches 29 ± 1°C. Also, the supply air temperature from RoCo had a consistent differential of 5°C (41°F) compared with the room temperature. Each HS reported comfortable values when using airflow rates between 50 to 60 cfm, and higher flow rates were reported to be uncomfortable due to the noise of the fan and the force of air impacting their bodies. Among the 40 HS, eight did not request RoCo due to their high tolerance to warm-hot environments. These HS reported comfortable values throughout the experiment. Lastly, the approved protocol for the smart nozzle occurred during the last 10 minutes of the experiment.

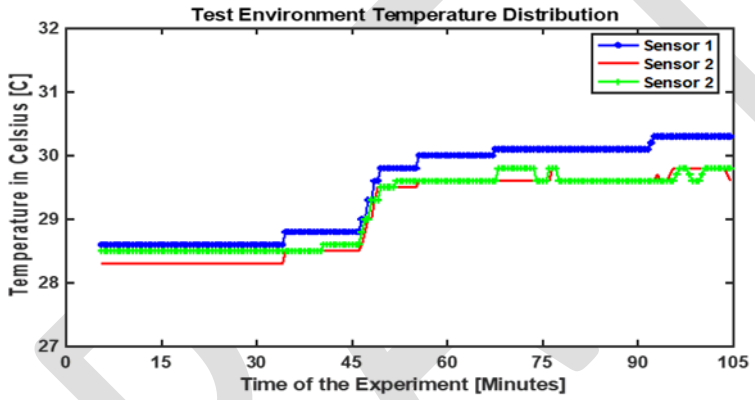

Figure 2.13. Test environment temperature distribution.

2.5.1 Experimental Results

RoCo's objective is to allow HS to manage and regulate their personal thermal environment. The results of the HS experiments indicate that RoCo positively impacts HS comfort levels and allows them to maintain their thermal comfortable level. However, the results also demonstrate high variability among HS due to their own individuality. Therefore, the results presented in this section will show the most significant responses obtained in the experiments.

2.5.2 Effective Cooling

RoCo's air jet aims at the upper body (i.e., chest and stomach) since this is the most effective area for heat transfer with the human body. For this reason, heat flux sensors were distributed over the torso to measure the effect of RoCo on the human body heat flux. Thus, the difference of the heat rejected when using RoCo and the heat rejected when NOT using RoCo is the effective cooling. Figure 2.14 shows the general trend of measured heat flux over the time of the experiment. As expected, the heat flux when RoCo is operating, represented by the green line, is higher due to a higher temperature difference between the human body and RoCo's air jet. The red line represents the heat flux of the HS when not using RoCo. To estimate effective cooling, the difference of the means between the green and red line were considered. Table 2.6 shows the effective cooling for some HS during the last two rounds of experiments. The measured effective cooling for this range of experiments was 2–10 W, and the project's target

effective cooling is 23 W. The difference between the calculated and target effective cooling is in the ambient temperature difference during the experiment. Nevertheless, the calculated effective cooling shows a linear correlation to the CFD estimation [15], as shown in Figure 2.15.

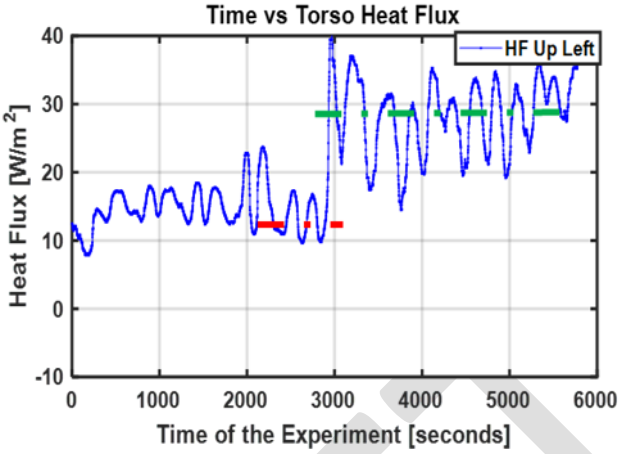

Figure 2.14. Heat flux measurement for no-RoCo and RoCo.

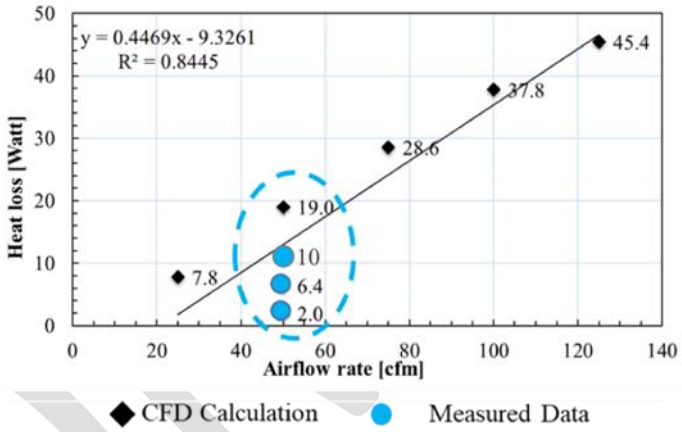

Figure 2.15. Comparison of CFD and experimental data.

Table 2.6. Effective cooling calculations.

ID	CFM	Effective cooling due to RoCo (W)
HS1	50	6.4
HS 2	50	4
HS 3	50	4
HS 4	50	2
HS 5	60	10

Body Temperature Analysis

To regulate the personal space of HS, RoCo helps reduce the human body's skin temperature. As expected, human body temperature follows the temperature profile of the room, and RoCo helps reduce this temperature as soon as it starts operating. The results suggest that RoCo

reduces skin temperature by approximately 1 K. An analysis of variance (ANOVA) showed statistically that the differences in skin temperature due to RoCo are significant in the experiments, as demonstrated in Figure 2.16.

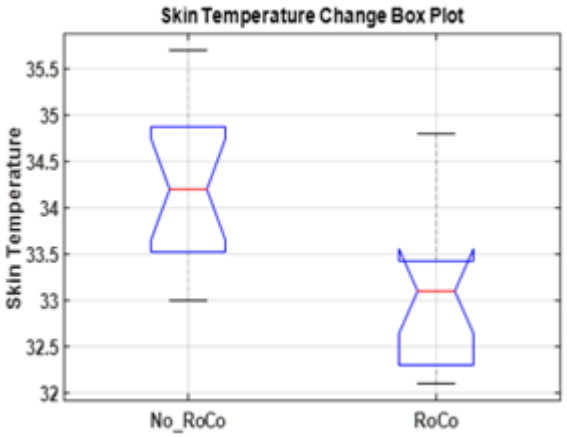

RoCo Statistics	
Average	33.1 °C (95.1°F)
Std	0.80
P-value	0.00053

Figure 2.16. ANOVA skin temperature.

2.5.3 Heart Rate Analysis

An important aspect of the human body thermoregulatory system is the heart due to its function to respond to hot or cold environments. The results suggest that the heart rate of most HS reduced or increased its variability. This effect is associated with the reduction of heat stress due to RoCo that allows the human body to ease the process of thermoregulation. An ANOVA analysis shows the statistically significant effect on the heart rate. This is due to RoCo since nothing else during the experiment changed. Figure 2.17 shows the statistics obtained from the ANOVA analysis.

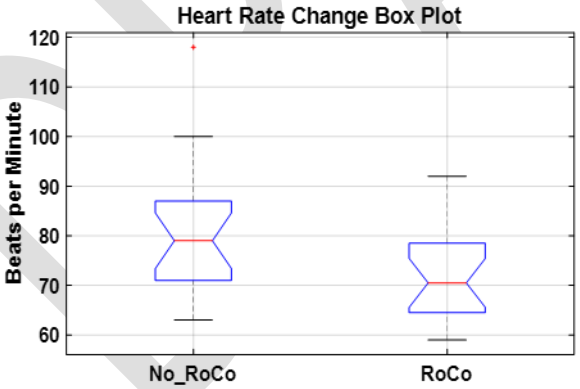

No RoCo Statistics	
Average	80.1 BPM
Std	12.86

RoCo Statistics	
Average	71.65 BPM
Std	8.70
P-value	0.0198

Figure 2.17. ANOVA heart rate.

2.5.4 Subjective Response

During the experiment, HS were required to report their thermal sensation and comfort level values every 10 minutes. Figure 2.18 shows a sample of the subjective response from four HS. Most HS required RoCo during the second hour of the experiment. At that time, all reported to be neutral, uncomfortable, or very uncomfortable when requesting RoCo. Meanwhile, as RoCo started operating, all reported an increase in their comfort level until reaching “very-comfortable,” as shown in Figure 2.18. Therefore, the subjective results demonstrate that the presence of RoCo has a positive effect on the comfort level of HS.

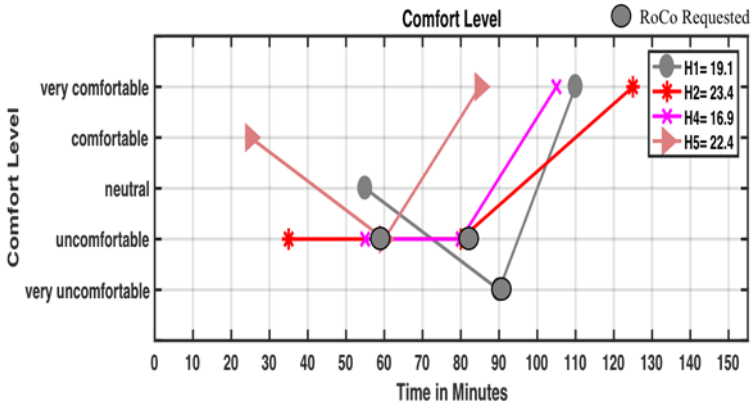

Figure 2.18. Sample of subjective responses from HS.

3 IHP Development

3.1 IHP Development Background

The DOE Building Technologies Office (BTO) long-term goal is to maximize the energy efficiency of the US building stock by 2030. Maximizing building energy efficiency is an essential facilitating step to enable market uptake of nZEBs, including net-zero energy homes. To achieve this vision, the energy used by the energy service equipment (e.g., equipment that provides space heating [SH], space cooling [SC], water heating) must be significantly reduced, by 50% or more, compared with today's best common practice. One promising approach to achieve this is to produce one piece of equipment that provides multiple services. ORNL developed a general concept design for such an appliance, called the *IHP*. The IHP concept was summarized in the final report for International Energy Agency (IEA) Heat Pumping Technologies (HPT) Annex 40 [16] with full details available in related reports [17, 18].

3.2 Variants of the IHP Layout

There are two primary versions of the IHP: geothermal (or GS-IHP) and AS-IHP. ORNL activities have focused on developing four different embodiments of the IHP in collaboration with manufacturing partners. The first focused on an electric GS-IHP and is now a commercially available product marketed by the partner ClimateMaster, Inc. (CM). The other three are AS-IHPs (two electric-driven and one natural gas engine-driven), which were also developed collaboratively with manufacturing partners. All three AS-IHP developments have reached the prototype packaged system stage and have completed field evaluation. Details are provided in the following sections.

3.2.1 Summary of GS-IHP System Development, Analyses, and Test Results

Figure 3.1 shows a conceptual installation. The system uses a variable-speed (VS) compressor, a VS indoor blower (for SH/SC distribution), and VS pumps for ground heat exchanger (GHX) fluid circulation and hot water (HW) circulation. A 190–400 L (50–105 gal) water heater (WH) tank is included. Figure 3.1 depicts a horizontal GHX installed in the existing home foundation excavation, but the system can use any geothermal heat source or sink (e.g., vertical bore GHX, ground water, surface water).

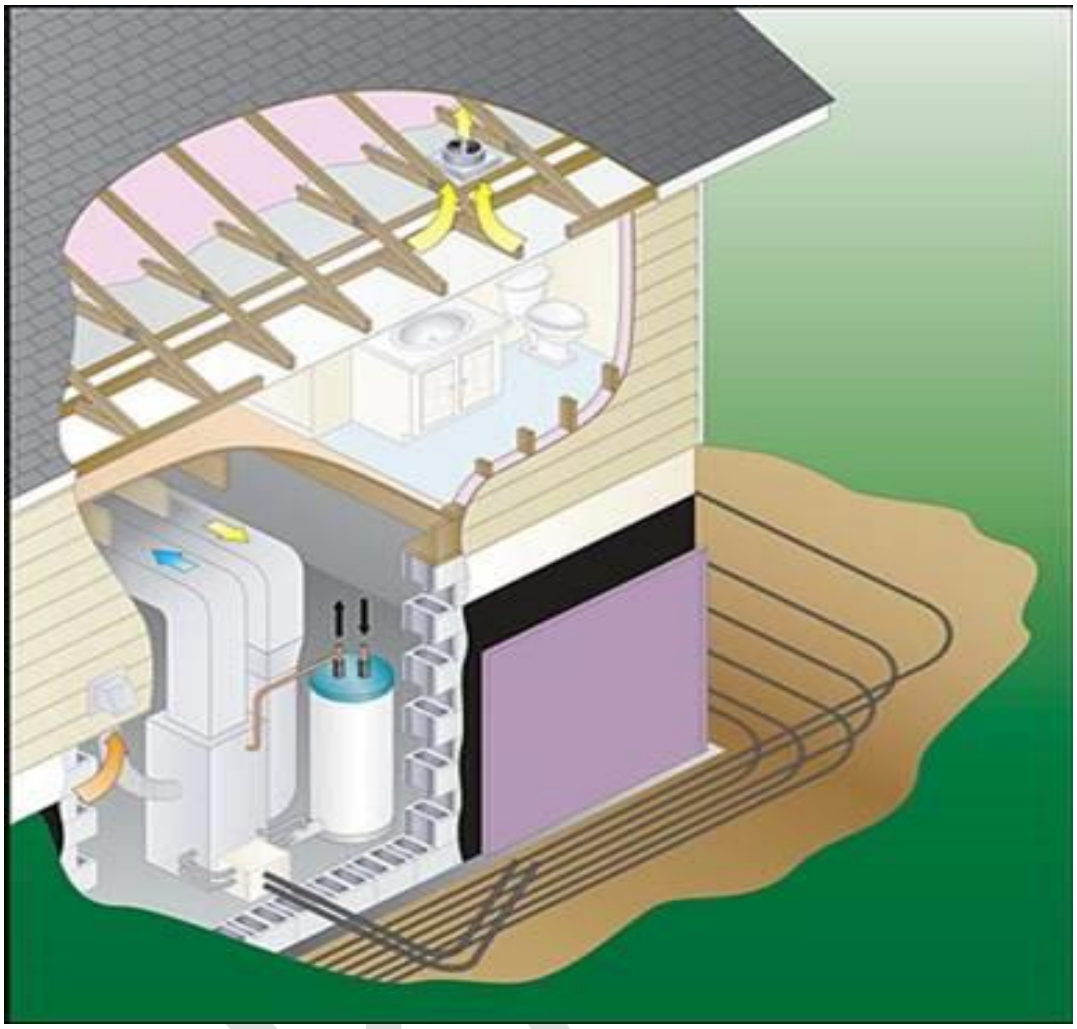

Figure 3.1. Conceptual installation of residential GS-IHP.

GS-IHP Field Demonstration Project Summary

The material in this section is summarized from the full project report [19].

In 2012, CM announced a new product, which is currently marketed as the Trilogy 45 Q-Mode.[2] It is available in two nominal SC capacity sizes: 7 kW (2 tons) and 14 kW (4 tons). Rated performance per the US Air-Conditioning, Heating, and Refrigeration Institute (AHRI) ground loop HP conditions [20] for the larger capacity unit are heating COPs of 5.1 and 3.3 at minimum and maximum speeds, respectively, and cooling COPs of 13.2 and 6.3 at minimum and maximum speeds, respectively [21]. The smaller capacity unit has slightly higher efficiencies at maximum compressor speeds: 3.6 heating COP and 7.1 cooling COP. Table 3.1 summarizes the system rating and design performance compared with those of a conventional electric commercial rooftop HP unit (RTU) with a conventional electric storage WH.

[2] https://www.climatemaster.com/Homeowner/side-links/products/product-details/trilogy

Table 3.1. Summary of GS-IHP vs. conventional RTU + electric storage WH.

	Base (electric RTU/HP and WH)	**GS-IHP**
Compressor/number	**Scroll/1-speed**	**Scroll/VS**
Refrigerant type	R410A	R410A
Design cooling seasonal COP	3.8	N/A
Design cooling rating	14.1 kW at 35°C outdoor temperature[a]	5.3 kW at minimum speed[b] 14.1 kW at maximum speed[b]
Design heating rating	13.2 kW at 8.3°C outdoor temperature[a] 8.2 kW at −8.3°C outdoor temperature[a]	7.0 kW at minimum speed[b] 17.6 kW at maximum speed[b]
Design water heating capacity; dedicated WH	4.5 kW (conventional electric WH)	~8.2 kW, low speed ~11.7 kW, high speed (110°F entering HW temperature; 35–80°F entering water temperature (EWT) from GHX loop)[c]
Design cooling plus WH capacity; combined mode	N/A	5.3 kW cooling + 7.0 kW, low speed 14.1 kW cooling + 20.2 kW WH, high speed (43.3°C entering HW temperature)[c]
Rated cooling efficiency	3.34 energy efficiency ratio (EER) at 35°C outdoor temperature 3.8 seasonal COP[a]	13.2 COP at minimum speed[b] 6.3 COP at maximum speed[b]
Rated heating efficiency	3.05 COP at 8.3°C outdoor temperature[a] 2.26 COP at −8.3°C outdoor temperature[a]	5.1 COP at minimum speed[b] 3.3 COP at maximum speed[b]
Design water heating efficiency; dedicated WH	1.0 COP (conventional electric WH)	2.5–5.0 COP (43.3°C entering HW temperature; 35–80°F EWT from GHX loop)[c]
Design cooling plus WH efficiency; combined mode	N/A	Up to 8.8 COP combined, low speed Up to 5.6 COP combined, high speed (43.3°C entering HW temp.)[c]
Unit dimension (in.)	45 L × 47 H × 76 W	25.4 L × 56 H × 30.6 W
Unit weight	590 lb, RTU	448 lb, Trilogy water source HP (WSHP)
Electrical	13.0 kW, RTU 4.5 kW, WH tank	8.5 kW, HP unit 4.5 kW, WH tank

[a]Certified per American National Standards Institute (ANSI)/AHRI Standard 210/240.
[b]Certified per ANSI/AHRI/ISO/ American Society of Heating, Refrigerating and Air-Conditioning Engineers (ASHRAE) Standard 13256-1. The Trilogy can be adjusted at installation to 17.6 kW maximum cooling capacity, as was done at the Oklahoma City site; a 17.6 kW cooling capacity conventional RTU HP was used for the baseline comparisons at that site as noted in later sections of this report.
[c]CM [21].

The system features a VS compressor, a VS blower for indoor air circulation, and VS pumps for GHX loop and domestic hot water (DHW) loop circulation. The system provides variable

SC, SH, and water-heating capacity as needed by modulating over setpoint temperature ranges. Four different operating modes are available, as listed below:

- SC (factory set at 5.3–14.1 kW for the larger unit; installer adjustable to maximum 17.6 kW)
- SH (1.5–17.6 kW for larger unit)
- Combined water-heating plus SC (SC + WH)
- Dedicated water heating (DWH) year-round

Additionally, the VS compressor and blower allow the unit to increase/decrease dehumidification (DH) (i.e., moisture removal) capacity as necessary in response to space relative humidity (RH) levels when in SC modes to maintain comfort levels in the conditioned space without sacrificing efficiency. Similarly, the air delivery temperature can be adjusted as needed in SH mode. Compact HX designs are used for the air/refrigerant SH/SC coil and the GHX loop/refrigerant and HW/refrigerant coils. This reduces the required system refrigerant charge and associated environmental risks.

Demonstration Site and Tested GS-IHP System Descriptions

CM and ORNL selected two commercial/institutional building sites for the field demonstration project. The first was a commercial kitchen attached to a day care facility located in a large church building in Knoxville, Tennessee. Knoxville is in climate Zone 4A ("mixed-humid" per Figure 3.2 and Table 3.2). The second was a homeless shelter dormitory-type building (~743 m^2 total floor space) in Oklahoma City, Oklahoma in climate Zone 3A ("warm-humid"). CM and its subcontractors (City Heat & Air Conditioning of Knoxville and Comfortworks, Inc. of Goldsby, Oklahoma) designed and installed the GS-IHP systems. Figures 3.2–3.10 provide photos and GHX schematics for the two installations. At the Knoxville site, a single GS-IHP provided SH, SC, and DHW services for a 43 m^2 kitchen and adjoining 5.6 m^2 pantry. The occupancy schedule is 8:00 a.m. to 5:00 p.m., Monday through Friday, except for holidays.

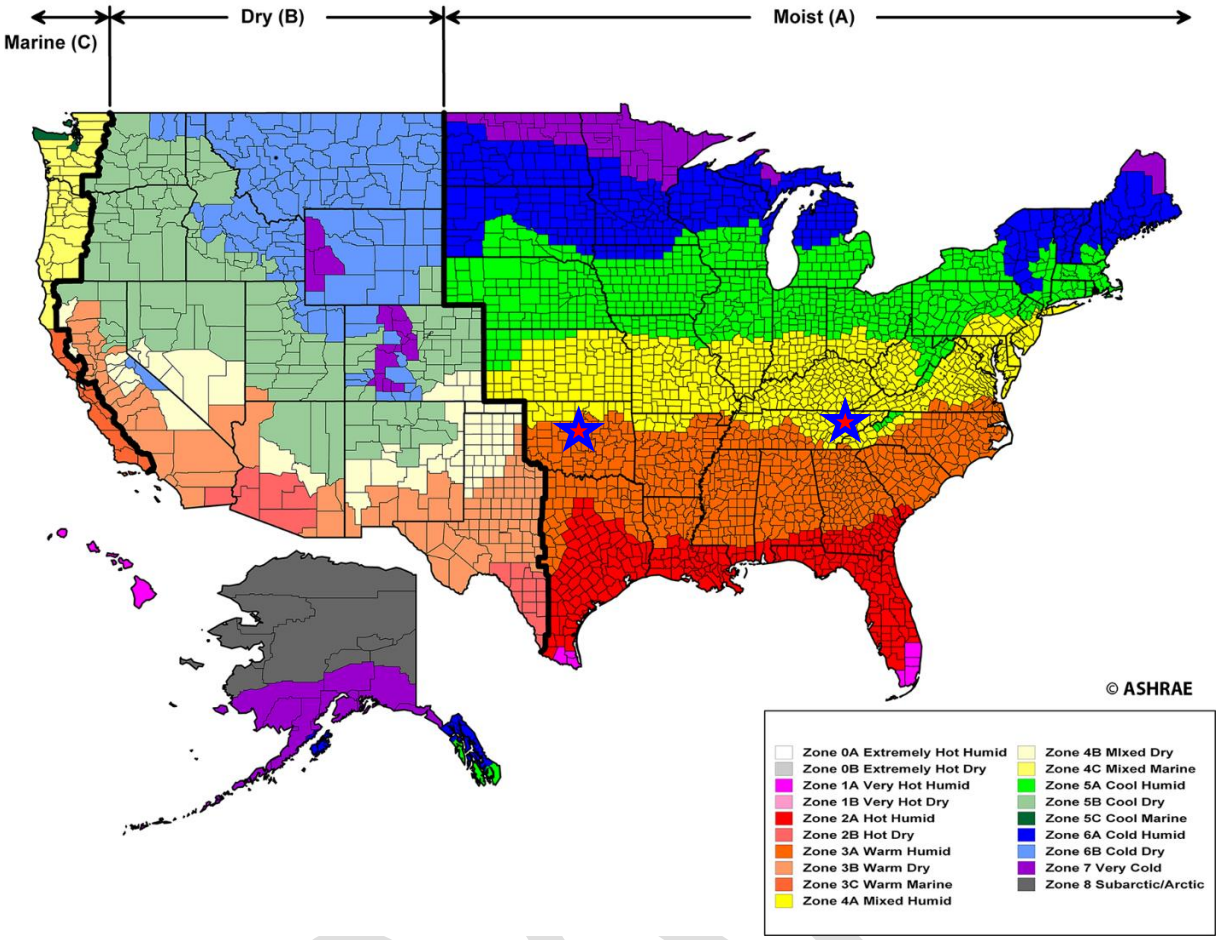

Figure 3.2. Map of US climate zones. Stars indicate GS-IHP demonstration site locations. (Source: ANSI/ASHRAE/IESNA Standard 90.1-2019 [11].)

Table 3.2. Description of US climate zones. (Source: ANSI/ASHRAE/IESNA Standard 90.1-2019 [11].)

Zone number	Name	Thermal criteria
0	Extremely hot	6,000 < CDD 10°C
1	Very hot/humid (1A), dry (1B)	5,000 < CDD 10°C ≤ 6,000
2	Hot/humid (2A), dry (2B)	3,500 < CDD 10°C ≤ 5,000
3A and 3B	Warn/humid (3A), dry (3B)	CDD 10°C < 3,500 and HDD 18°C ≤ 2,000
3C	Warm/marine	CDD 10°C ≤ 2,500 and HDD 18°C ≤ 2,000
4A and 4B	Mixed/humid (4A), dry (4B)	CDD 10°C ≤ 3,500 and 2,000 < HDD 18°C ≤ 3,000
4C	Mixed/marine	CDD 10°C ≤ 1,500 and 2,000 < HDD 18°C ≤ 3,000
5A, 5B, and 5C	Cool/humid (5A), dry (5B)	CDD 10°C ≤ 3,500 and 3,000 < HDD 18°C ≤ 4,000
5C	Cool/marine	CDD 10°C ≤ 1,000 and 3,000 < HDD 18°C ≤ 4,000
6A and 6B	Cold/humid (6A), dry (6B)	4,000 < HDD 18°C ≤ 5,000
7	Very cold	5,000 < HDD 18°C ≤ 7,000
8	Subarctic	7,000 < HDD 18°C

Figure 3.3. Aerial view of the Knoxville site. (Photo source: Google Maps.)

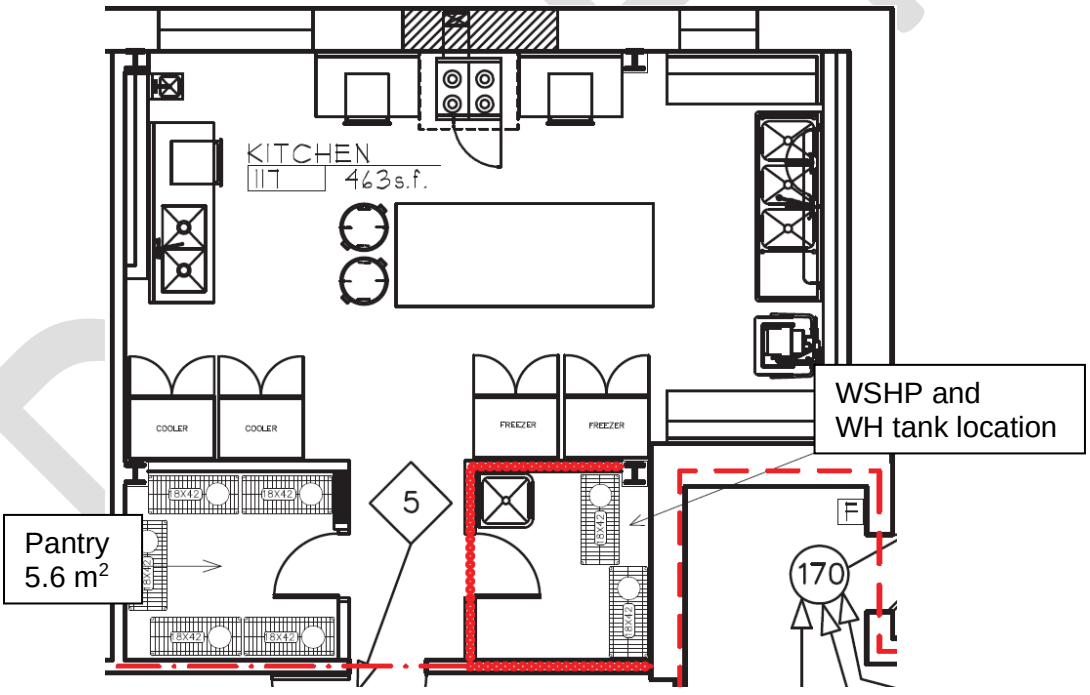

Figure 3.4. Kitchen floor plan of the Knoxville site.

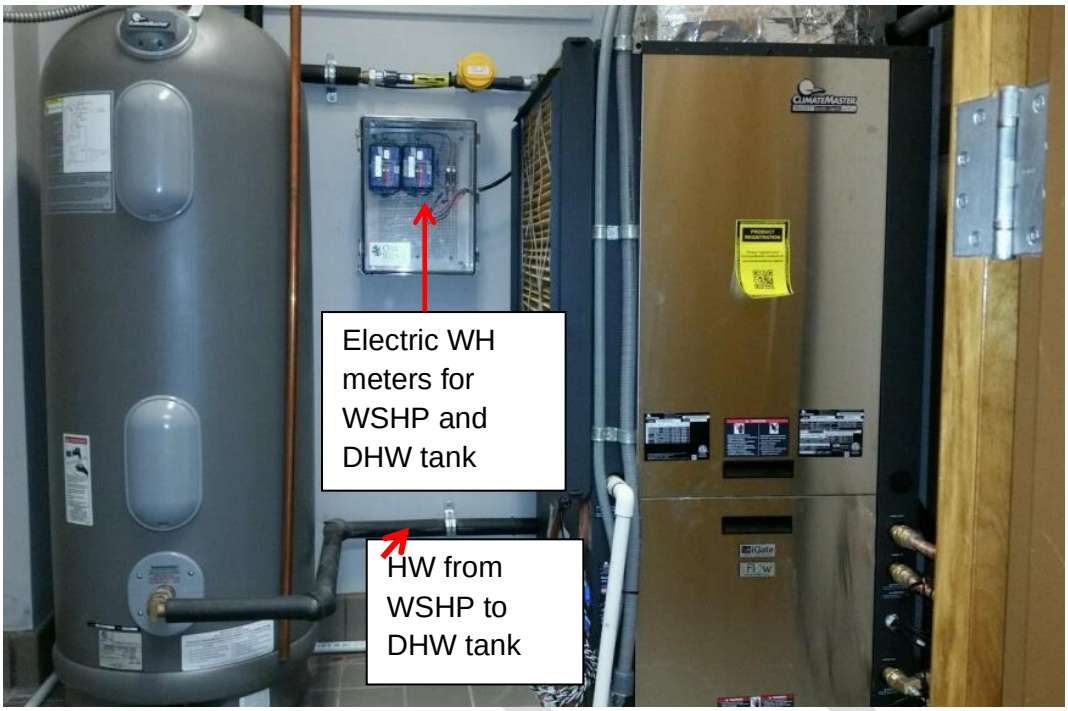

Figure 3.5. Trilogy WSHP system as installed at the Knoxville site.

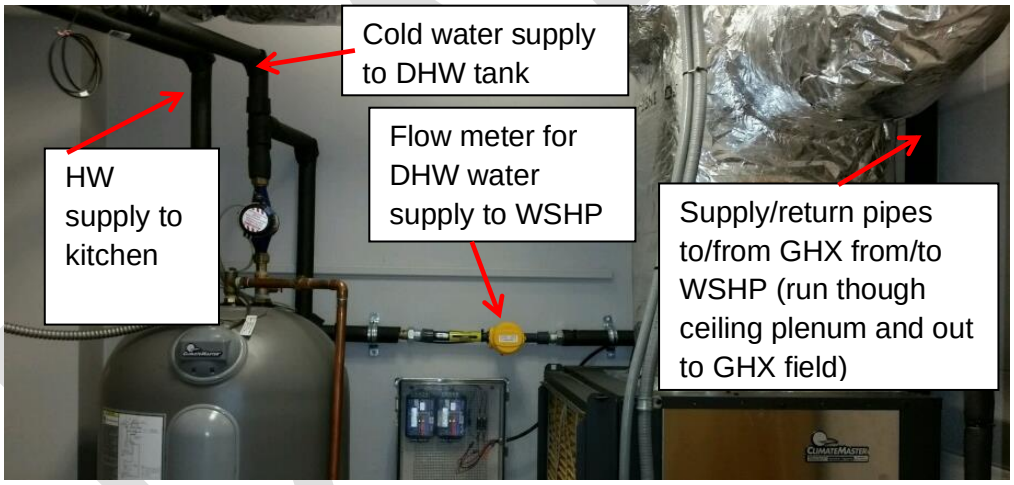

Figure 3.6. WH piping connections and flowmeters at the Knoxville site.

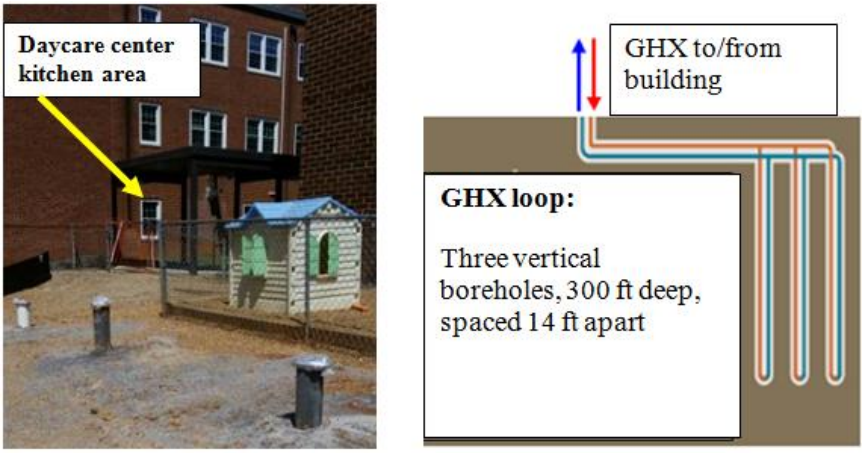

Figure 3.7. GHX loop location and schematic for Knoxville site. (Graphic source: CM.)

Figure 3.8. Oklahoma City site host building.

Figure 3.9. Oklahoma City host building mechanical room; instrumented Trilogy is on left hand side against back wall; Trilogy HW tanks are on the right. (Source: CM.)

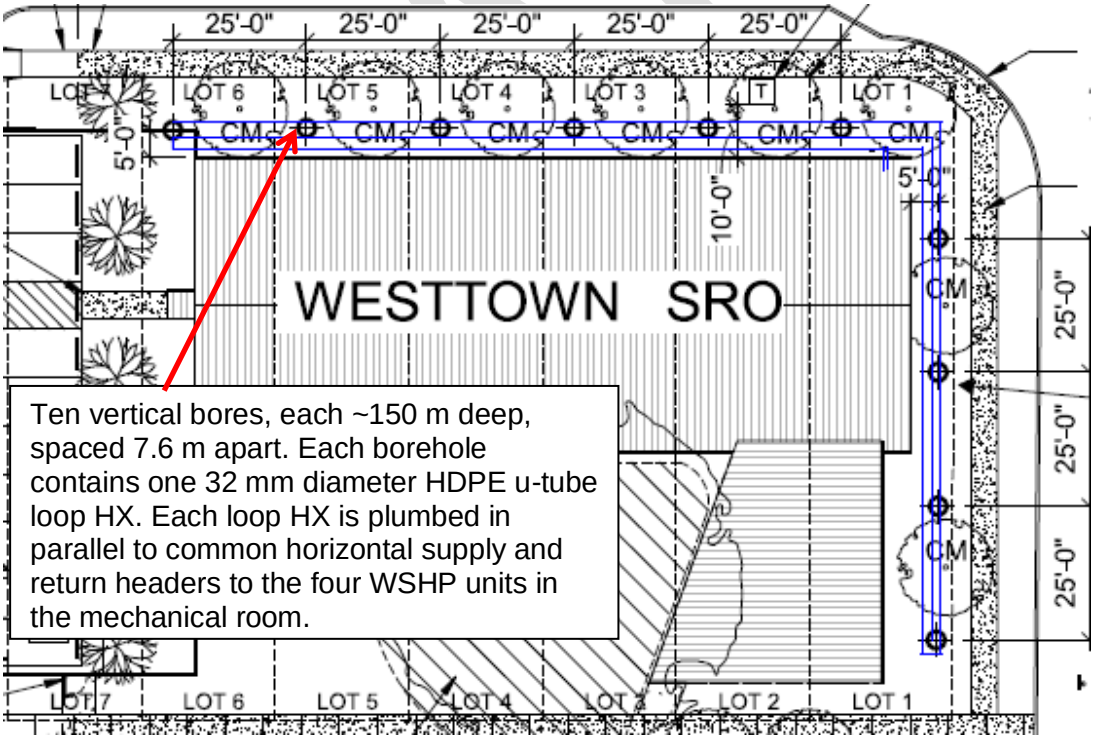

Figure 3.10. GHX loop location and details for Oklahoma City site. (Source: CM.)

The Oklahoma City installation includes two Trilogy-based GS-IHP systems with 400 L HW tanks, each providing HVAC/WH to 10 residential units (~230 m^2 each). Because of the higher peak design cooling loads at this site, the Trilogy units were set up during installation to provide peak cooling capacity of 17.6 kW each. Two additional non-IHP GS HPs provide HVAC for common areas of the building. The total nominal cooling capacity for all four HP systems is 63 kW, and all are connected to a common GHX loop (Figure 3.9). Each WSHP unit uses its own

internal loop circulator pump; no central system pump is used. Only one GS-IHP was instrumented and monitored in detail. The residential areas of the building are occupied continuously.

The two Trilogy HW tanks are connected to a common building HW distribution system. This system includes a HW recirculation loop to minimize the wait time for HW at the fixtures in each residential unit; the recirculation pump energy use was not monitored. Only one of the tanks was instrumented to attempt to determine the HW energy delivered to the building HW distribution system.

Instrumentation, Data Acquisition Systems, and Field Data Analysis Approach

The test systems were installed and commissioned to ensure proper operation at both sites. Data acquisition systems (DAS) were designed and installed at each site. Data monitoring at the Knoxville site began on August 18, 2015 and continued until August 18, 2016 with only one ~3 day outage. Because of construction delays at the Oklahoma City site, data acquisition installation was delayed. Partial data monitoring for SH and SC performance began on January 31, 2016. Full data collection, including WH mode operation, began May 19, 2016 and continued through September 19, 2016, but there were several outages, as noted below. Therefore, monitored data were not available to support a full year's performance summary as was the case for the Knoxville site.

The Oklahoma City site data gaps January through August 2016 include:

- April: DAS unavailable at the beginning April 28 at 3 p.m. through May 19 at 1 p.m.
- June: data missing from June 10 at 6 p.m. through June 15 at 6 p.m.
- August: DAS offline August 12–16
- September: DAS offline September 3–7

Data were collected in 15-second intervals, averaged into 1-minute intervals, and sent to a remote server at ORNL via the internet. Table 3.3 summarizes the DAS sensor accuracy. During data collection, the GS-IHPs were operated as normal with a wall thermostat to control SH and SC operation and a WH tank thermostat to control WH operation.

Table 3.3. Instrumentation used to measure GS-IHP system performance.

Monitoring point	Manufacturer	Model number	Accuracy range
Trilogy WSHP unit and WH tank element energy consumption	Continental Control Systems	WattNode models WNC-3Y-208-MB and WNB-3Y-208-P, respectively	±0.5% W reading for 5–100% rated current (±1% of reading for 1–5% rated current)
Line voltage	Continental Control Systems	WattNode model WNC-3Y-208-MB	±0.5% V reading
Supply/return temperatures, Trilogy to/from GHX loop	Omega	PM-1/10-1/8-6-1/8-P-3; platinum resistance temperature device (RTD), immersion	±(0.03 + 0.0005 |T|)°C from 0–100°C[a]
Supply/discharge temperatures, Trilogy to/from DHW tank	Omega	PM-1/10-1/8-6-1/8-P-3; platinum RTD, immersion	±(0.03 + 0.0005 |T|)°C from 0–100°C[a]
Supply/return temperatures, DHW tank to/from building HW distribution network	Omega	PM-1/10-1/8-6-1/8-P-3; platinum RTD, immersion type	±(0.03 + 0.0005 |T|)°C from 0–100°C[a]

Flow, GHX loop	Omega	FMG3001-PP	±0.8%, maximum (~3.8–76 l/m)[b]
Flow, DHW tank loop	Omega	FMG3001-PP	±0.8%, maximum (~3.8–38 l/m)[b]
Flow, building water supply to DHW tank	Omega	FTB8007B-PT	±1.5% (0.83–83 l/m)
ID space temperature	Trilogy onboard sensor	Thermistor included with CM thermostat	±0.56°C (±1.0°F)
ID space RH (%)	Trilogy onboard sensor	Johnson Controls model HT-6703	±3% RH
WH upper tank wall temperature	Trilogy onboard sensor	Thermistor mounted to WH tank wall	±0.56°C (±1.0°F)
Temperature in/out Trilogy air coil	Omega	Type T TC	0.75% full scale
RH% in/out Trilogy air coil	Omega	HX92AC-D	±2.5% RH from 20–80% RH; ±3.1% RH below 20% and above 80% RH at 22°C with temperature coefficient of ±0.1% RH/°F output
Ambient temperature	Local airport weather data	Ecobee website accessed via Trilogy control system	N/A

[a]All RTDs underwent five-point calibration over an expected temperature operating range of about -1-60 °C (30–140°F) against a NIST traceable thermometer; linear fit to temperature standard with R^2 of 1.000.
[b]Results of factory calibration against NIST traceable standard over expected operating flow ranges.

SH, SC, and WH energy delivered by the GS-IHP was computed for each mode using the following equations.

SC delivered (SC Mode):

$$Q_{SC} = V_{GroundLoop}\rho_{GroundLoop}c_{GroundLoop}(LWT - EWT) - W_{IHP} \quad (1)$$

SC delivered (SC + WH Mode):

$$Q_{SC} = Q_{WH,IHP} - W_{IHP} \quad (2)$$

SH delivered (SH mode):

$$Q_{SH} = V_{GroundLoop}\rho_{GroundLoop}c_{GroundLoop}(EWT - LWT) + W_{IHP} \quad (3)$$

Water heating delivered by IHP to the WH tank and connecting lines between tank and IHP (DWH mode):

$$Q_{WH,IHP} = V_{DHWLoop}\rho_{DWHLoop}c_{DWHLoop}(LDHWT - EDHWT) \quad (4)$$

Water heating delivered to building

$$Q_{WH} = V_{Hot}\rho_{Hot}c_{Hot}(T_{Hot}^{*} - T_{Cold}) \quad (5)$$

*Note 1: T_{Hot} was taken to be the maximum of (1) the leaving HW temperature measured by an immersion RTD sensor in the HW exit line to the building distribution system or (2) the upper tank wall temperature measured by a thermistor located near the upper element. Many of the HW draws experienced at both sites were of such small volumes and short durations that the RTD response time was too slow to capture an accurate measure of the leaving HW temperature.

Where:

- EWT is the GHX loop fluid temperature entering WSHP (RTD)
- LWT is the GHX loop fluid temperature leaving WSHP (RTD)
- $EDHWT$ is the domestic HW temperature entering WSHP (RTD)
- $LDHWT$ is the domestic HW temperature leaving WSHP (RTD)
- T_{Cold} is the cold water supply temperature to WH tank (RTD)
- T_{Hot} is the HW temperature leaving WH tank (see footnote)
- V is the fluid flow rate
- ρ is the fluid density
- c is the fluid specific heat

Energy consumption for the GS-IHP is measured directly by two watt-hour meters: one for the Trilogy unit (W_{IHP}) and one for the WH tank backup elements (W_{tank}). For the combined SC/WH mode, the energy consumption was apportioned to each output proportional to the output capacity and stored along the load data for each time step. This implicitly assumes that the efficiency, or COP, is the same for SC and WH in the combined mode.

The energy delivery and measured energy use for the GS-IHP in each mode were totalled for each month and season and compared with the estimated energy used by a baseline electric RTU/electric WH system sized to meet the same loads. Baseline RTU performance was estimated using performance curves that accounted for variations in outdoor temperature and humidity, indoor temperature and humidity, time- and temperature-controlled defrosting, cyclic losses, and supplemental resistance heating. Defrost cycles were assumed to be 5.8% of the operating time at outdoor temperatures below 40°F, and the defrost tempering heat energy was assumed to be equal to the cooling done during the reverse cycle defrost. The measured cooling load was not divided into sensible and latent parts. Since the GS-IHP varies its VS blower speed (rpm) to adjust the split of sensible and latent cooling required by the space, it is assumed to deliver the minimum total cooling energy required to maintain comfortable indoor conditions. In contrast, the baseline RTU unit does not have a VS indoor blower and therefore cannot adjust the ratio of sensible and latent cooling delivered. This results in either insufficient latent cooling and discomfort or in excess latent cooling and wasted energy. As such, assuming that similar comfort levels are maintained by both systems, the SC savings calculated for the GS-IHP over the RTU system are conservative.

Note 2: Additionally, late in the project it was discovered that the flowmeter at the Knoxville site providing the V_{Hot} measurement was subject to some flow oscillations in the cold-water line. Because of the nature of the meter, these oscillations caused the flow measurement to be higher than the actual flow. This erroneous flow was filtered out of the data by checking the corresponding temperature of the HW leaving the tank. When oscillations caused the measured flow, the HW temperature sensor was sufficiently far from the tank, so it did not increase in temperature. Any flow data without a corresponding increase in HW temperature or that was composed of less than three pulses from the flow meter were removed from the dataset. This could have inadvertently eliminated some small flow events (<0.2 gal), so the calculation of the water heating energy delivered to the building is likely conservative.

Note 3: There was significant uncertainty at the Oklahoma City site about where to place the DHW flow meter due to the presence of a building HW recirculation system and because there were two IHP systems with water tanks. With the amount of instrumentation budgeted for the project, it was impossible to obtain a good measure of the WH energy delivered to the building HW distribution system from each individual tank with any confidence. Therefore, the tank and connecting line standby heat losses measured for the Knoxville system (~23% combined) were assumed to also apply to the Oklahoma City system. This a somewhat conservative assumption because the IHP in Oklahoma City experienced heavier and more continuous WH loads than the Knoxville system. The system in Oklahoma City spent an average of ~12% of its total test period hours in WH modes compared with <5% for the Knoxville system. With longer run times and heavier WH loads, the HW tank and connecting line standby heat losses should be a smaller fraction of the total load.

Knoxville Site System Performance Summary

Table 3.4 summarizes the overall GS-IHP performance monitoring results for the Knoxville site from 2 p.m. on August 18, 2015 through 12 a.m. on August 18, 2016, along with the assumptions and limitations of the comparison. Only SC and WH operation data were included in the table because no SH operation was required during the test year at the Knoxville site.

Table 3.4. Knoxville site GS-IHP summary performance comparison vs. baseline system.

	GS-IHP	Baseline RTU + electric WH
SC (from SC and SC + WH modes)		
Total SC delivered (kWh)	16,729	16,729
Sensible cooling delivered (kWh)	14,227	14,227
Sensible heat ratio (SHR)	0.85	0.85
SC energy use (kWh); % savings vs. baseline	2,165; 46.3%	4,032
SC COP	7.73	4.15
WH (from demand WH and SC + WH modes)		
Total HW used (gal)	19,262	19,262
Average working day HW use (gal/day)	78.3	78.3
WH output from WSHP to WH tank (kWh)	2,730	--
Water heating delivered to building (kWh)	2,106	2,106
Total WH energy use (kWh); % savings vs. baseline	646; 72.4%	2,340
GS-IHP backup tank element energy use (kWh)	1.5	--
Water heating COP	3.26	0.90[3]
Water heating COP excluding tank/line losses	4.23	1.00
Misc. energy consumption from controls, etc. (kWh)	151	151
Overall		
Energy use (kWh)	**2,962**	**6,519**
% energy savings	**54.6%**	**--**
Carbon equivalent emissions (CO_2 metric tons)[4]	**2.04**	**4.49**
CO_2 emission savings (metric tons)	**2.45**	**--**

The following assumptions were made.

1) Baseline RTU SHR—a measure of latent cooling or DH capacity—is the same as the baseline estimated for Trilogy WSHP.
2) Baseline RTU is a 48,000 Btu/h (4-ton) rated cooling capacity unit (see Table 3.1 for other ratings).
3) Baseline RTU fan power is 365 W/0.47 L/m or 365 W/1,000 cfm [22] (taken from the current AHRI 210/240 ratings procedure).
4) Baseline RTU miscellaneous energy use is the same as that measured for the Trilogy WSHP.
5) Energy use for the combined SC + WH mode is divided between SC and WH proportional to the output capacities. Essentially, the COP for WH and SC in the combined mode is assumed to be the same. This slightly lowers the SC efficiency due to the higher

[3]Minimum energy factor rating for existing 50 gal electric storage WH manufactured before April 15, 2015 as rated per DOE test procedure. https://www1.eere.energy.gov/buildings/appliance_standards/product.aspx/productid/27.
[4]Estimated using a kWh-to-CO_2 conversion factor of 6.89×10^{-4} metric tons/kWh.

condensing pressures required for the SC + WH mode and raising the WH efficiency relative to the SC-only and dedicated WH mode efficiencies.

6) The Trilogy sensible cooling and subsequent SHR are calculated based on the cubic feet per minute provided by the Trilogy unit, an assumption of 1.2 kg/m^3 (0.075 lbm/ft^3) air density, and measured return and supply air temperatures.
7) The baseline system uses the existing electric WH at the site; the rated energy factor (EF) is 0.9, which is the minimum EF required for electric WHs manufactured before April 1, 2015.

The SC mode energy savings are likely somewhat conservative because the IHP and baseline RTU were assumed to maintain similar comfort sensible and latent SC loads. Since the RTU does not have a VS blower like the IHP, it would likely have to consume more energy to meet the same latent SC loads.

Figure 3.11 provides a graphical comparison of the monthly average overall SC COPs for the GS-IHP and baseline RTU/HP. The GS-IHP SC COPs in the plot include SC delivered in SC-only and SC + WH modes.

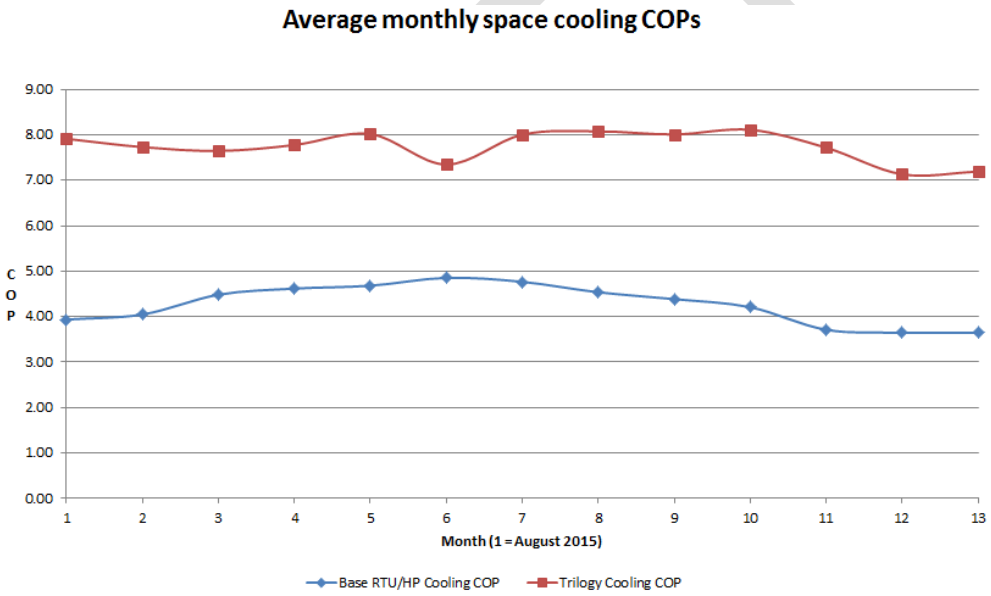

Figure 3.11. Knoxville site Trilogy WSHP vs. baseline RTU/HP SC monthly average COPs.

Figure 3.12 compares the hourly outdoor air temperature (OAT) and EWT of the Trilogy in both modes. In the hottest parts of the summer, the EWT was consistently cooler (by >11°C [>20°F]) than the outdoor (OD) air, which minimized the condensing pressure, leading to improved SC mode efficiency. In the winter months, the EWT was much warmer than the OD air, benefitting the GS-IHP WH mode efficiency. The EWT at the end of the monitoring period was essentially the same as when the unit began operating in August 2015. This indicates that, despite the heavily SC-load dominated operation all year and the addition of the antifreeze solution in January, there was no discernable warming of the ground surrounding the GHX bores during this first year of operation. The GHX loop could have been somewhat shorter, reducing system cost but sacrificing some energy-saving potential due to reduced efficiency.

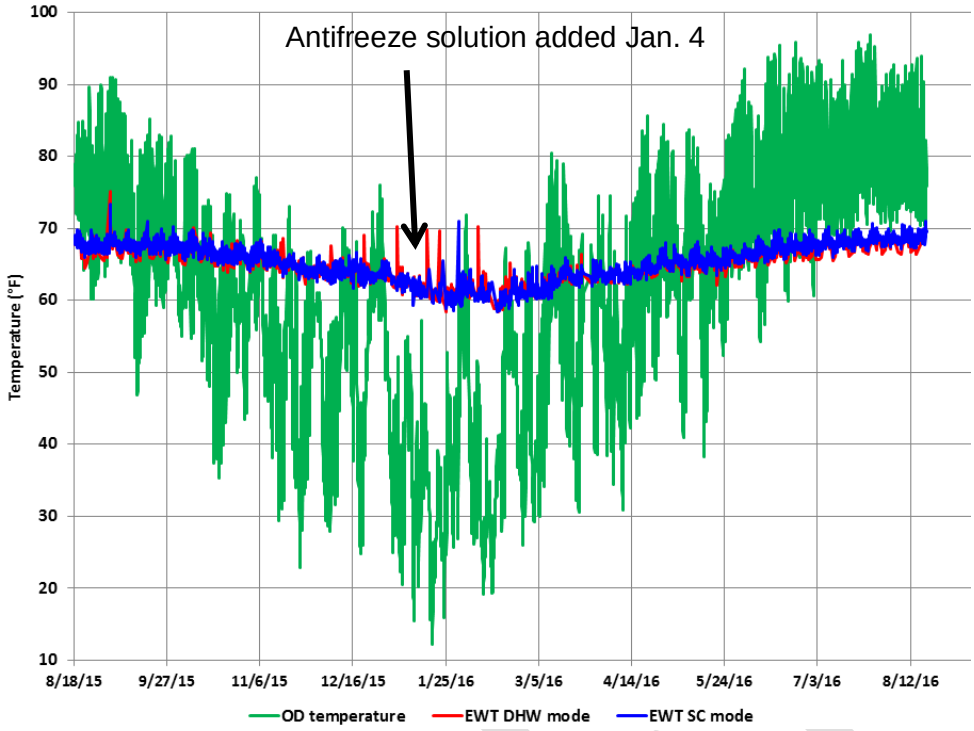

Figure 3.12. Knoxville site Trilogy WSHP EWT vs. OAT.

Also, the kitchen staff kept the SC setpoint low, as evidenced by the space temperature history during the test period shown in Figure 3.13. During the occupied periods (i.e., weekdays), the air temperature in the kitchen ranged as low as ~18°C (~64°F).

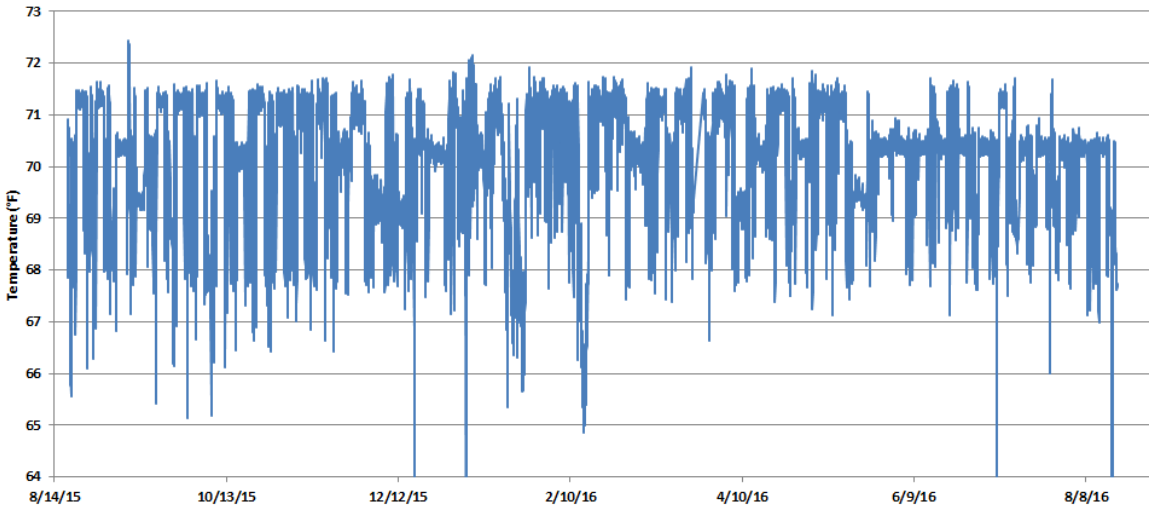

Figure 3.13. Knoxville site kitchen space temperature measured at thermostat during test year.

In addition to the energy savings, the GS-IHP system significantly reduced the hourly average kilowatt demand at the Knoxville site. The monthly peak hour kilowatt demand is shown in Table 3.5 for the GS-IHP and baseline systems. The maximum average hourly demand each month for the GS-IHP was 54–78% lower than that of the baseline system.

Table 3.5. Knoxville site peak hourly kilowatt demand by month, GS-IHP vs. baseline.

Month	GS-IHP demand (kW)	Date	Baseline demand (kW)	Date
August 18–31, 2015	1.705	--	4.545	--
September 2015	2.923	9/2/15, 12–1 p.m.	4.349	9/2/15, 1–2 p.m.
October 2015	1.642	--	5.290	--
November 2015	1.888	11/6/15, 12–1 p.m.	5.444	11/10/15, 1–2 p.m.
December 2015	1.603	--	7.110	--
January 2016	1.593	--	5.508	--
February 2016	1.538	--	5.407	--
March 2016	1.664	--	5.969	--
April 2016	1.510	--	5.647	--
May 2016	1.778	--	5.676	5/20/16, 2–3 p.m.
June 2016	2.301	6/14/16, 12–1 p.m.	10.425	6/16/16, 12–1 p.m.
July 2016	1.682	--	5.557	--
August 1–18, 2016	1.331	--	5.280	--
Total period	2.923	9/2/15, 12–1 p.m.	10.425	6/16/16, 12–1 p.m.

The kitchen staff behavior was perhaps the most significant factor influencing the IHP system peak demand at this specific location. Figure 3.14 illustrates the hourly IHP system, tank element power, and baseline RTU system power, along with outdoor temperature, HW tank temperature (at the top element location), thermostat cooling setpoint temperature, and HW consumption for the week beginning August 30, 2015. The IHP (purple line) and baseline system (red line) September peak demands occurred on Wednesday of that week. The IHP peak demand is not coincident with the outdoor temperature (orange line). Instead, it coincides with the point where the kitchen staff abruptly lowered the thermostat set temperature (light blue line), causing the system to increase to almost maximum compressor speed (light purple line) for about an hour to meet the sudden increase in SC demand. On the previous day—with similar OD temperatures and slightly lower peak HW usage (green line) but no sudden setpoint reduction—the IHP peak was only about half (1.52 kW vs. 2.92 kW). In contrast, the baseline system—which does not have variable capacity capability to improve efficiency—peak demand (red line) was estimated to be only about 0.2 kW lower (4.11 vs. 4.32 kW). Similar thermostat adjustments were also largely responsible for the IHP system peaks in November and June. The average hourly compressor speed absent abrupt thermostat adjustments was generally ~50–70% of maximum.

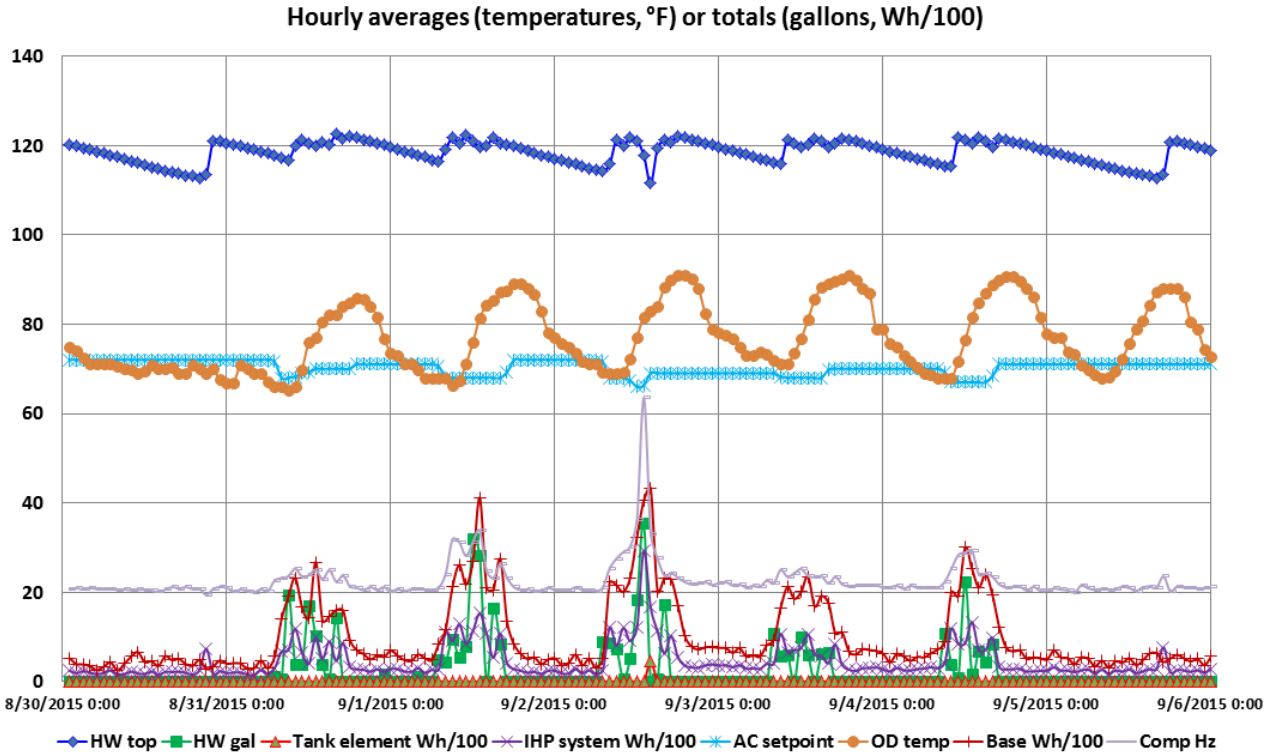

Figure 3.14. Knoxville site maximum IHP hourly peak demand week. (Note: the IHP and tank element power values are divided by 100 to make all the parameters fit on the chart.)

Energy cost savings for the Knoxville site were computed based on the energy and demand savings and the July 2016 commercial rate data from the local electric utility.[5] During June, July, August, and September, energy and demand charges were $0.12171/kWh and $13.92/kW. For all other months, the rates were $0.12130/kWh and $13.13/kW. Costs and savings for the GS-IHP vs. the baseline are given in Table 3.6. Total estimated energy cost savings were ~64%. Almost two thirds of the savings were due to the lower demand charges.

Table 3.6. Knoxville site GS-IHP HVAC/WH energy cost savings (August 18, 2015–August 18, 2016).

	Baseline RTU/HP and electric WH	**GS-IHP**
Electricity consumption	$792	$360
Electricity demand	$1,052	$312
Total costs	$1,844	$672
Energy cost savings vs. Baseline	--	$1,172
% cost savings vs. Baseline	--	63.6%

Oklahoma City Site GS-IHP System Performance Summary

The assumptions listed for Table 3.4 for the Knoxville site data analyses (reiterated with two differences as noted) also apply to the Oklahoma City site data analyses. The following assumptions were made.

[5]Knoxville Utilities Board, *General Power Rate—Schedule GSA*, July 2016. http://www.kub.org/wps/wcm/connect/3bfe2f80424c71338027b1d8d4cab33c/GSAJuly.pdf?MOD=AJPERES&CACHEID=3bfe2f80424c71338027b1d8d4cab33c.

1) Baseline RTU SHR is the same as that estimated for Trilogy WSHP.
2) Baseline RTU is a 17.6 kW rated cooling capacity unit (vs. 14.1 kW for the Knoxville site due to lower design load).
3) Baseline RTU fan power is 365 W/0.47 m^3/s, or 365 W/1,000 cfm [22].
4) Baseline RTU miscellaneous energy use is the same as that measured for the Trilogy WSHP.
5) Energy use for the combined SC + WH mode is divided between SC and WH proportional to the output capacities. Essentially, the COP for WH and SC in the combined mode is assumed to be the same. This slightly lowers the SC efficiency due to the higher condensing pressures required for the SC + WH mode and raising the WH efficiency relative to the SC-only and dedicated WH mode efficiencies.
6) The Trilogy sensible cooling and subsequent SHR are calculated based on the cubic feet per minute provided by the Trilogy unit, an assumption of 1.2 kg/m^3 (0.075 lbm/ft^3) air density, and measured return and supply air temperatures.
7) The baseline system requires a new electric WH. The rated EF is 0.94, which is the minimum EF required for electric WHs manufactured after April 1, 2015. For the Knoxville site, the original electric WH, which was installed before April 2015, was used with an EF of 0.9.

Tables 3.7–3.9 summarize the Oklahoma City GS-IHP performance for SH, SC, and WH operation, respectively.

Table 3.7. Oklahoma City site SH performance comparison, IHP vs. baseline RTU/HP.

Month	IHP (COP)	SH delivered (kWh)	IHP SH energy use (kWh)	Baseline RTU energy use (kWh)	IHP energy savings (%)	IHP SH energy cost ($)	Baseline RTU energy cost ($)	IHP energy cost savings (%)
January 31	4.86	26.93	5.54	10.37	46.6	0.32	0.59	46.6
February	4.85	2,101.82	433.43	915.40	52.7	24.84	52.45	52.7
March	5.04	1,062.94	211.02	426.51	50.5	12.09	24.44	50.5
April 1–28	5.27	263.43	49.94	99.99	50.0	2.86	5.73	50.0
Total	4.94	3,455.12	699.94	1,452.57	51.8	40.11	83.21	51.8

Table 3.8. Oklahoma City site SC cooling performance comparison, IHP vs. baseline RTU/HP

Month	IHP (COP)	Total SC delivered (kWh)	Total IHP SC energy use (kWh)	Baseline RTU energy use (kWh)	IHP energy savings (%)	IHP SC energy cost ($)	Baseline RTU energy cost ($)	IHP energy cost savings (%)
April 1–28	7.17	98.48	13.73	25.92	47.0	0.79	1.49	47.0
May 19–31	8.39	950.14	113.19	247.30	54.2	6.49	14.17	54.2
June[a]	7.08	3697.49	522.51	1,045.08	50.0	29.94	59.88	50.0
July	6.60	4,594.56	695.99	1,356.30	48.7	39.88	77.72	48.7
August[b]	6.80	3,229.54	475.22	939.58	49.4	27.23	53.84	49.4
September[c]	8.05	366.95	45.56	98.87	53.9	2.61	5.67	53.9
Total	6.93	12,937.16	1,866.19	3,713.05	49.7	104.32	212.76	49.7

[a]gap in data from June 10–15
[b]gap in data from August 12–16
[c]gap in data from September 3–7

Table 3.9. Oklahoma City site WH performance comparison, IHP vs. baseline RTU/HP. (Note: performance at this site is estimated assuming the ratio of WH delivered to the building is the same as measured at the Knoxville site.)

Month	Daily HW use (gal/d)	IHP (COP)	Total WH delivered to bldg. (kWh)	Total IHP WH energy use (kWh) (tank element kWh)	Baseline WH energy use (kWh)	IHP WHenergy cost ($)	Baseline WHenergy cost ($)
May 19–31	161	4.12	127.17	30.84 (0.21)	133.19	1.77	7.63
June[a]	167	4.27	286.64	67.09 (3.68)	302.64	3.84	17.34
July	182	4.72	1,008.41	213.81 (4.99)	1062.5	12.25	60.88
August[b]	181	4.45	808.35	181.59 (9.77)	853.48	10.41	48.909
September[c]	280	4.12	530.84	128.94 (0.68)	564.25	7.39	32.33
Total	189	4.44	2,761.42	622.28 (19.11)	2,916.05	35.66	167.09
% savings				78.7%			78.7%

[a]gap in data from June 10–15
[b]gap in data from August 12–16
[c]gap in data from September 3–7

As shown in Table 3.7, the IHP system demonstrated an overall SH COP of almost 5.0 and energy and cost savings of ~52% over the 61.7 days for which data were available. Energy cost savings were computed using the standard residential service rates from the Oklahoma Gas and Electric Company (OGE).[6] OGE charges a standard rate of $0.0573/kWh year-round with a slightly higher rate ($0.068) in June through September for consumption in excess of 1,400 kWh/month and a lower rate ($0.0173) in November through May for consumption under 600 kWh/month. For analysis purposes, the standard rate was assumed to be applied all year. The total electric cost savings for the monitored unit were ~$43. Assuming the average SH daily load and efficiency for the entire heating season would be the same as that of the monitored period, total SH energy and cost savings are estimated to be ~2,060 kWh and $118.

For SC operation, data were available for 117.6 days, over which the IHP demonstrated a COP of ~6.9 with almost 50% energy and electric cost savings compared with the estimated performance of the baseline RTU (Table 3.8). The delivered SC energy to the building is a combination of the SC delivered in two modes: SC only and SC + WH. Approximately 87% of the total SC load was delivered in SC-only mode operation. Total electricity cost savings for the monitored unit were ~$105. OGE also offers residential customers a time-of-use (TOU) rate option for June–October. From 2–7 p.m., the electricity use rate is $0.14/kWh, and for all other hours the rate is $0.027/kWh. With the TOU rate, the IHP's SC energy cost savings for the period would drop slightly to ~$100.

[6]OGE, *Standard Pricing Schedule: R-1 Residential Service*, August 2012. https://oge.com/wps/wcm/connect/de21b39f-2d52-402f-82e6-a6826999d724/3.00+R-1.pdf?MOD=AJPERES&CACHEID=de21b39f-2d52-402f-82e6-a6826999d724.

Assuming the average SC daily load and efficiency for the entire cooling season would be the same as that of the monitored period, the total SC energy and cost savings are estimated to be ~2,760 kWh and ~$158.

Estimated WH performance at the Oklahoma City site is given in Table 3.9. Operation data were available for 109.6 days. For that period, the IHP's estimated WH mode COP was ~4.45 with ~79% energy and electricity cost savings compared with the baseline electric WH, while delivering almost 715 L/d of HW to the residential units in the building (~71.5 L/day/unit). The WH energy delivered to the building is a combination of the WH delivered to the building in two modes: dedicated WH and SC + WH with over 80% coming during the SC + WH operating mode. Total electricity cost savings for the monitored unit were ~$131. With the TOU rate assumption, IHP WH energy cost savings for the period would drop slightly to ~$125.

Assuming the average WH daily load and efficiency for the entire year would be the same as that of the monitored period, total WH energy and cost savings are estimated to be ~12,460 kWh and ~$714.

Figure 3.15 compares the hourly OAT and EWT of the Trilogy for SH, SC, and WH operating modes (combined SC + WH mode does not use the GHX). In the hottest parts of the summer, the EWT was consistently cooler than the OD air, which minimized the condensing pressure and improved SC mode efficiency. In the winter months, the EWT was warmer than the OD air on average, benefitting the GS-IHP SH and WH mode efficiency.

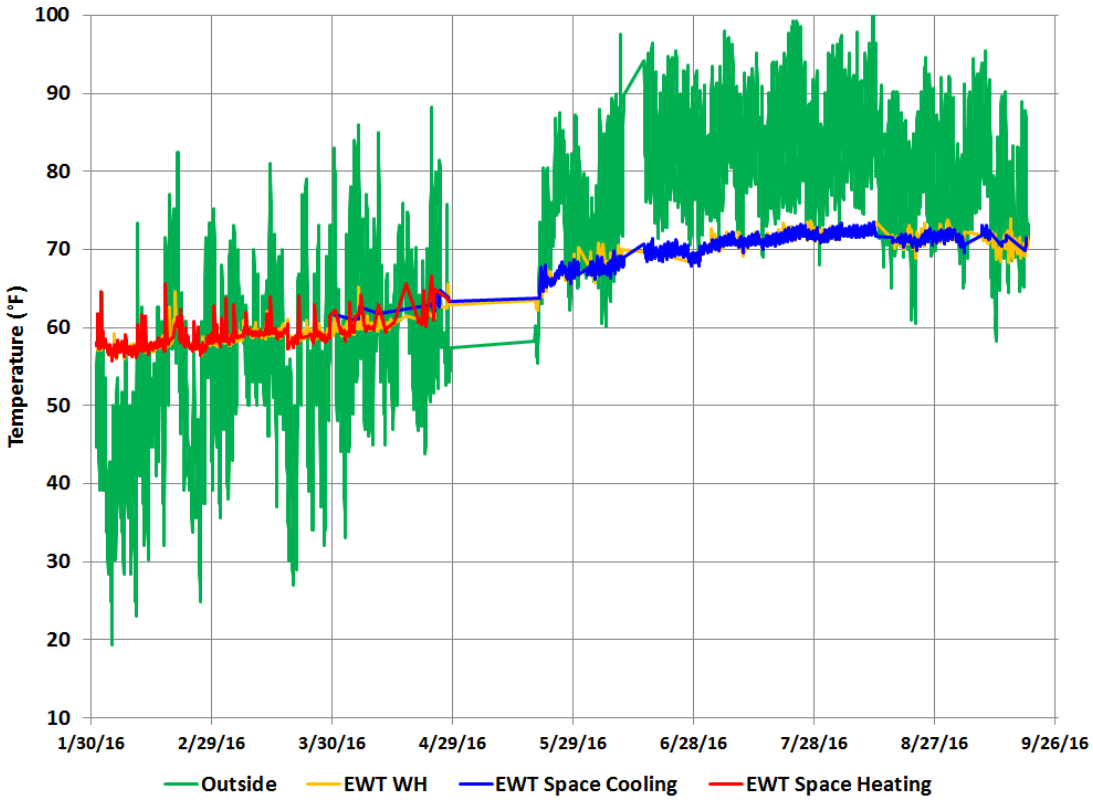

Figure 3.15. Oklahoma City site Trilogy WSHP EWT vs. OAT.

The monthly hourly average peak kilowatt demand at the Oklahoma City site is shown in Table 3.10 for the GS-IHP and baseline systems.

Table 3.10. Oklahoma City site peak hourly kilowatt demand by month, GS-IHP vs. baseline.

Month	GS-IHP demand (kW)	Date	Baseline demand (kW)	Date
January	0.937	--	2.869	--
February	3.388	2/27/16, 4–5 a.m.	10.283	2/26/16, 4–5 a.m.
March	3.139	3/19/16, 1–2 a.m.	10.574	3/19/16, 2–3 a.m.
April	4.437	4/13/16, 6–7 p.m.	7.302	4/2/16, 4–5 a.m.
May	2.289	5/25/16, 6–7 p.m.	6.605	5/28/16, 4–5 p.m.
June	6.367	6/14/16, 5–6 p.m.	7.960	6/14/16, 5–6 p.m.
July	5.671	7/27/16, 5–6 p.m.	9.869	7/25/16, 6–7 p.m.
August	7.024	8/3/16, 5–6 p.m.	9.144	8/3/16, 4–5 p.m.
September	4.315	--	8.070	--
Total period	7.024	8/3/16, 5–6 p.m.	7.201	2/26/16, 4–5 a.m.

Comparing Table 3.10 with Table 3.5 shows that the Trilogy system peak demand was generally higher at the Oklahoma City site than at the Knoxville site. Several factors contributed to this difference. First, the Trilogy WSHPs at the homeless shelter were configured to deliver a maximum cooling capacity of 17.6 kW due to the higher design loads at the shelter vs. those at the commercial kitchen at the Knoxville site. The higher SC loads at the shelter required the Trilogy to run at generally higher compressor drive frequencies (hertz) and, thus, higher compressor speeds, sometimes reaching peaks of almost 70 Hz (~4,200 compressor rpm). In contrast, the Trilogy unit at the Knoxville site seldom experienced compressor drive frequencies higher than ~40 Hz. Therefore, hourly SH or SC energy use (i.e., hourly power demands) for the IHPs at the Oklahoma City site was higher.

Additionally WH demands at the shelter were larger and more constant than at the Knoxville kitchen facility. As a result, the backup electric elements in the WH tanks were used more frequently than those at the Knoxville site. Although the total elements usage at the shelter was modest (~19 kWh from May–September and only ~1 kWh for January–April), sometimes element operation coincided with peak air-conditioning demand periods. This resulted in the IHP system experiencing occasional sharp, short-term peaks during summer months.

Installation Costs at Each Site

Actual system installation cost data were compiled for each site and are listed below. In addition to the actual cost for the Knoxville site, an assumed “mature market” installation cost estimate was made for use in the payback analysis discussed in this report. Payback estimates (high and low) were made for a GS-IHP system of the Knoxville site design vs. the baseline RTU/HP and electric WH using the range of GS-IHP installation cost estimates.

The primary variable affecting GS-IHP system installation cost is the external geothermal heat source/sink. As noted, this usually involves drilling/excavating and installing a GHX loop—usually of the vertical bore field type. For the Knoxville site, three “out of normal” installation issues were experienced that negatively affected the actual system costs.

- First and most important were the drilling issues related to the urban location. The primary complication was that provisions had to be made to recover all the drilling cuttings and fluids to avoid overloading city storm sewers. A vacuum pump truck had to accompany the drill rig to the site to accomplish this recovery, which significantly increased drilling costs.

- Secondly, the space available for the GHX field at the site was limited, so a horizontal boring machine was used to run the GHX header pipes from the GHX field to the building. In most cases, a much less expensive trenching machine is used to dig a trench for the headers. The space issue also limited the maximum distance between the boreholes to 4.3 m instead of CM's normally recommended 6–8 m spacing.
- Finally, the GHX header piping needed to be partly exposed to ambient air because it was impossible to run the headers under the building to the WSHP location next to the kitchen facility due to existing underground infrastructure. The header piping had to be run up the outside wall and through a ceiling plenum above the WSHP (Figures 3.16 and 3.6), which added ~1 day to the installation time. This situation occurs only rarely in the experience of the installing contractors. It also required an antifreeze solution to be added to the water in the GHX loop in early January 2016 to avoid any potential loop freeze problems. This added an estimated $700 to the system cost (the cost of the antifreeze plus an additional site visit) and slightly reduced the system performance relative to a water-only loop.

The installation contractor estimated that for a more rural location without all these complicating factors, the GHX install costs would be reduced by a factor of 2–3.[7]

Figure 3.16. Knoxville site GHX loop headers attached to a wall outside the kitchen facility.

No "out of normal" GHX installation issues occurred at the Oklahoma City site.

The Knoxville site GS-IHP installation cost estimate is as follows:

- GHX actual (per installer billing): $38,000 (~$138/m bore)
- GHX mid (without issues): $15,000 (~$56/m bore) (compared with US average costs of $49/m bore in the South and $42.62 in the Midwest [23])
- GHX low (mature market estimate): $9,600[8] (~$35/m bore)
- Trilogy unit: $9,800[9] (compared with ~$5,100 typical cost for nonpremium WSHP [23])

[7]Personal communication, M. Davis (City Heat and Air) to Van Baxter, August 26, 2016.
[8]Personal communication, D. Ellis (Comfortworks, Inc.) to Van Baxter, August 29, 2016. Estimated mature market GHX installation cost including drilling, u-tube pipe loop insertion, backfill/grouting boreholes, trenching and header pipe to building, and filling/flushing the GHX pipe loop.
[9]Personal communication, D. Ellis (Comfortworks, Inc.) to Van Baxter, August 29, 2016. Estimated mature market selling price for Trilogy unit including DHW tank, installation, and commissioning.

- Indoor installation: $1,600[10]
- Totals
  - high: $49,400
  - low: $26,400
  - mature market: $21,000

Knoxville site baseline RTU/HP + electric WH system install cost estimate:

- New RTU unit: $4,100 for 14 kW (4-ton) unit per [24]
- Roof curb: $1,500
- Structural: $1,700
- Plans/permits: $2,000
- Crane: $1,000
- Connection to existing ductwork: $1,000
- Total: $11,300

Excepting the RTU, baseline installation cost estimates were based on costs given in the Gas Engine Heat Pump field demonstration report by Vineyard et al. [25]. Before the IHP was installed, heating and cooling for the site kitchen facility were supplied by a central system that served the entire building. Because there are heavy internal loads in the kitchen due to refrigerator/freezer units, cooking equipment, dishwasher, and other tools, the existing system had inadequate cooling capacity during workdays. Thus, for the baseline system used in this comparison, it is assumed that a new RTU/HP dedicated to the kitchen area will be installed, which would require some structural roof modifications to accommodate the unit weight and new ductwork from the RTU to the existing kitchen ductwork. For the baseline water heating, it was assumed that the existing electric WH would be used, so no install costs related to WH were included.

The Oklahoma City site installation (new building) cost estimate is as follows:[11]

Total system estimate:

- GHX actual (per installer billing): $51,200 (~$33.5/m bore)
- Equipment (four WSHP units plus ERV): $39,100
- Indoor GHX loop and DHW tank connections: $6,500
- Totals: $141,200

Subtotal estimate for one Trilogy IHP (assumes GHX loop with 381 bore m (1,250 bore ft) total):

- GHX: $12,800 (~$33.5/m bore)
- Equipment: $9,800
- Indoor GHX loop and DHW tank connections: $2,025

[10]Includes removing existing WH tank, connecting WSHP to GHX headers, installing water piping connections between WSHP and DHW tank, and connecting to existing building air ducts and water pipes.

[11]Personal communication, D. Ellis (Comfortworks, Inc.) to Van Baxter, August 28, 2016. Total system equipment cost includes two Trilogy (IHP) WSHPs with 400 L DHW tanks and two non-IHP WSHPs with thermostats and miscellaneous materials along with one energy recovery ventilator (ERV) at $6,800. Ductwork cost was $50,700 for the entire building and was assumed to be the same for IHP and baseline installations.

- Totals: $24,625

Oklahoma City site baseline RTU/HP + electric WH system install cost estimate:

- New RTU unit: $4,300 for 17.6 kW (5-ton) unit [24]
- Roof curb: $1,500
- Structural: $1,700
- Plans/permits: $2,000
- Crane: $1,000
- Connection to existing ductwork:$1,000
- New 105 gal electric WH $1,900[12]
- Total: $13,400

Summary Cost and Payback Assessment

A payback analysis is provided in Table 3.11 based on the Knoxville site system design and the three GS-IHP cost assumptions given above. The "high" cost assumption uses the GHX cost as billed by the contractor for the Knoxville site. The "low" cost assumption is given based on the contractors' estimate that GHX cost could have been up to one third of the actual cost if not for the "out of normal" conditions noted previously. The mature market cost assumption is based on experience with many installations in Oklahoma. Finally, an alternative GHX financing approach was considered. For this case, the utility was assumed to install and own the GHX [26]. A GHX cost recovery charge of 2% of the GHX installation cost is added to the electric bill, reducing the total annual energy cost savings to the building owner [23]. Using the energy cost savings from Table 3.6, the payback for the GS-IHP ranges from ~8.5 to >30 years for the low- to high-GHX cost ranges, assuming the building owner pays the cost of the GHX installation up front. Assuming the utility installs and owns the GHX (i.e., building owner pays only for the Trilogy and associated indoor installation), the payback period could drop to <1 year.

[12]Price quote from Home Depot in September 2016 for 105 gal electric WH ~$1,500; assumed $400 for installation.

Table 3.11. Knoxville site payback analysis.

	Equipment costs ($)		GHX installed cost ($)	Total cost($)	Cost difference ($)	Energy cost savings($)	Payback (yrs)
	Price	Installation					
Conventional RTU/HP and electric WH	4,100	7,200	N/A	11,300	N/A	N/A	N/A
GS-IHP; high GHX cost assumption	9,800	1,600	38,000	49,400	38,100	1,172	**32.5**
GS-IHP; low GHX cost assumption	9,800	1,600	15,000	26,400	15,100	1,172	**12.9**
GS-IHP; mature market cost	9,800	1,600	9,600	21,000	9,700	1,172	**8.3**
GS-IHP; mature market GHX cost; utility owns GHX assumption	9,800	1,600	N/A	11,400	100	980[a]	**0.1**

[a]Utility adds cost recovery surcharge totaling 2% of GHX installation cost per year to bill ($192).

GS-IHP Field Demonstration Conclusions and Observations

These demonstrations were performed in Knoxville and Oklahoma City. The Knoxville site was a small commercial kitchen that experienced a year-round SC load and heavy HW demands during the work week (Monday–Friday). The Oklahoma City site was a homeless shelter (dormitory-like facility) that featured relatively balanced SH and SC and WH loads with SC being the largest. Both sites allowed the GS-IHP to take advantage of its combined SC + WH mode that featured extensive recovery of the normally wasted system condenser heat for water heating.

During August 2015–August 2016, the Knoxville site GS-IHP provided 53.7% total source energy savings compared with a baseline electric RTU/HP and electric WH. Peak demand savings were 54–78% per month. Energy savings of 54.6% and energy cost savings of 55.9% were achieved (almost evenly split between reduced demand charges and electricity consumption savings). The GS-IHP also saved a significant amount of carbon emissions, which were ~2.45 metric tons for the August 2015–August 2016 test year. If trading for carbon credits ever become a reality, then additional cost savings would be realized. These savings significantly exceeded the project technical performance goal of ≥45% energy and carbon emission reductions. No SH loads were experienced for this site; only SC and WH operation was required for the entire test year.

For the Oklahoma City site, DAS installation delays prevented the collection of a full year of performance data. However, enough data were obtained to allow a reasonable estimate of SH, SC, and WH energy savings and efficiency vs. the baseline system.

- SH: from Table 3.7, total energy savings of ~753 kWh (~52%) and average COP of ~4.9
- SC: from Table 3.8, total energy savings of ~1,847 kWh (~50%) and average COP of ~6.9
- WH: from Table 3.9, total energy savings of ~2,293 kWh (~78%) and average COP of ~4.4

Over the actual monitoring period, the GS-IHP at the site demonstrated total site electricity savings of ~4,890 kWh (~60%) and carbon-emission savings of ~3.4 metric tons, greatly exceeding the project's technical goal. Assuming that the daily average loads and COPs above are the same for the balance of the year for each mode, the total annual energy savings are estimated to be ~12,460 kWh with carbon-emission savings of ~8.6 metric tons. The WH savings indicated above are estimated assuming that the system at the Oklahoma City site experienced the same HW tank and connecting line standby heat losses (as a percentage of the total load) that were measured at the Knoxville site.

This field study successfully demonstrated the energy savings, environmental savings, and operational benefits of GS-IHP technology for small commercial building applications. Both demonstration systems significantly exceeded the project technical objectives of >45% energy and carbon-emission savings (>50% at both sites). The best applications of the GS-IHP system are buildings or specific small zones of buildings that have high HW loads coincident with high SC loads.

Payback analyses were conducted for the Knoxville site system based on the annual energy savings demonstrated. The specific site conditions (e.g., limited area, local regulations) caused drilling costs to be about three times higher than what is typical for the area. For the actual GHX cost, simple payback vs. the baseline RTU/HP/electric WH system were >30 years (Table 3.11). With more typical GHX costs for the area, the payback is approximately 13 years. For a mature market cost assumption based on experience at the Oklahoma City site, the payback drops to ~8 years for many installations, which is still likely higher than what is acceptable for most commercial building owners. Assuming an alternative GHX financing option were available in which the local utility (or another entity) installed and owned the GHX loop and amortized the cost via a surcharge on the electric bill, system payback could be reduced to ~0.1 year.

The economics of GS-IHPs will vary from site to site for several reasons, including the following.

- Regional differences in drilling costs, local site conditions and requirements, and financing options can cause the GHX loop installation costs to vary widely, even within a given region. Where local site conditions are unfavorable (e.g., restricted area, local permitting/regulation restrictions, as experienced at the Knoxville site), GHX installation costs can be prohibitive.

- Local electricity rate structures could limit the operating cost savings achievable, leading to higher payback periods.

3.2.2 Electric AS-IHP System Development, Analyses, and Test Results

Full details of the AS-IHP concept development can be found in Murphy et al. [18] with a shorter summary in the Annex 40 final reports [16, 27]. Most of the material in this section is summarized from the two prototype system development reports [28, 29].

Figures 3.17 and 3.18 show conceptual installations for the two different AS-IHP prototype systems developed. Each system uses a VS compressor, VS indoor blower (for SH/SC distribution), and VS outdoor fan. One system (Figure 3.17) also includes an integral HW circulation pump that might be single-, multi-, or VS. One electric AS-IHP prototype and the gas engine-driven AS-IHP prototype are of this general configuration. The second electric

prototype system (Figure 3.18) has a separate dedicated HP water heater/DH unit that can provide DWH and dedicated year-round DH. A 190 L (50 gal) WH tank is included. Both prototype electric AS-IHP systems have 10.5 kW (3-ton) nominal cooling capacities, and the prototype gas engine AS-IHP was a nominal 17.6 kW (5-ton) size.

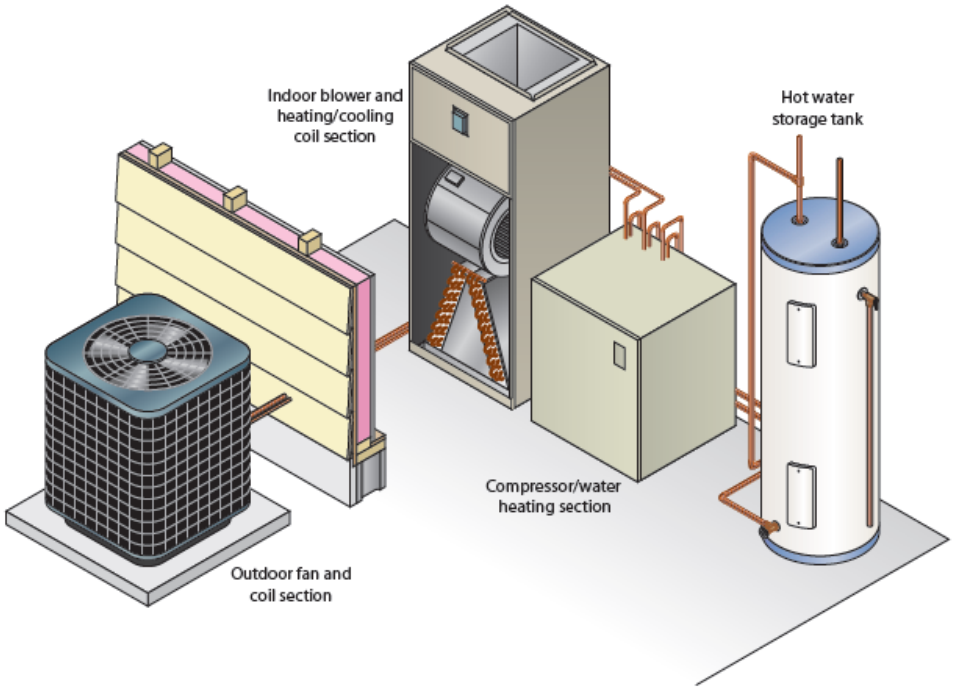

Figure 3.17. Conceptual installation of AS-IHP system concept 1.

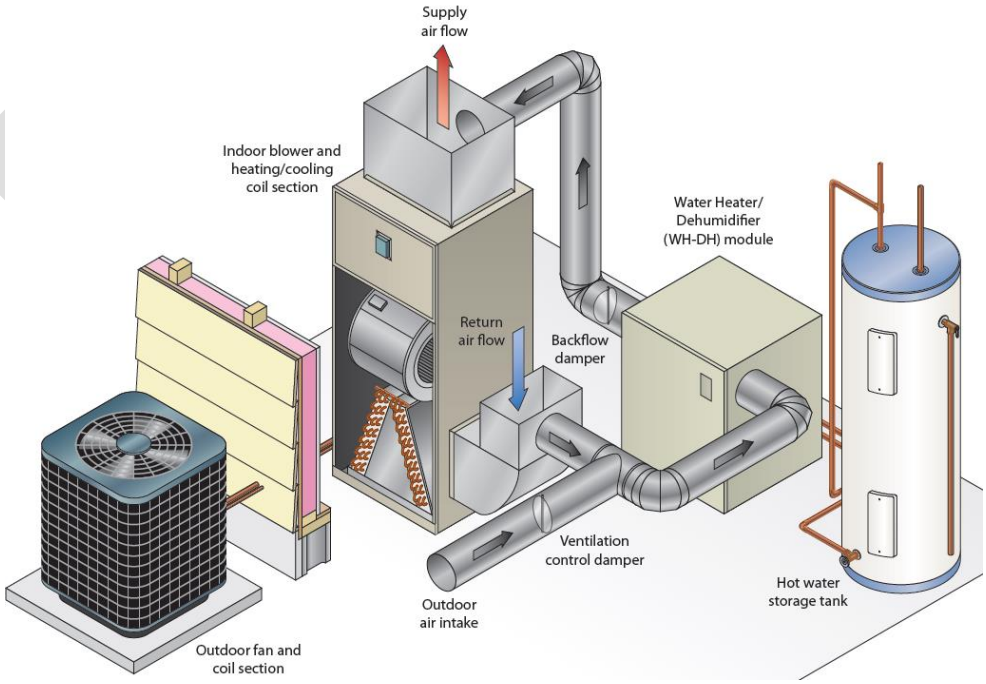

Figure 3.18. Conceptual installation of AS-IHP system concept 2.

Electric AS-IHP 1—Single-Compressor or Combined System

ORNL and an ASHP manufacturing partner, Nortek Global HVAC, collaborated to design and develop a prototype of an AS-IHP based on the concept in Figure 3.17 suitable for existing residential applications using R-410A refrigerant. A nominal 10.6 kW (3-ton) design cooling size was selected for development. ORNL and manufacturer team members engaged in an iterative process of prototype analysis/design, lab testing, and redesign based on lab results. Three generations of prototypes were developed, which led to field testing. The design uses a VS compressor, blower, and fan. Dual electronic expansion valves are used to provide a wide range of refrigerant flow control. The final prototype design used compact HX designs for all three system HXs (indoor and outdoor air coils and refrigerant-to-water HX).

Field performance observations

A 1-year field test was initiated in a 223 m^2 (2,400 ft^2) test house (Figure 3.19) in Knoxville, Tennessee in May 2014. Pictures of the field test system are included in Figure 3.20, and the DAS is shown in Figure 3.21.

Figure 3.19. Field test site in Yarnell Station neighborhood, Knoxville, Tennessee.

Figure 3.20. Prototype installation: (left) indoor sections (HW storage tank, compressor and water heating module, and indoor fan coil); (right) outdoor fan coil section.

Figure 3.21. Field data monitoring system.

Before the field testing started, the test house occupancy simulation was set up. The water draw schedule used at the site was based on the latest Building America water draw generator [30]. Latent, sensible, and other building internal loads were based on the Building America House Simulation Protocols [31]. Occupancy simulation devices followed a schedule input via a database that is read by a programmed controller for operating space heaters to simulate sensible heat and humidifiers to simulate latent heat. HW loads (e.g., dishwasher, clothes washer, showers, sinks) were simulated by operating solenoid-controlled water valves according to the programmed schedule with an average HW use of 213 L/day. Figure 3.22 shows the HW valves and controller setup. Temperature control setpoints of 49.0°C (120°F) for WH, 24.4°C (76°F) for SC, and 21.7°C (71°F) for SH were implemented in the system controls before starting data monitoring. The primary operating modes experienced during this period were:

- SC only (Dedicated SC)
- SC + desuperheater (DS) WH (SC + DS)
- SC + FC WH (SC + WH)
- SH only

Figure 3.22. HW use control valves.

Prototype Field Performance Summary and Observations

Both the SC and SH seasonal COPs were lower than those estimated using the AHRI 210/240 [21] procedures with the rated values for the prototype, as seen in Table 3.12. The AHRI estimates were computed using the minimum (i.e., more efficient thermal envelope) and maximum (i.e., less efficient thermal envelope) house load line assumptions (DHRmin and DHRmax) and using the actual demonstrated test house load lines.

Table 3.12. Site-measured seasonal SH and SC COPs vs. estimated AHRI 210/240 [21] ratings for prototype system.

Mode	Field measured	AHRI 210/240	% deviation field vs. rated
SH $SCOP_h$	2.05	For DHRmin load: 2.98 For DHRmax load: 2.44 For house loads: 2.64	31 16 22
SC $SCOP_c$	5.14	For default load and 0.2 Cd: 5.49 For house loads: 5.60	6 8

Field measurements on two single-speed (SS) ASHPs were taken in the Knoxville area in 2011–2012. Both were tested in one two-story house; SS unit 1 conditioned the downstairs, and unit 2 conditioned the upstairs. Heating season measurements showed a $SCOP_h$ of 1.52 and 1.76 for units 1 and 2, respectively [32]. These are 32% lower and 22% lower than the $SCOP_h$ rating for the units of 2.26 (per AHRI 210/240 based on DHRmin load line). This is like the 31% deviation in Table 3.12 from the estimated AHRI rating for the field prototype based on the DHRmin load line. However, for cooling operations, the two SS ASHPs had field-measured $SCOP_c$s of 2.08 and 2.46 (a 45% and 35% deviation from rated), whereas the field AS-IHP prototype field-measured $SCOP_c$ was 5.14 (only a 6% deviation from estimated rating).

There are several reasons why the AS-IHP field prototype's measured SH COP is lower than expected.

- Blower energy use is higher at the field site than was measured in the lab test phases of the project due to higher duct system external static pressure losses. This is somewhat peculiar for the changes made in the test house ducting system to accommodate the AS-IHP. However, residential duct systems generally have higher pressure losses than implicitly assumed in AHRI 210/240. (This also negatively affects the SC seasonal COP.)

- The $SCOP_h$ procedure does not account for defrost tempering heat usage which accounted for >10% of the total field system energy use in February alone.

- The indoor temperature during the heating season averaged close to 72°F, whereas lab testing and the HSPF procedure assume 70°F.

- The standard house load line used in the HSPF procedure is lower than that experienced at the test house during the 2014/2015 winter test season.

- Many of the issues related to the SH control for the field-test prototype could also be an unintended consequence of using a generic, low-cost, two-stage thermostat to control a VS system. Setting up optimal sequence timing to control the compressor speed based only on a high- or low-stage thermostat input is a significant challenge. This approach is unlikely to provide good results in all homes due to differences in equipment sizing relative to the actual heating load and the thermal mass of the home.

Table 3.13 compares the average heating and cooling degree days for Knoxville with those experienced during the 2011–2012 and 2014–2015 test years. The 2014–2015 test year weather for Knoxville was somewhat cooler than the long-term averages per ASHRAE [33] for the heating (~12% colder) and cooling seasons (~8% cooler). The 2011–2012 actual weather (when the two SS ASHPs were tested) was a bit warmer than normal—22% warmer during the heating season and 14% warmer during the cooling season.

Table 3.13. Average vs. 2014–2015 test site heating and cooling degree days.

Location	Annual °F-days heating (18.3°C base)	Annual °F-days cooling (18.3°C base)
Knoxville		
Average[1]	1997	841
2011–2012[2]	1553	958
2014–2015[2]	2136	825
2014–2015[3]	2233	778

[1]1986–2010 averages, ASHRAE [33].
[2]Test year actuals from National Oceanic and Atmospheric Administration for Knoxville McGhee-Tyson airport weather station [34].
[3]For test year May 3, 2014–May 2, 2015; site-measured actual.

It is not unusual for actual measured HP HSPFs to be degraded by 30% or more compared with the HSPF rating (based on the DHRmin load line) due to the reasons cited previously and other miscellaneous effects, such colder-than-normal winters. The higher house load effect alone likely accounts for more than half the degradation.

Estimated field prototype AS-IHP energy savings vs. baseline minimum efficiency system at test site

The annual energy use of a baseline system (3.8 $SCOP_c$ and 2.26 $SCOP_h$ [Region IV] SS ASHP and electric WH) that meets the field test site loads was estimated. The HSPF and SEER ratings for the baseline unit were adjusted downward by 27 and 40%, respectively, based the average field-measured deviations from rated efficiencies experienced by the SS ASHPs previously field tested in a similar size nearby house in the Knoxville area [32]. The results for this comparison are shown in Table 3.14. Since the tank and HW distribution line losses from the HW storage tank were unaccounted for in the AS-IHP field performance, they were also omitted from the baseline equipment efficiency (e.g., baseline WH COP = 1.0). The table shows that the largest percentage and absolute savings come from water heating at 61% and 1,905 kWh, respectively. SC and SH energy savings are estimated at 1,800 kWh (55%) and 1,461 kWh (20%), respectively. The estimated total annual savings for the AS-IHP vs. estimated baseline energy use at the Knoxville site are about 38%. Heavy reliance on backup electric elements for SH and defrost tempering and higher indoor blower energy usage (vs. lab-measured performance) were significant contributing factors, causing the lower-than-expected SH performance of the AS-IHP field prototype system. A smaller rated capacity IHP combined with a better insulated house (closer to the DHRmin load assumption used by the AHRI 210/240 procedure) would be a much closer match to the preferred application and would possibly have yielded total energy savings of ~45% or more at the test site.

Table 3.14. AS-IHP 2014–2015 measured performance vs. estimated baseline performance at the test site.

Mode		AS-IHP	Baseline system estimated performance	Percent savings over baseline
SC	COP (SEER)	5.14 (17.52)	2.29 (7.80)	
	Delivered (kWh)	7,416	7,416	
	Consumed (kWh)	1,444	3244	55%
SH	COP (HSPF)	2.06 (7.01)	1.65 (5.62)	
	Delivered (kWh)	12,125	12,125	
	Consumed (kWh)	5,899	7,360	20%
Water Heating	COP	2.68	1	
	Delivered (kWh)	3,104	3,104	
	Consumed (kWh)	1,199	3,104	61%
Total	**Consumed (kWh)**	**8,542**	**13,708**	**38%**

Applying the AS-IHP system to commercial buildings for which the annual loads are dominated by WH and SC needs would also be expected to yield much higher annual energy savings than were demonstrated during this residential field test.

Electric AS-IHP 2

ORNL has been engaged with another manufacturing partner (Lennox Industries) to develop a field-test prototype of the second AS-IHP concept system, as shown in Figure 3.28.

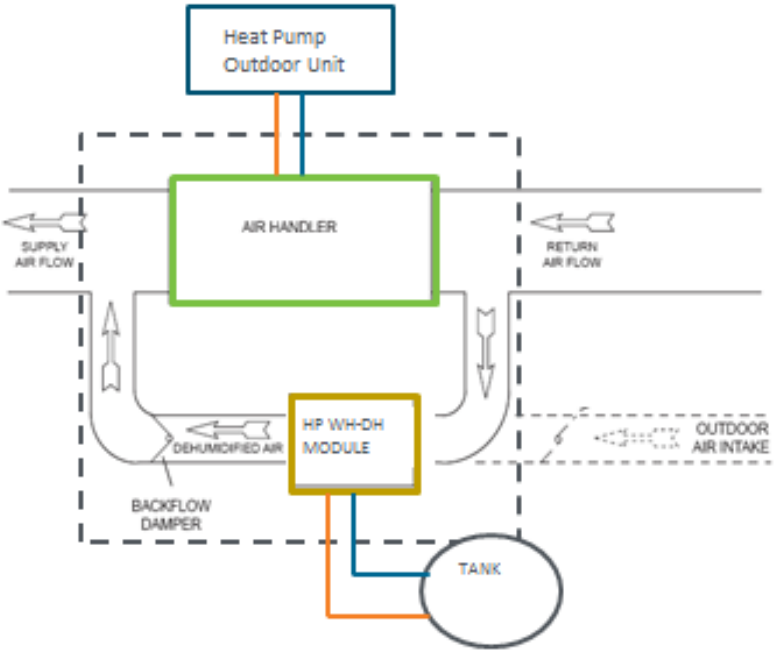

Figure 3.23. Two-box AS-IHP concept schematic.

WH-DH module and AS-IHP system field-test prototype design summary

The WH-DH module design is based on US Patent 8,689,574 B2 [35]. Figure 3.29 is a photograph of the field-test WH/DH unit with its side panels removed to show the control board. Figure 3.30 provides a CAD drawing of the general layout of the field-test prototype WH/DH design.

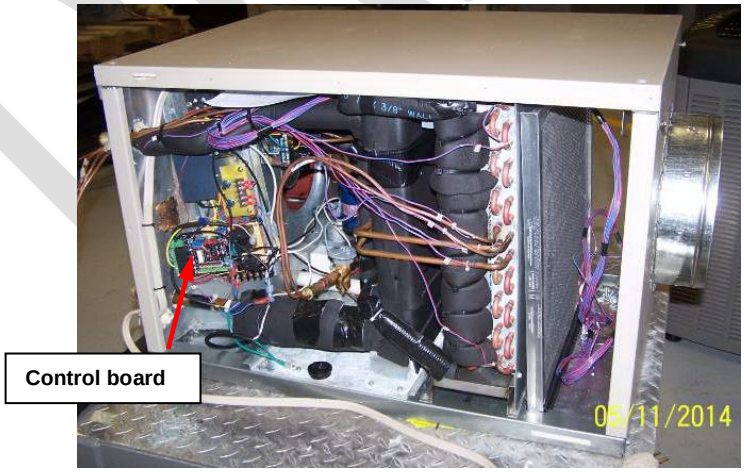

Figure 3.24. Field-test WH/DH prototype.

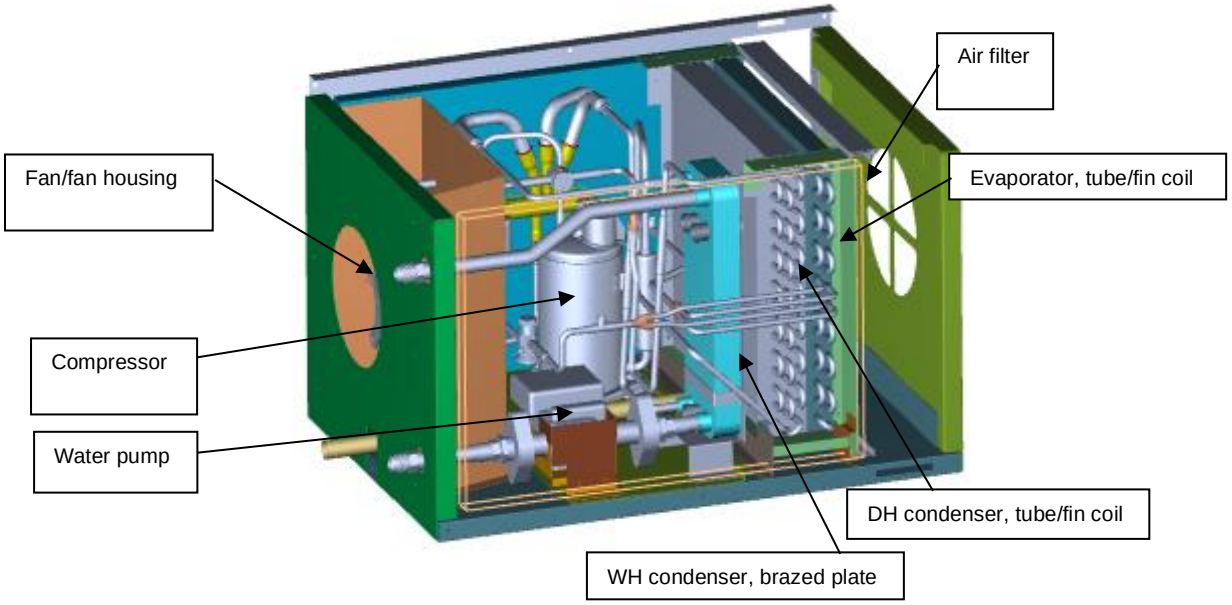

Figure 3.25. CAD drawing of field-test prototype WH/DH module.

A drawing of the AS-IHP field-test system arrangement is provided in Figure 3.31. The system design intent was to pair the WH/DH field-test prototype with a Lennox high-efficiency, VS XP-25 ASHP. The XP-25 family of ASHP products has rated $SCOP_c$s of 5.9–7.0 and $SCOP_h$s of 2.8–3.0 [36]. The model selected for the field-test AS-IHP was rated at 10.1 kW of cooling with a $SCOP_c$ of 6.3 and DOE Climate Region IV $SCOP_h$ of 2.9. Significant components of the WH/DH are a SS compressor, SS water pump, VS fan, fin-and-tube refrigerant-to-air evaporator, brazed plate refrigerant-to-water condenser, and fin-and-tube refrigerant-to-air condenser, as depicted in Figure 3.30. A solid-state microcontroller manages the competing requests for service with WH having priority over DH. The VS blower initially used the same speed for WH, DH, and fresh-air ventilation (V) modes. Early in Summer 2016, a control change was implemented to slow the WH/DH fan during V mode (details are provided in the DH performance discussion below).

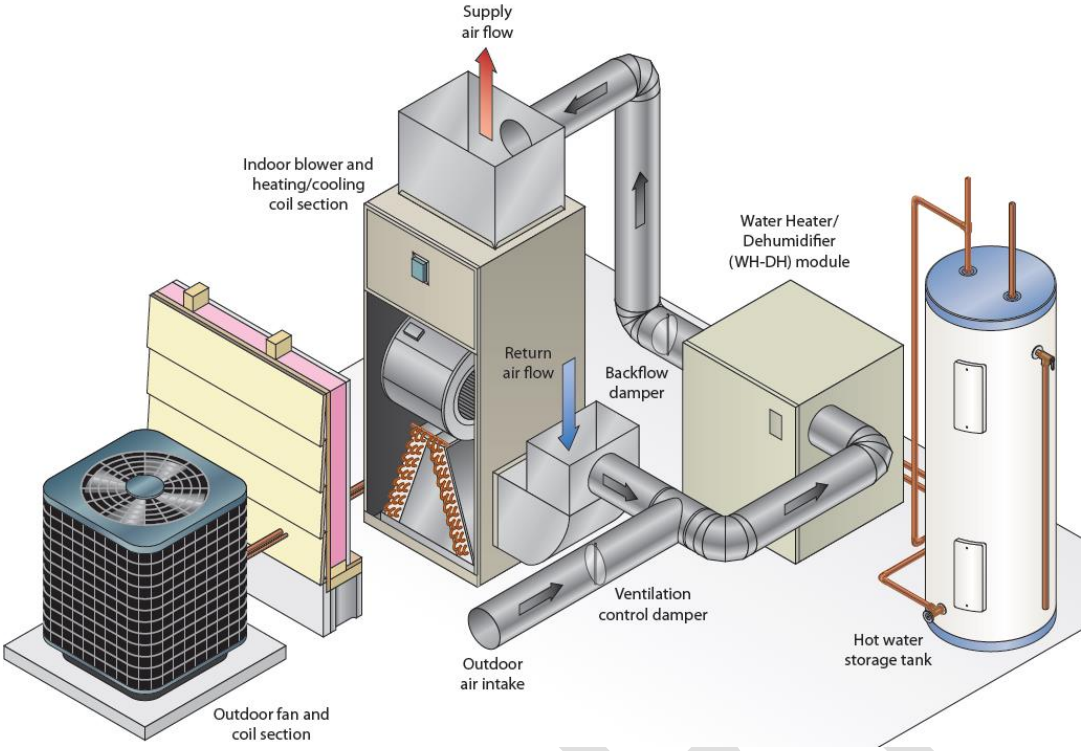

Figure 3.26. Two-unit AS-IHP field-test system arrangment.

Field Test Setup

The XP-25 ASHP and WH/DH prototype were shipped to ORNL in early 2015 and installed in June–July 2015 at the Knoxville test house (Figure 3.19) for a 1-year field test. A photo of the field-test system is included in Figure 3.32, and the field DAS is shown in Figure 3.21. Full data monitoring of the AS-IHP system began in August 2015 and continued through September 2016. Monitoring the WH/DH module continued through May 2017 to evaluate the effect of some design and control modifications implemented due to the initial test-year results.

Figure 3.27. Field-test prototype during installation. ASHP indoor air handler and WH/DH prototype shown with rain gauges for condensate collection to monitor DH and latent cooling loads.

The same house occupancy simulation protocol used for the AS-IHP 1 field test was also used for the test of AS-IHP 2 prototype system.

The field DAS was set up to collect data at 15 second intervals with 1 minute, 15 minute, 1 hour, and daily averages. Data were stored on servers located at ORNL. A dedicated internet connection was set up to allow the Lennox project team to monitor data collection in real time.

Equipment setup

The space-conditioning system included zone controls and dampers that allowed the upstairs and downstairs zone temperatures to be controlled independently. The zoning system also controlled the ASHP airflow based on fixed airflow values that were assigned to each zone during system commissioning. The thermostat setpoints were 71.0°F (21.7°C) for the heating seasons and 76.0°F (24.4°C) for the cooling seasons. The ASHP operating mode was switched manually between heating only and cooling only as needed.

The WH/DH was connected to a standard electric storage WH with copper pipe and a concentric fitting that was inserted in place of the typical drain at the bottom of the WH (Figure 3.33). The power to the lower thermostat/element was disconnected and rewired to provide a low-voltage signal to the WH/DH when WH was required.

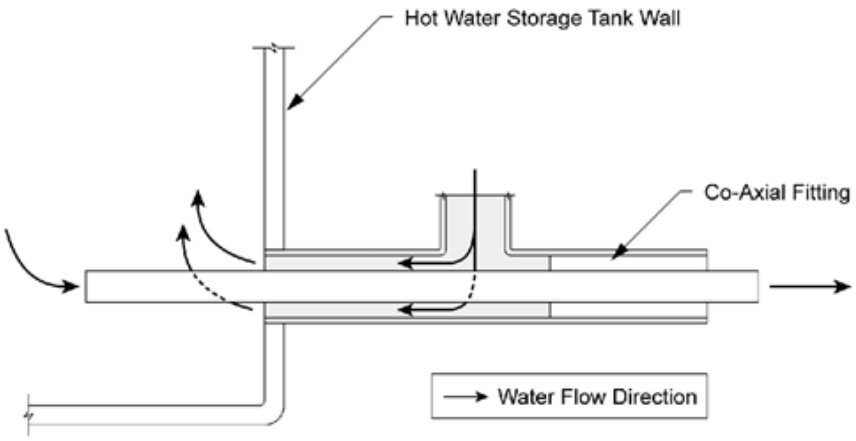

Figure 3.28. Schematic of coaxial tank water fitting.

The return air for the WH/DH was ducted from the return plenum of the HP. The supply air was ducted separately from the WH/DH with one duct terminating on the second floor of the house and the other on the first floor. Controlled fresh-air intake is one difference between the field-test system and the baseline equipment. A constant 45 cfm (21 L/s) of outdoor air was provided to the house. Homes with tightly sealed envelopes need mechanical fresh air V to maintain acceptable indoor air quality.

Instrumentation

The ASHP was instrumented for air-side heating and cooling capacity measurements, as well as additional measurements of refrigerant-side pressures and temperatures. The condensate drained from the evaporator coil was also measured to provide a check on the air-side latent capacity measurement. The WH/DH was instrumented for water-side WH capacity measurements and air-side capacity measurements for DH and the cooling by-product from the WH mode. Like the ASHP, the condensate drained from the WH/DH was also measured

to provide a check on the air-side latent capacity. Solid-state transducers were used to measure the total and component energy use of the ASHP and WH/DH.

WH/DH Module DH Mode Performance

During AS-IHP system test year (October 2015–September 2016)

The WH/DH was called to dehumidify when a low-voltage alternating current (AC) signal was supplied. In a typical installation, this would be provided by a humidistat. However, since the home was already instrumented with humidity sensors, the data logger was used to provide the contact closure functionality of a humidistat. The call for DH mode was supplied to the WH/DH when the Level 1 or Level 2 humidity sensors read over 55% RH, and it was removed when both sensors read below 51% RH. The WH/DH maintained the humidity in the house excellently with the highest hourly average humidity measurement during the study being 54.8%.

One issue observed during WH/DH operation involved the evaporation of condensate remaining on the evaporator coil during V mode (i.e., essentially, all the hours when neither the DH nor WH mode operation occurred). The DH and WH modes condense moisture from the air on the evaporator coil, as shown in the top plot of Figure 3.34. The blue highlighted sections indicate that the unit is operating in DH mode. In this mode, the unit provides positive latent cooling and negative sensible cooling (i.e., heating). The house humidity is reduced as moisture is removed from the air. The pink highlighted sections indicate operation in the V mode. In this mode, the unit provides negative latent cooling (i.e., evaporates moisture into the air) and sensible cooling due to the evaporative cooling effect. This increases the house humidity and negates part of the work done during the DH mode. Based on a comparison of the air-side latent capacity during the DH mode and the latent capacity calculated based on the measured condensate leaving the unit, approximately 33% of the condensed moisture was being evaporated during the V mode. This results in an effective DH efficiency that is one-third lower than its steady-state efficiency. The first step taken to mitigate this effect involved reducing the airflow through the unit during the V mode. The initial equipment setup required the V airflow to be like that of the WH and DH (~300 cfm) to ensure the proper outdoor air V rate of 45 cfm. This was due to the small size of the fresh-air intake duct relative to the WH/DH return duct. In June 2016, a damper was added to the WH/DH return duct upstream of the fresh-air intake. This damper was closed during the V mode, reducing the airflow to the required V rate since the unit was now pulling in 100% fresh air instead of a mixture of fresh air and indoor air. This also significantly reduced the V mode fan power to ~13 vs. ~53 W before installing the damper. The bottom plot in Figure 3.34 shows DH and V cycles of the WH/DH after the damper was installed, as well as reduced airflow composed of 100% fresh air for V. During the V mode, the condensate evaporation was significantly reduced, as indicated by the latent capacity being only slightly negative. The DH cycle frequency was also reduced, and the humidity in the home increased at a much slower rate, although the outdoor conditions were slightly drier for the data shown in the bottom plot of Figure 3.34. Once again, a comparison between the air-side latent capacity measured during the DH mode and the condensate collected from the WH/DH indicated that only 5% of the condensed moisture was evaporated back into the air during the V mode. This is a significant reduction compared with the 33% evaporation rate seen before the return air damper was installed.

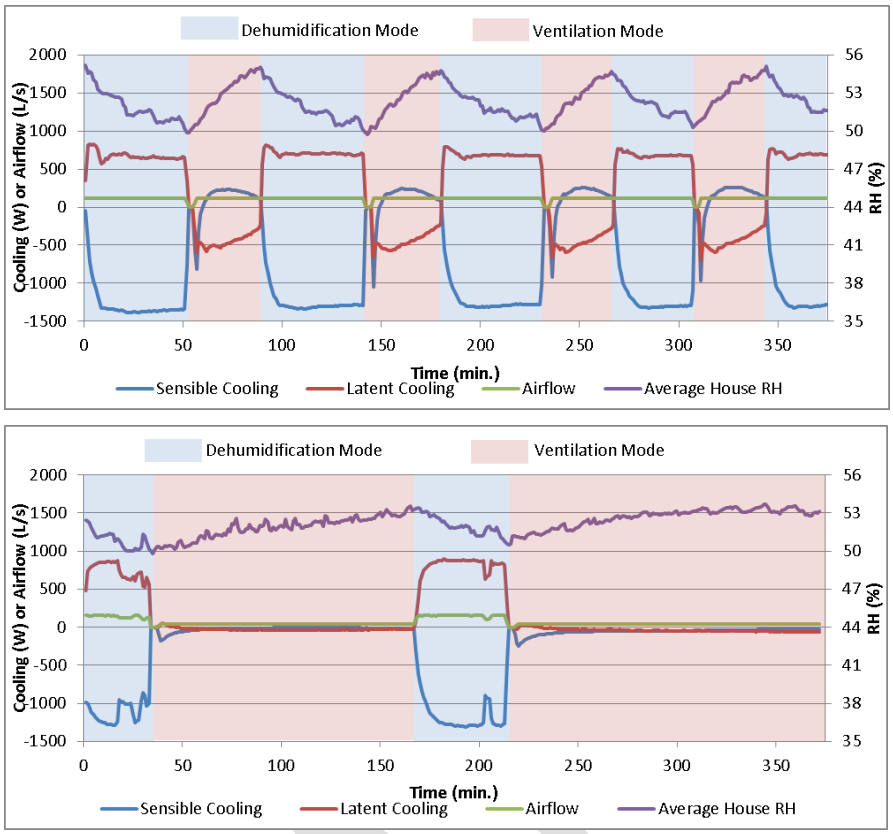

Figure 3.29. WH/DH cycling between DH mode and V mode with condensate evaporation during V for equal V and DH airflow rates (top plot) and with reduced airflow during V mode (bottom plot) [37].

The monthly run time and average efficiency based on the measured air-side latent capacity are shown in Figure 3.35. As noted, condensate evaporation in the V mode likely resulted in increased DH run time for all months before and including June 2016. July and August 2016 showed significant (i.e., >100 hours per month) DH run time due to high outdoor humidity. September 2016 had a higher average outdoor humidity than October–December 2015 but had significantly less DH run time, illustrating the reduction in the re-evaporation of condensate during V mode. For the months with significant run time, the efficiency for DH was ~1.5–2.1 L/kWh. There were measurement issues related to the air-side capacity of the WH/DH for August–October 2015, so this period was excluded from the calculation of the average DH efficiency of 1.7 L/kWh.

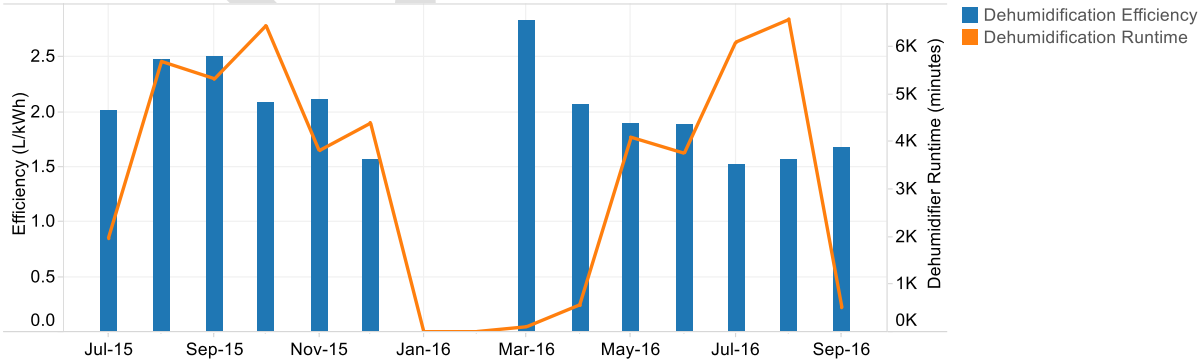

Figure 3.30. Monthly DH efficiency and run time [36].

WH/DH Module WH Mode Performance

The monthly WH efficiencies for the WH/DH are shown in Figure 3.36. The different lines indicate system performance at various points as heat is generated by the WH/DH unit (HP), transferred to the storage tank, and leaves the storage tank to be used in the house. The blue line shows the COP of the HP only, which does not account for backup resistance heat use and losses associated with the interconnecting lines and storage tank. These COPs range from a low of 2.3 in January to a high of 3.1 in August. As mentioned earlier, there were no HW draws for 20 days in January. Without the flow of cold makeup water into the tank, the EWTs seen by the WH/DH will be at least as high as the lower thermostat “make” temperature of approximately 112°F (44.4°C). The higher EWTs seen by the WH/DH when recovering from standby losses compared with recovering from HW use resulted in lower-than-average COPs for January.

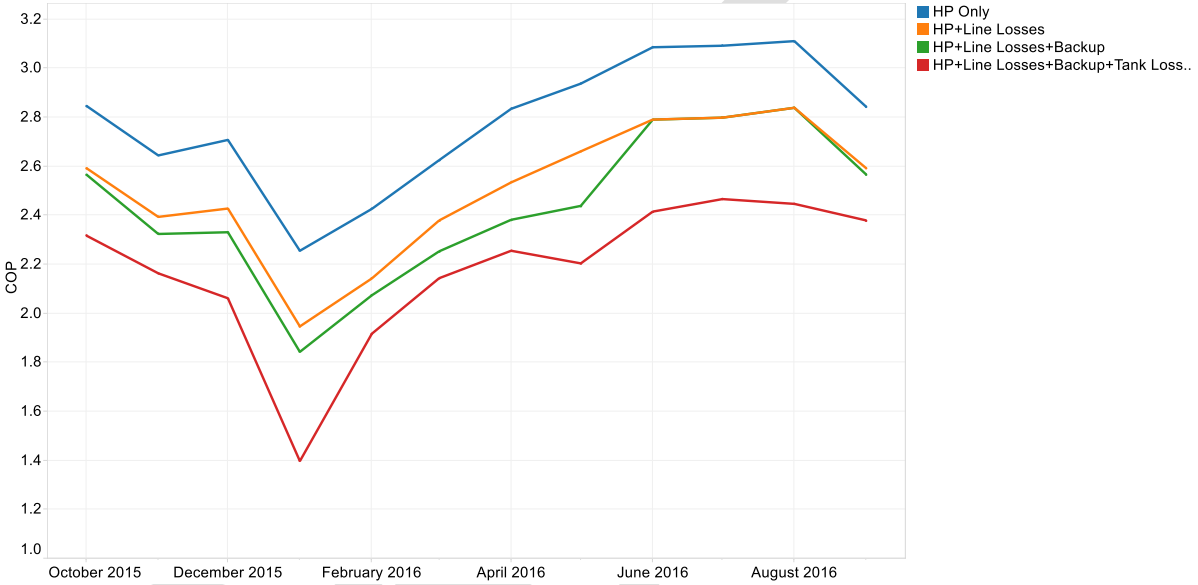

Figure 3.31. Monthly average WH mode COPs of the WH/DH HP with and without backup resistance heat use and heat losses from the storage tank and water lines connecting the WH/DH to the storage tank [36].

The orange line in Figure 3.36 shows the COP of the WH/DH when accounting for heat loss in the water lines that connect the WH/DH to the storage tank. Immersion temperature sensors located on both ends of the interconnecting water lines allowed the heat loss to be measured. Despite the water lines being insulated, the measured heat loss from these lines averaged 9.8% of the heat provided by the WH/DH HP. Examining a 1-week snapshot of data indicated that, on average, the water lines lost 76% of their heat relative to the garage temperature between WH cycles. The copper water lines were 35.8 ft (10.9 m) long and0.75 in. (1.9 cm) diameter. Over the test year there were 2007 WH cycles. The heat loss from the water in the lines during periods when the WH/DH was off is estimated to be 738 kBtu (216 kWh) or 6.2% of the WH delivered by the WH/DH. Using the average garage temperature, average water temperature in the lines, and insulation thickness, the heat loss from the lines when the WH/DH was operating in WH mode was calculated to be 453 kBtu (133 kWh) or 3.8% of the WH provided by the WH/DH. Combining the calculated off-cycle and WH cycle line losses yields a calculated value of 10.0% heat loss, which agrees well with the measured line losses of 9.8%.

The green line in Figure 3.36 shows the system COP when including backup resistance heat use but excluding tank losses. After filtering the data for periods when the WH/DH was shut

down for sensor maintenance or other issues, the backup resistance energy use for the yearlong period was just 60.2 kWh or 5.4% of the total energy used for WH.

Finally, the red line in Figure 3.36 shows the COP of the entire system. This was calculated by dividing the measured WH energy being delivered to the house at the outlet of the storage tank by the total energy use of the WH/DH and backup resistance elements. Based on the measured data, the tank losses are 9.9% of the WH energy delivered to the tank (omitting data from 20 days in January of no HW use). This value aligns with the performance expectations of a typical electric storage WH tank having a rated EF of 0.9, which is the minimum allowable EF for electric storage WHs manufactured before April 2015 in the United States.

The annual WH mode COPs for the WH/DH were 2.75, 2.48, 2.39, and 2.19 for the HP only, HP with line losses, HP with line losses and backup resistance use, and entire WH/DH system, including tank/line losses and backup resistance heat use, respectively. To achieve the highest overall system WH efficiencies, it is important to limit the length and diameter of the water lines connecting the WH/DH to the storage tank as much as possible, insulate these lines, and use a well-insulated storage tank.

AS-IHP System SC Performance

The monthly and seasonal SC performance of the ASHP and the effect of the WH/DH operation on SC are summarized in Table 3.15. The average monthly cooling COPs of the ASHP were between 4.32 and 5.59 with a seasonal average of 4.44. The WH mode of the WH/DH provides SC as a by-product of its operation. The DH mode also generates sensible heating in addition to latent cooling with a net SH effect, as indicated by negative values in the table. The “free cooling” effect that the WH operation has on the overall AS-IHP system (i.e., ASHP and WH/DH combined) SC efficiency results in monthly cooling COPs for the system between 4.46 and 10.84. The very high system COPs during April and October indicate a larger ratio of “free cooling” from the WH/DH to cooling supplied by the ASHP. However, much of the SC delivered by the WH/DH in these months was likely not satisfying a real demand for SC, and the house was being overcooled. Therefore, the WH/DH cooling effect for these 2 months was not included in the seasonal average SC COP for the system. With this consideration, the system’s seasonal average SC COP was 4.72, which was 6.3% higher than the COP of the ASHP alone. For the cooling season, this 6.3% efficiency increase results in estimated SC energy savings due to the operation of the WH/DH of 122 kWh.

Table 3.15. SC data for the ASHP and AS-IHP system, including the cooling and heating byproducts of the WH/DH [36].

Month	April 2016	May 2016	June 2016	July 2016	Aug. 2016	Sept. 2016	Oct. 2016	Totals
System SC delivered (kWh)	191	674	1,819	2,317	2,304	1,812	271	9,189[a]
ASHP	122	526	1,697	2,242	2,233	1,680	141	8,641
WH/DH mode	-4[b]	-30	-23	-56	-50	-5	-23[b]	191
WH/DH WH mode	73[b]	178	144	132	121	137	153[b]	938
ASHP SC energy use (kWh)	22	99	385	517	517	383	25	1948
ASHP average COP	5.57	5.34	4.41	4.34	4.32	4.39	5.59	4.44
System average COP	8.68	6.84	4.72	4.48	4.46	4.77	10.84	4.72[a]
Average OD temperature (°C)	15.7	18.9	25.1	26.4	26.3	23.7	15.1	21.6
While ASHP cooling	25.0	25.3	28.1	28.4	28.0	26.9	23.4	27.6
ASHP run hours	22.5	95.0	300.5	400.3	409.7	329.3	31.4	1,588.7

[a]Total system SC delivered and average system COP do not include WH/DH cooling/heating effects for April and October because the cooling demand was very low for these months; therefore, the WH/DH operation likely did not significantly affect the cooling load experienced by the ASHP.
[b]Only includes days of the month when the ASHP was in the cooling mode.

AS-IHP System SH Performance

The monthly and seasonal SH performance of the ASHP and the effects of the WH/DH operation on SH are summarized in Table 3.16. As noted, when the WH/DH operates in WH mode, it provides SC as a by-product. However, for the heating season, the latent cooling provides no energy benefit or penalty, so the data shows only the sensible cooling. Similarly, for the limited run time in the DH mode, Table 3.16 only accounts for the sensible heating. The monthly SH COPs for the ASHP only are 2.00–3.43. The lowest COPs correspond to months with high backup resistance heat use. For January 2016, backup resistance heat use accounted for approximately one third of the total SH energy use. The average ASHP SH COP during the evaluation period was 2.38. When the cooling and heating by-products of the WH and DH modes of the system are accounted for, the overall AS-IHP system SH COP is reduced to 2.23—a 6.3% reduction. For the heating season, this 6.3% reduction in overall efficiency results in an estimated SH penalty due to operation of the WH/DH of 330 kWh.

Table 3.16. SH data for the ASHP and AS-IHP system, including the cooling and heating byproducts of the WH/DH [37].

Month	Oct. 2015	Nov. 2015	Dec. 2015	Jan. 2016	Feb. 2016	March 2016	April 2016	Totals
Total sensible heating delivered (kWh)	172	1,344	1,687	4,029	2,723	1,192	384	11,651[a]
ASHP	171	1,431	1,764	4,158	2,974	1,408	505	12,411
WH/DH mode	43[b]	77	77	0	0	1	1[b]	199
WH/DH WH mode	-42[b]	-164	-154	-129	-251	-216	-122[b]	-1078
SH energy use (kWh)								
Total	50	502	677	2,076	1,289	478	153	5,225
Backup	0	0	120	684	299	32	1	1,136
Defrost	0	0	19	54	24	8	0	105
Average ASHP COP	3.43	2.85	2.61	2.00	2.31	2.94	3.29	2.38
Average system COP	3.44	2.68	2.49	1.94	2.11	2.49	2.51	2.23[a]
Average OD Temp (°C)	15.1	11.5	10.6	1.5	5.4	12.5	15.7	10.3
While ASHP heating	10.2	5.9	5.3	0.2	2.1	5.8	7.6	3.3
Run hours	27.0	260.2	289.2	592.0	449.0	241.3	87.9	1,946.6
Defrost hours	0.0	0.0	4.0	10.7	5.1	2.1	0.2	22.1

[a]Total system SH delivered and average system COP do not include WH/DH cooling/heating effects for April and October because the heating demand was very low for these months; therefore, the WH/DH operation likely did not significantly affect the heating load experienced by the ASHP.
[b]Only includes days of the month when the ASHP was in the heating mode.

The SC and SH average measured seasonal efficiencies (COP or SEER in Btu/Wh) for the ASHP unit deviated significantly from AHRI 210/240 (AHRI 2008) rated values, as seen in Table 3.17. The AHRI estimates were computed using the minimum and maximum house load line or design heating requirement (DHRmin and DHRmax) assumptions and for the actual measured test house load lines during the 2015–2016 field-test period. Figure 3.32 compares these heating and cooling loads with the AHRI 210/240 heating and cooling load lines based on the rated heating capacity Q(47) at 8.3°C ambient and the rated cooling capacity Q(95) at 35°C.

Table 3.17. Site-measured seasonal SH and SC COPs vs. estimated AHRI 210/240 ratings for ASHP unit used in AS-IHP system.

Mode	Site-measured SCOPs	AHRI 210/240 ratings	% deviation, field vs. rated
SH $SCOP_h$	2.38	Region IV HSPF: For DHRmin load: 2.93[a] For DHRmax load: 2.22 For house loads: 2.34	 −18.8 +7.0 +1.8
SC $SCOP_c$	4.44	SEER: For default load and Cd: 6.30 For house loads: 6.90	 −29.5 −35.7

[a]From AHRI (2016) [21].

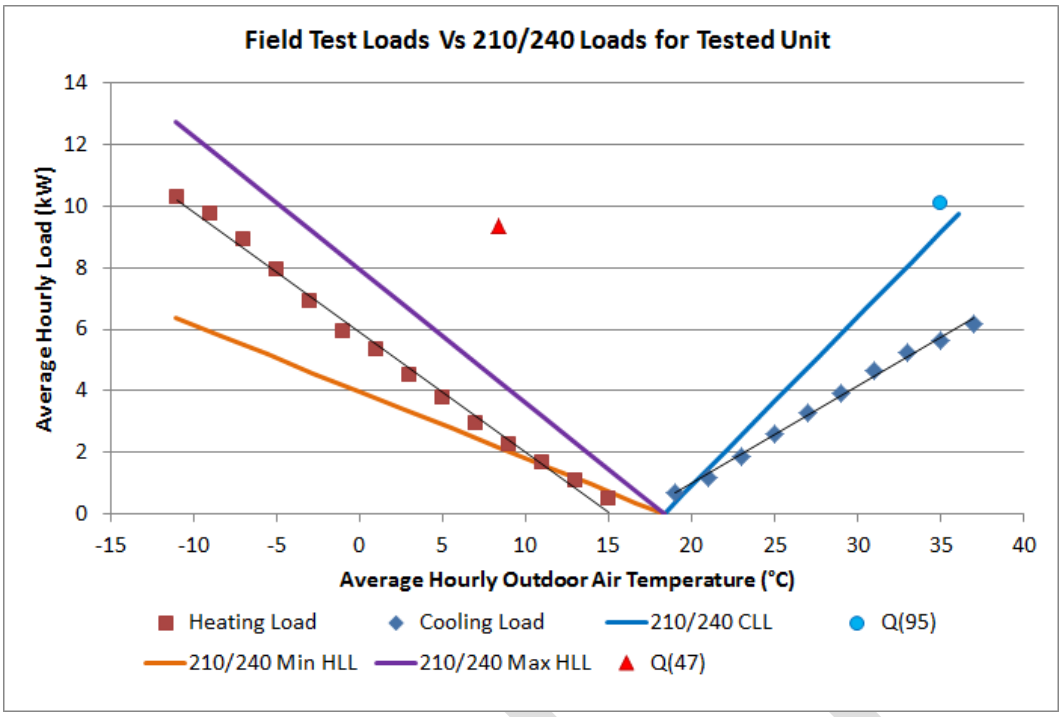

Figure 3.32. Field-test house 2015–2016 heating and cooling load lines vs. AHRI 210/240 load lines (maximum and minimum).

The ASHP of the AS-IHP field-test prototype might show these deviations compared with its rating values for several reasons.

- Blower energy use is higher at the field site due to higher duct system ESP than those assumed for the rating calculations. This is somewhat peculiar to the zoned distribution system used at the test house and to other changes made in the ducting system to accommodate the AS-IHP. However, residential duct systems generally have higher ESPs than the ~37 Pa (0.15 in. water gauge) implicitly assumed in AHRI 210/240.

- The control algorithm used by the zone controller caused the ASHP to operate at higher speeds than the space loads would warrant during times when both zones simultaneously called for SC or SH [37]. This reduced the energy savings that could have accrued from lower speed operation during mild weather periods in SH and SC seasons. (The effect was greater in the SC season.) Additionally, the data indicate that the compressor speed was allowed to vary even though the supply airflow was dictated by the zone(s) calling for conditioning. This results in the system running at suboptimal combinations of compressor speed and airflow, which also reduces efficiency.

- The $SCOP_{hS}$ procedure does not account for defrost tempering heat usage. This accounted for ~2% of the total field system SH energy use during the test year.

- The indoor temperature during the heating season averaged 21.9°C, whereas the $SCOP_{hS}$ calculation procedure assumes 21.1°C.

- The indoor dry bulb temperature during the cooling season averaged 24.4°C, whereas the $SCOP_{cS}$ procedure assumes 26.7°C.

- The standard minimum house-heating load line used in the $SCOP_{hS}$ procedure has a lower slope than that experienced at the test house (Figure 3.32). This results in a lower design-heating load than that experienced by the test house. This is primarily why ~22% of the

total SH seasonal energy use for the field-test system was from backup resistance heat (Table 3.16) even though the 2015–2016 SH heating season in Knoxville was warmer than average, having ~18% fewer heating degree days based on the local airport weather station (Table 3.18).

- The test year cooling season in Knoxville was significantly warmer than average, having ~39% more cooling degree days as measured at the local airport weather station (Table 3.19). This resulted in many more hours of high-speed operation during SC than is normally expected, adding to the impacts from the zoned duct system.

Table 3.18 compares average heating and cooling degree days for Knoxville with those experienced during the 2011–2012 and 2015–2016 test years.

Table 3.18. Average vs. 2015–2016 test site heating and cooling degree days.

Location	**Annual °F days heating** (18.3°C base)	**Annual °F days cooling** (18.3°C base)
Knoxville		
Average[a]	1,997	841
2011–2012[b]	1,553	958
2015–2016[b]	1,642	1,170
2015–2016[c]	1,864	1,070

[a]1986–2010 averages from ASHRAE [33].
[b]Test year actual values from National Oceanic and Atmospheric Administration [34] and [38] for McGhee Tyson Airport weather station.
[c]For test year October 2015–September 2016; site-measured actual.

Estimated AS-IHP Savings vs. Baseline

The annual energy use of a baseline system (3.8 $SCOP_c$ and 2.26 $SCOP_h$ [Region IV] SS ASHP and electric WH) meeting the field-test site loads was estimated. The HSPF and SEER ratings for the baseline unit were adjusted downward by 27 and 40%, respectively, based on the average field-measured deviations from rated efficiencies experienced by SS ASHPs previously field tested in the Knoxville area [31]. The results for this comparison are shown in Table 3.19. Since the HW tank heat losses were unaccounted for in the AS-IHP field test, they were also omitted from the baseline equipment efficiency (e.g., baseline WH COP of 1.0). This comparison assumes that the baseline ASHP meets the same total DH load as the prototype AS-IHP system. The largest percentage of savings come from WH at 58% (1,593 kWh). The WH energy savings estimate includes the effect of the 20-day period in January when the HW load was zero, so this savings estimate is likely somewhat conservative. SC + DH are estimated at 1,812 kWh (45%), and SH energy savings are estimated at 1,836 kWh (26%). The estimated total annual savings for the AS-IHP vs. the estimated baseline energy use at the Knoxville field-test site are ~38%. Heavy reliance on backup electric elements for SH and defrost tempering coupled with higher indoor blower energy usage vs. manufacturer's data were likely the primary causes of the lower-than-expected AS-IHP field-test prototype system SH performance.

Table 3.19. AS-IHP system 2015–2016 energy savings vs. estimated baseline system performance at the test site (based on 13 SEER ASHP field tests in 2011–2012).

Mode		AS-IHP	Baseline system estimated performance[a]	Percent savings over baseline
SC + DH	Delivered (kWh)	9,189	9,189	
	Consumed (kWh)	2,201	4,013	45%
SH	Delivered (kWh)	11,651	11,651	
	Consumed (kWh)	5,225	7,061	26%
Water heating	COP	2.39	1	
	Delivered (kWh)	2739	2,739	
	Consumed (kWh)	1,146	2,739	58%
Total	**Consumed (kWh)**	**8,572**	**13,813**	**38%**

[a]Estimated per average measured performance of two 13 SEER ASHPs tested in the Knoxville area in 2011–2012 [32].

3.2.3 Gas Engine-Driven AS-IHP System Development Summary

Gas engine-driven heat pumps (GHP) can be an attractive economic choice in parts of the United States where typical engine fuels—such as natural gas, propane, or liquefied petroleum gas—can be less expensive than electricity. Compared with conventional fuel-fired furnace heating systems, GHPs are projected to reduce SH fuel consumption by 35% and water heating fuel consumption by 80%. GHPs can also significantly reduce summer cooling electric peak demand by over 80% compared with electric air-conditioning systems [39].

ORNL and its partners—Southwest Gas Corp (SWG), a gas utility company, and Intellichoice Energy, engineering consultancy company—have been collaborating to develop a multifunction (or IHP type) GHP for commercial and residential building applications. The system design was based on the needs of the SWG market located in the Southwestern United States (Figure 3.33). This area is a part of the US warm-dry climate zone (Figure 3.2) and is characterized by very long, very hot summers but also very cold winters in some areas due to elevation.

Figure 3.33. SWG utility service area.

Commercial Gas Engine-Driven AS-IHP Summary

Commercial system development was completed first, and NextAire Inc., a manufacturing partner, introduced a system to the US market in 2012 (Figure 3.34). Its design cooling capacity was ~39 kW (~11 tons) at 35°C outdoor temperature with a COP of 1.1; the design heating capacity was ~42 kW (~142,000 Btu/h) at 8.3°C with a COP of 1.5 [40]. The system also provides ~18 kW of water heating via engine heat recovery at maximum engine speed (2,400 rpm).

Figure 3.34. Commercial gas engine AS-IHP installed on the roof at the field demonstration site.

Most of the material in this section is summarized from the final report on a field demonstration project conducted during 2014–2015 in Las Vegas, Nevada [Vineyard, et al]. A commercial building with approximately 4,150 m^2 that consisted of retail space, offices, kitchen space, and warehouse storage hosted the demonstration (Figure 3.35). Approximately 325 m^2 of space was conditioned by the GHP-RTU. The remainder of the building was conditioned by conventional electric RTUs. The space conditioned by the GHP-RTU included a training room, two machine rooms, and warehouse storage.

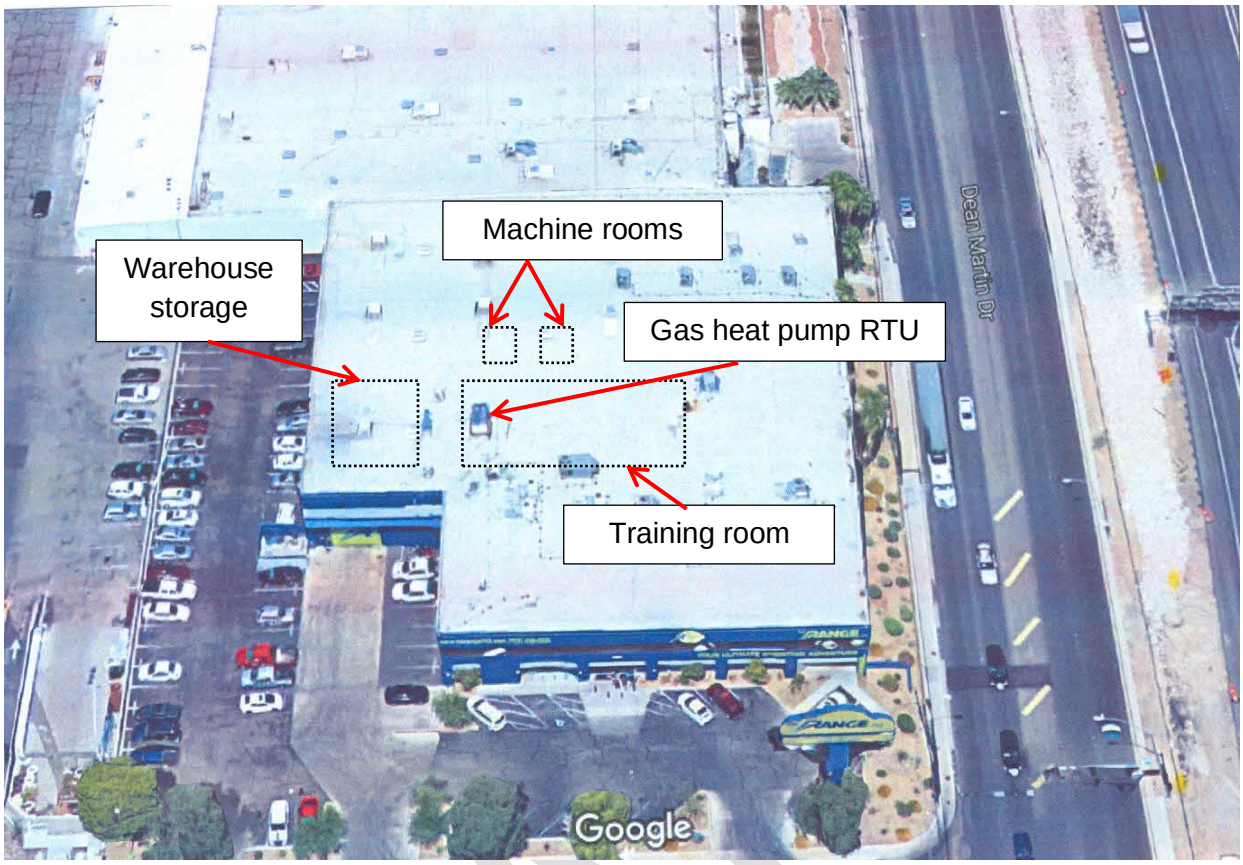

Figure 3.35. Aerial view of the demonstration site. (Source: Google Maps)

The energy cost savings and a payback analysis are summarized in Table 3.20. Equipment costs for the base electric RTU HP were obtained from the manufacturer. The gas AS-IHP RTU cost was obtained from the manufacturer and is based on a cost for selling a quantity of 1,000 units per year. The installation cost for the gas AS-IHP was $3,000 higher than that of the base electric RTU due to the cost of reinforcing the roof to support the additional weight of the gas unit. The total cost difference between the gas AS-IHP and the baseline system is $6,000, giving a payback for the gas AS-IHP ranging from 3.5 to 3.7 years, depending on the type of WH used in the base system.

Table 3.20. Commercial gas engine AS-IHP energy cost savings and payback vs. baseline electric RTU with electric and gas WHs.

	Equipment cost ($)	**Installed cost ($)**	**Total cost (S)**	**Cost difference ($)**	**Energy cost savings ($)**	**Payback (years)**
Conventional RTU	10,000	6,250	16,250			
Gas AS-IHP vs. base RTU with gas WH	13,000	9,250	22,250	6,000	1,619	**3.7**
Gas AS-IHP vs. base RTU with electric WH	13,000	9,250	22,250	6,000	1,706	**3.5**

Residential Gas Engine-Driven AS-IHP Development Summary

A prototype residential scale version of a GHP was developed and lab and field tested. Full details of the residential system development are found in Momen et al. [41], and a summary can be found in the HPT Annex 40 final report [16]. Lab test results confirmed a cooling capacity of ~17 kW at 35°C outdoor temperature with a COP of 1.1; a heating capacity of ~20 kW at 8.3°C with a COP of 1.5; and a water heating capacity of ~9 kW of water heating via engine heat recovery. Eight prototype systems were field tested in the Las Vegas area. The energy cost savings results vs. an electric baseline system are summarized in Table 3.21. Figure 3.36 provides a photograph of the prototype design final configuration.

Table 3.21. Prototype demonstrated energy costs vs. baseline system at Las Vegas test sites

Site #	Baseline energy costs ($)	Gas AS-IHP prototype energy costs ($)	Savings (%)
1	3,083	2,877	6.7
2	3,061	2,660	13.1
3	2,356	2,068	12.2
4	1,569	1,442	8.0
5	3,163	2,760	12.7
6	3,237	2,819	12.9
7	3,379	2,798	17.2
8	3,680	3,375	8.3

Figure 3.36. Final version of the prototype residential gas engine AS-IHP.

The prototype design was optimized to have the smallest possible footprint, the lowest possible electric consumption, and the best possible efficiency. Unfortunately, its production cost was estimated to be about $15,000 [41]. SWG estimates that a unit cost target should be $8,000 for the gas HP to penetrate the market.

This cost is too high for the system to be commercially viable. Therefore, ORNL and its partners undertook a project under a DOE technology commercialization fund (TCF) support [42] to reduce the manufacturing cost and improve the residential gas AS-IHPs commercial viability. To achieve this goal, the following objectives were identified:

- Identify and implement a different engine that meets the capacity, efficiency, and reliability targets
- Value engineer the unit to reduce the cost of the components and manufacturing
- Complete a commercialization study to identify entry points to the market

To date, the results of this project indicate that a cost reduction of at least 43.5% is achievable (Figure 3.37). Although this is positive, the unit cost remains too high to penetrate the bulk of the US residential market. However, it is at a level that early adopters (e.g., homeowners and home builders focused on sustainability and maximum energy efficiency) might be willing to install systems.

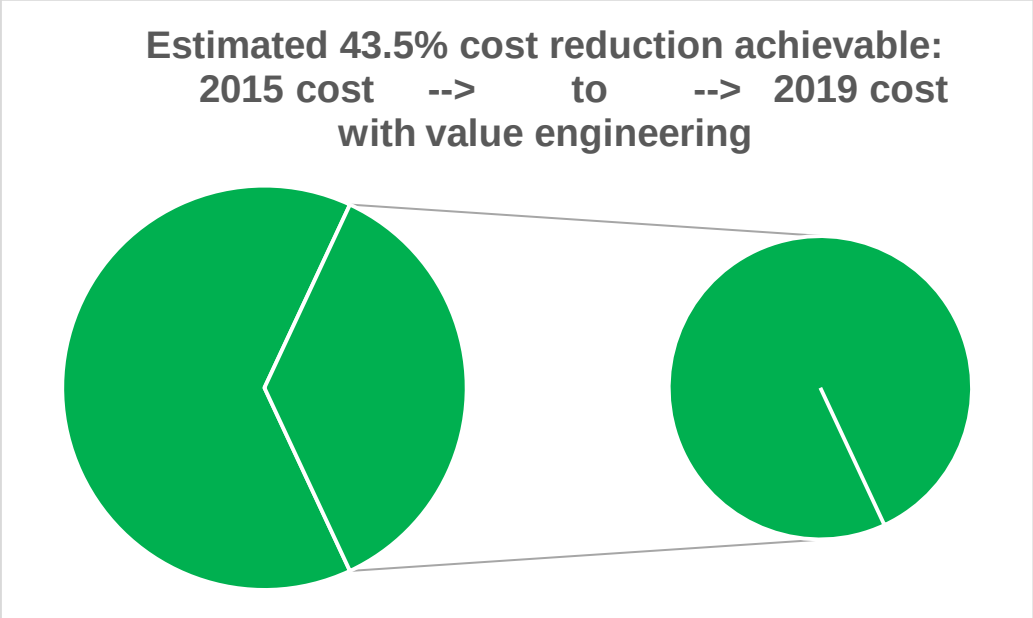

Figure 3.37. The TCF project shows potential to reduce the cost of prototype residential gas engine AS-IHP by ~43.5%.

An in-depth market study was conducted as part of the TCF project. One principle recommendation from the study is to add additional high-value features or amenities to the system where feasible. One such feature could be to enable the system to include electric generation capability to allow the system to continue operation during loss of electric grid events and possibly run some essential electric appliances as a side benefit. Some investigation into this possibility was already undertaken [41]. One possible implementation approach during grid outage situations is to increase the engine speed to maximum and engage a 5 kW AC generator component. The generator would produce approximately 1.6 kW AC power for fans and other electricity needs of the HP system, along with ~1–2 kW of additional electric power for emergency external needs, such as lighting and refrigerators. With an average electricity demand of 2–3 kW (40–60% of rated output), the 5-kW generator efficiency is high (~70%).

Cost reduction and value-added efforts are ongoing.

4 Test Facility for nZEB Technologies

4.1 Background: NZERTF, Gaithersburg, Maryland

The residential-style net-zero home on the NIST main campus offers a unique test bed for residential air-conditioning technologies. Several air-conditioning systems can be installed in the home in parallel so that the selected system can be operated at nearly the same weather conditions and load profile. With this in mind, a small duct high-velocity (SDHV) HP was installed in parallel with a conventionally ducted air-source HP to answer the following question: Can an SDHV HP system whose ductwork is much easier to install than a conventional duct system provide comparable energy-use efficiency? The two systems were installed side by side in the house with one system operating for a week and the other system operating for a week in an alternating fashion for a whole cooling and heating season. The main parameters that could answer the question were measured on both systems—namely, electrical energy use and cooling/heating thermal energy. Human comfort performance of the two systems is described in a complementary publication by Kim et al. [43].

A more complete description of the net-zero home is found in Fanney et al. [44]. The net-zero house (Figure 4.1) includes a detached two-car garage. It is a two-story, three- to four-bedroom house with three full bathrooms and is separated from the garage by a breezeway. The first floor includes a utility closet for the clothes washer and dryer and a future multisplit HP indoor unit, a kitchen and dining area, a family room, an office (optional bedroom), a full bathroom, and a foyer open to the second floor. The second floor comprises a master bedroom with an adjoining bathroom, two additional bedrooms, a second bathroom, and a hallway. The house includes a full 135 m^2 (1,435 ft^2) basement. The detached garage contains the data acquisition/control equipment associated with the facility. The front of the house faces true south and accommodates two solar systems: a 10.2 kW photovoltaic system located on the main roof and four 2.2 m^2 (24 ft^2) solar thermal collectors on the roof of the front porch.

(a)

(b)

Figure 4.38. NZERTF: (a) left front at ground level and (b) right front elevated view.

Because of the home's air tightness, it is mechanically ventilated according to ASHRAE Standard 62.2 [45]. NZERTF uses a heat recovery ventilator to provide outdoor air to all bedrooms. The ventilator operates to deliver 136 m^3h^{-1} (80 cfm) for 45 minutes of every hour. This system operates independently of the HVAC systems and has a separate duct system.

Many investigations have been performed to examine the performance of various HVAC systems in low-load homes. The largest body of work has been performed by the national laboratories funded by DOE's Building America Program [46].

Poerschke and Rudd [47] studied the efficacy of using small duct airflow distribution systems in several different home-run configurations. Their goal was to optimize air distribution and minimize temperature differences in the test homes. They showed that this could be done with their central manifold systems while maintaining air-distribution energy efficiencies between 0.16 and 0.22 W cfm^{-1}. They attempted to design air-distribution manifolds and small duct (i.e., PVC pipe) combinations that allowed for better balance when changes were made to a run. This work could provide good data for a training dataset in many multifactor optimization algorithms.

Duct design methods should change to reflect the operating regimes of multispeed and variable-speed equipment. The ducting should be designed to optimize the lifetime performance of the system, meaning the ducting should give the best performance for the most likely static pressures (i.e., airflow rates) that will occur. Duct design tools should incorporate more detailed load information along with weather data files and operational models to produce a ducting system optimized for the lowest lifetime air-moving cost to the consumer. This is a complicated, multi-objective optimization problem that has been examined by many

researchers, such as Besant and Asiedu [48], Tsal et al. [49], Caldas and Norford [50], and Jorens et al. [51]. Residential duct designers need a product that can be used by nonexpert practitioners to design residential duct systems for the lowest lifetime cost.

Martin et al. [52] performed testing on the same SDHV system as was installed in NZERTF. They examined the energy use and dehumidification performance of the SDHV in a hot-humid climate (zone 2a). Their design-cooling load was only 13% greater than that of NZERTF. The 14 SEER, variable-speed, SDHV system used 8.2% less energy in the cooling season than a 13 SEER single-speed system and 16.7% more energy than a 22 SEER, variable-capacity system, but the SDHV system maintained lower humidity levels overall than the other systems.

4.2 Test Setup

4.2.1 Test House

The first and second floors have a combined living area of 252 m^2 (2,713 ft^2). Including the basement (actively conditioned) and attic (passively conditioned), the total floor space is 425 m^2 (4,578 ft^2). The building has a total conditioned volume of 1,268 m^3 (44,773 ft^3), which includes the attic and basement spaces. The window-to-wall area ratio for the first floor's north, south, east, and west sides are 0.167, 0.201, 0.143, and 0.048, respectively. In the same order, the second floor is 0.123, 0.285, 0.050, and 0.050. The outside perimeter length of the basement and first floor is 47.155 m (154 ft, 8.5 in.), and the second floor is 42.418 m (139 ft, 2 in.). The building envelope was constructed by using a continuous air-barrier system to minimize infiltration with building ventilation provided by a heat recovery ventilation system. Five blower door tests were conducted at various stages of construction, and the final test, conducted after the house was complete, yielded an air exchange rate of 802 m^3h^{-1} (1,200 cfm) at 50 Pa (0.2 in wg) corresponding to 0.63 air changes per hour. Details can be found in Fanney et al. [44]. A detailed TRNSYS model of the house was developed by Balke et al. [53].

The house is in DOE climate zone 4A. This climate zone is defined as mixed humid with IP units CDD 50°F ≤ 6,300 and 3,600 < HDD 65°F ≤ 5,400 and SI units CDD 10°C ≤ 3,500 and 2,000 < HDD 18°C ≤ 3,000 (Table 3.1). The house design cooling and heating thermal loads are 4,722 W (16,114 $Btuh^{-1}$) and 5,667 W (19,336 $Btuh^{-1}$). This is equivalent to 11.11 Wm^{-2} and 13.33 Wm^{-2} at design day cooling and heating temperatures of 32.8°C (91°F) and -8.9°C (16°F).

The HPs were controlled by wall-mounted thermostats that measured temperature in the living room and dining room area, as shown in Figure 4.2. These were the only thermostats used, so all operations were as if the house were a single zone. The cooling season setpoint temperature was 23.8°C (75°F), and the heating season setpoint was 21.1°C (70 F).

(a)

(b)

Figure 4.39. Thermostat locations: (a) wide view and (b) detailed view.

4.2.2 Air-Duct Systems for the HPs

NZERTF has four separate air-duct systems: (1) a conventional duct system used with air-to-air or ground-source HPs, (2) an SDHV air-distribution system used in conjunction with an air-to-air SDHV HP, (3) a dedicated duct system associated with the heat recovery ventilator, and (4) a short-run supply air-duct system on the first and second floors for two ceiling-mounted cassette-type mini air handlers used with multisplit, variable-speed, air-source HPs. All four duct systems are within conditioned spaces. Further discussions will focus on the conventional and high-velocity duct systems.

The conventional duct system was designed for less than a 124.5 Pa (0.5 in wg) static pressure drop at supply and return duct airflow rates of 2,039 m^3h^{-1} (1,200 cfm) with all air supplies fully open. The insulated main trunk lines are located with the air handler in the basement. Multiple supply registers are in each room of the house. Return ducts are in central locations on the first and second floors.

The SDHV air-distribution system begins in the basement with an insulated main trunk line that outlines the basement perimeter, allowing takeoffs for individual room air-supply registers that supply the first floor. A large, insulated, supply riser feeds a similar ring in the attic. The trunk lines are 22.9 cm (9 in.) in diameter and are designed for an airflow rate of 2,039 m^3h^{-1} (1,200 cfm). The takeoff ducts that supply the individual registers are 6.35 cm (2.5 in.) in diameter.

4.2.3 Tested HPs and Measurement Uncertainty

The rated cooling and heating performance of the two HP systems at AHRI Standard 210/240 [22] conditions is shown in Table 4.1. The calculated loads and duct layout were determined by the original architectural firm by using a computer program that used ACCA Manual J [54] and ACCA Manual D [55]. Oversizing the variable speed equipment allows the equipment to operate at partial load for most of its run time and thus operate at a higher efficiency. A thorough discussion of selecting variable speed equipment based on efficiency and the

implications for human comfort can be found in Cummings and Withers [56] and Shirey et al. [57].

Table 4.7. Rated performance of the two HP systems.

System	SEER (Btu [Wh]$^{-1}$)	EER cooling (Btu [Wh]$^{-1}$)	HSPF region IV (Btu [Wh]$^{-1}$)	Cooling capacity, W (Btu h^{-1})	Heating capacity, W (Btu h^{-1})
Conventional (two-stage)	15.80	13.05	9.05	7,620 (26,000)	7,796 (26,600)
SDHV (variable-speed)	14.00	7.45	8.35	8,558 (29,200)	10,317 (35,200)
Calculated LOADS				4,723 (16,114)	5,667 (19,336)

Both systems were fully instrumented and connected to data acquisition devices that monitored them continuously with 10 second scans during the off-period and 3 second scans during the on-period. The data were saved and aggregated for each testing day. Figure 4.3 shows the measured points for each system. Figure 4.4 shows the conventionally ducted HP (CDHP) system, and Figure 4.5 shows the SDHV system at the installed locations in NZERTF.

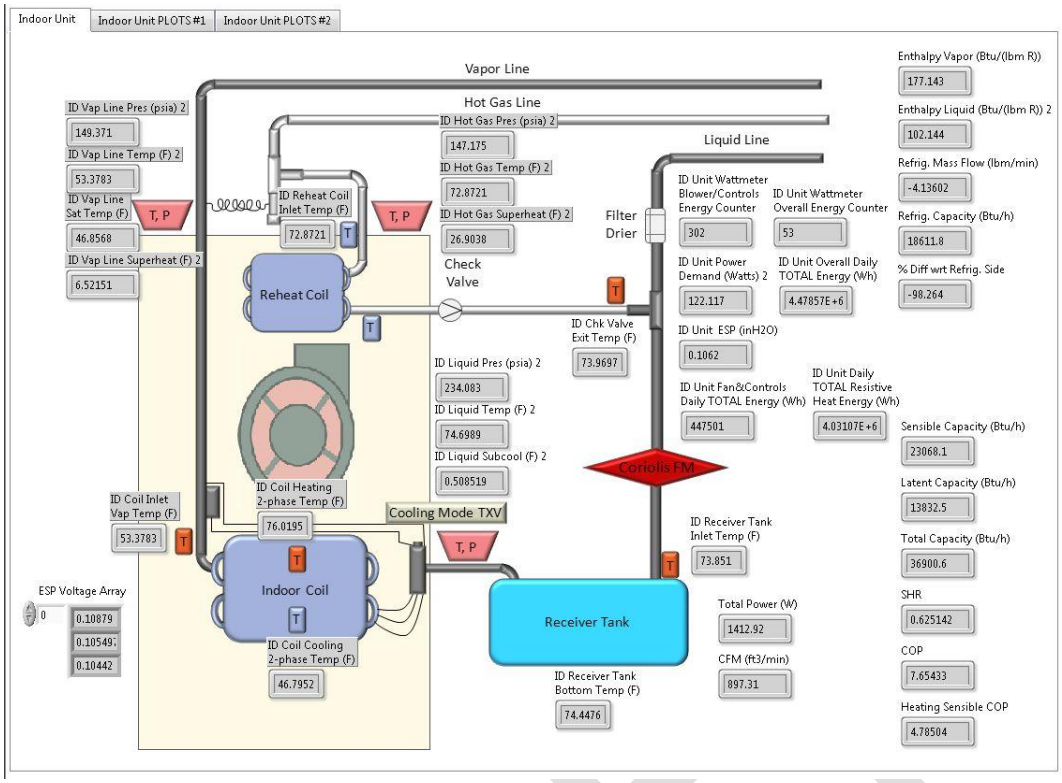
Indoor Unit
Indoor Unit PLOTS #1
Indoor Unit PLOTS #2
Vapor Line
Hot Gas Line
Liquid Line
ID Vap Line Pres (psia) 2
149.371
ID Vap Line Temp (F) 2
53.3783
ID Vap Line Sat Temp (F)
46.8568
ID Vap Line Superheat (F) 2
6.52151
T, P
ID Reheat Coil Inlet Temp (F)
72.8721
Reheat Coil
ID Hot Gas Pres (psia) 2
147.175
ID Hot Gas Temp (F) 2
72.8721
ID Hot Gas Superheat (F) 2
26.9038
Check Valve
Filter Drier
ID Unit Wattmeter Blower/Controls Energy Counter
302
ID Unit Wattmeter Overall Energy Counter
53
ID Unit Power Demand (Watts) 2
122.117
ID Unit Overall Daily TOTAL Energy (Wh)
4.47857E+6
ID Chk Valve Exit Temp (F)
73.9697
ID Unit ESP (inH2O)
0.1062
ID Liquid Pres (psia) 2
234.083
ID Liquid Temp (F) 2
74.6989
ID Liquid Subcool (F) 2
0.508519
ID Unit Fan&Controls Daily TOTAL Energy (Wh)
447501
ID Unit Daily TOTAL Resistive Heat Energy (Wh)
4.03107E+6
Coriolis FM
Enthalpy Vapor (Btu/(lbm R))
177.143
Enthalpy Liquid (Btu/(lbm R)) 2
102.144
Refrig. Mass Flow (lbm/min)
-4.13602
Refrig. Capacity (Btu/h)
18611.8
% Diff wrt Refrig. Side
-98.264
Sensible Capacity (Btu/h)
23068.1
Latent Capacity (Btu/h)
13832.5
Total Capacity (Btu/h)
36900.6
SHR
0.625142
COP
7.65433
Heating Sensible COP
4.78504
ID Coil Heating 2-phase Temp (F)
76.0195
ID Coil Inlet Vap Temp (F)
53.3783
Cooling Mode TXV
Indoor Coil
ID Coil Cooling 2-phase Temp (F)
46.7952
ESP Voltage Array
0.10879
0.10549
0.10442
ID Receiver Tank Inlet Temp (F)
73.851
Receiver Tank
Total Power (W)
1412.92
CFM (ft3/min)
897.31
ID Receiver Tank Bottom Temp (F)
74.4476

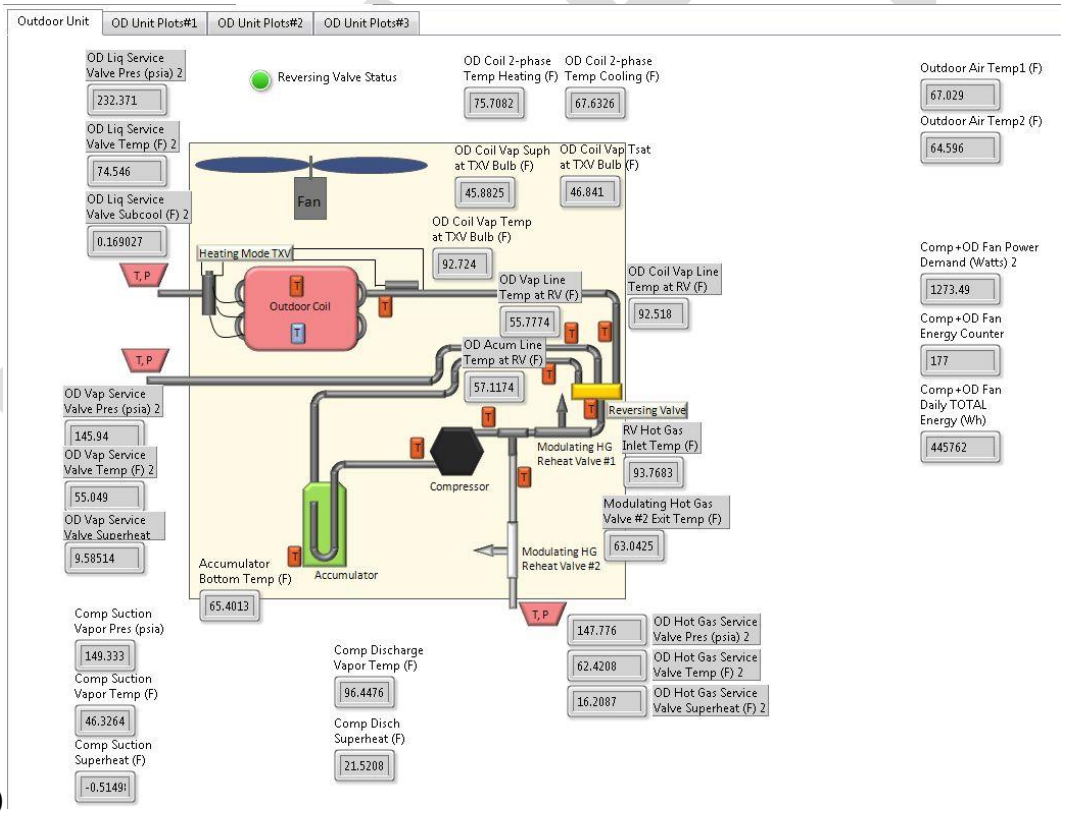
Outdoor Unit
OD Unit Plots#1
OD Unit Plots#2
OD Unit Plots#3
OD Liq Service Valve Pres (psia) 2
232.371
OD Liq Service Valve Temp (F) 2
74.546
OD Liq Service Valve Subcool (F) 2
0.169027
Reversing Valve Status
OD Coil 2-phase Temp Heating (F)
75.7082
OD Coil 2-phase Temp Cooling (F)
67.6326
Outdoor Air Temp1 (F)
67.029
Outdoor Air Temp2 (F)
64.596
Fan
OD Coil Vap Suph at TXV Bulb (F)
45.8825
OD Coil Vap Tsat at TXV Bulb (F)
46.841
OD Coil Vap Temp at TXV Bulb (F)
92.724
Heating Mode TXV
Outdoor Coil
OD Vap Line Temp at RV (F)
55.7774
OD Coil Vap Line Temp at RV (F)
92.518
Comp+OD Fan Power Demand (Watts) 2
1273.49
Comp+OD Fan Energy Counter
177
Comp+OD Fan Daily TOTAL Energy (Wh)
445762
OD Acum Line Temp at RV (F)
57.1174
Reversing Valve
RV Hot Gas Inlet Temp (F)
93.7683
OD Vap Service Valve Pres (psia) 2
145.94
OD Vap Service Valve Temp (F) 2
55.049
OD Vap Service Valve Superheat
9.58514
Modulating HG Reheat Valve #1
Compressor
Modulating Hot Gas Valve #2 Exit Temp (F)
63.0425
Modulating HG Reheat Valve #2
Accumulator Bottom Temp (F)
65.4013
Accumulator
Comp Suction Vapor Pres (psia)
149.333
Comp Suction Vapor Temp (F)
46.3264
Comp Suction Superheat (F)
-0.5149
Comp Discharge Vapor Temp (F)
96.4476
Comp Disch Superheat (F)
21.5208
147.776
62.4208
16.2087
OD Hot Gas Service Valve Pres (psia) 2
OD Hot Gas Service Valve Temp (F) 2
OD Hot Gas Service Valve Superheat (F) 2

(a)

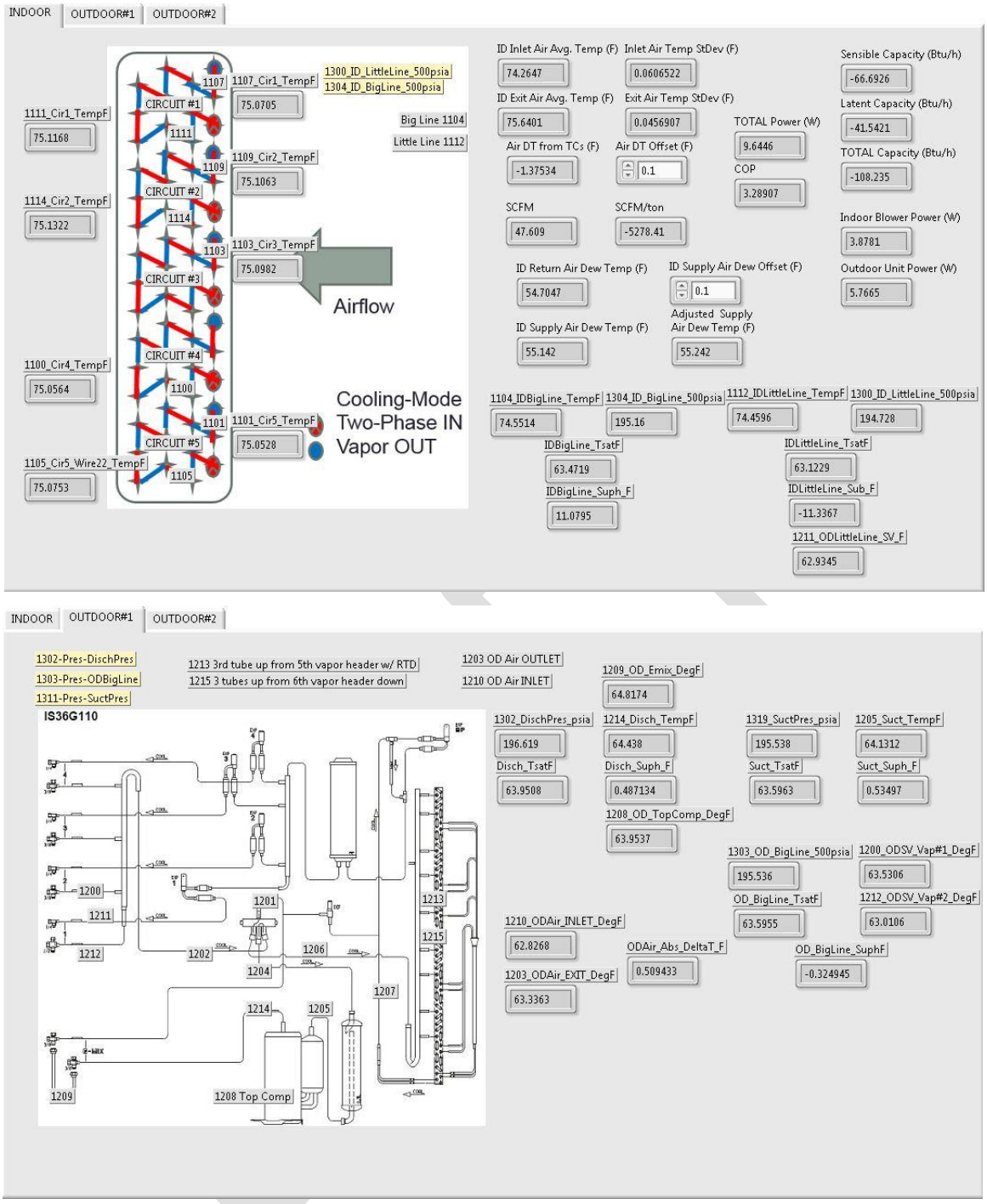

(b)

Figure 4.40. Measurement points for (a) two-stage CDHP and (b) SDHV, variable-speed HP.

(a)  (b) 

Figure 4.41. CDHP system indoor and outdoor units at NZERTF: (a) indoor air handler and (b) outdoor unit.

(a)  (b) 

Figure 4.42. SDHV system indoor and outdoor units at NZERTF: (a) indoor air handler and (b) outdoor unit.

Table 4.2 lists the measurement uncertainties for both systems at a 95% confidence level. A detailed uncertainty analysis was performed in Davis et al. [58]. The plus or minus uncertainties included with measured quantities are calculated as two standard deviations of multiple

measurements. The uncertainty of values calculated from a least squares fit is listed as twice the fit standard error (k = 2 coverage factor) unless stated otherwise.

Table 4.8. Measurement uncertainties.

Instrument	Range	Total uncertainty at a 95% confidence level
T-type thermocouples	-10–55°C (16–131°F)	±0.6°C (1.0°F)
High-pressure transducer	6,895 kPa (1,000 psig)	±0.25% of reading
Low-pressure transducer	3,447 kPa (500 psig)	±0.25% of reading
Air pressure differential (ESP[1])	0–187 Pa (0–0.75 in. H_2O)	±0.8% of reading
Indoor blower and controls power meter	0–300 VAC, 5 Amps, 1,000 W	±5 W
Indoor total power meter	0–300 VAC, 100 Amps, 20,000 W	±100 W
Outdoor unit power meter	0–300 VAC, 20 Amps, 4,000 W	±20 W
Supply air dewpoint temperature sensor	-28.8–49°C (-20–120 °F)	±1.0°C (1.8°F)
Coriolis refrigerant mass flow meter on CDHP	0–2,180 kg h^{-1} (0–80 lb min^{-1})	±0.15% of reading
Volumetric airflow rate	85–2,039 m^3h^{-1} (50–1,200 cfm)	5.5% of value
Sensible capacity	1,465–11,137 W (5,000–38,000 Btu h^{-1})	4–7%
Latent capacity	293–2,931 W (1,000–10,000 Btu h^{-1})	25–40%
Total capacity	2,931–11,137 W (10,000–38,000 Btu h^{-1})	7–10%
COP	0–6	8–12%

4.2.4 Results

The two systems operated side by side with one unit operating for 1 week followed by the other unit operating for 1 week. This weekly flip-flop, instead of a daily flip-flop, was necessary due to the large thermal inertia of the net-zero house. A net-zero house can go for weeks with no space conditioning given its low losses to the environment, so a weekly flip-flop was judged to be a better way to compare and remove the performance overlap of the two systems. CDDs and HDDs are used to normalize the results and provide a better comparison of the heating and cooling performance of the two systems. Even though the two systems operated side by side in a weekly alternating pattern, weather variability prevented the two systems from having an equal number of CDDs and HDDs.

4.2.4.1 Cooling Season

The cooling season weather conditions seen by the two systems are characterized in Figure 4.6 by using CDDs with respect to a base of 50°F (10°C). The conventionally ducted system experienced almost 31% more CDDs, even though the two systems were alternating operations weekly.

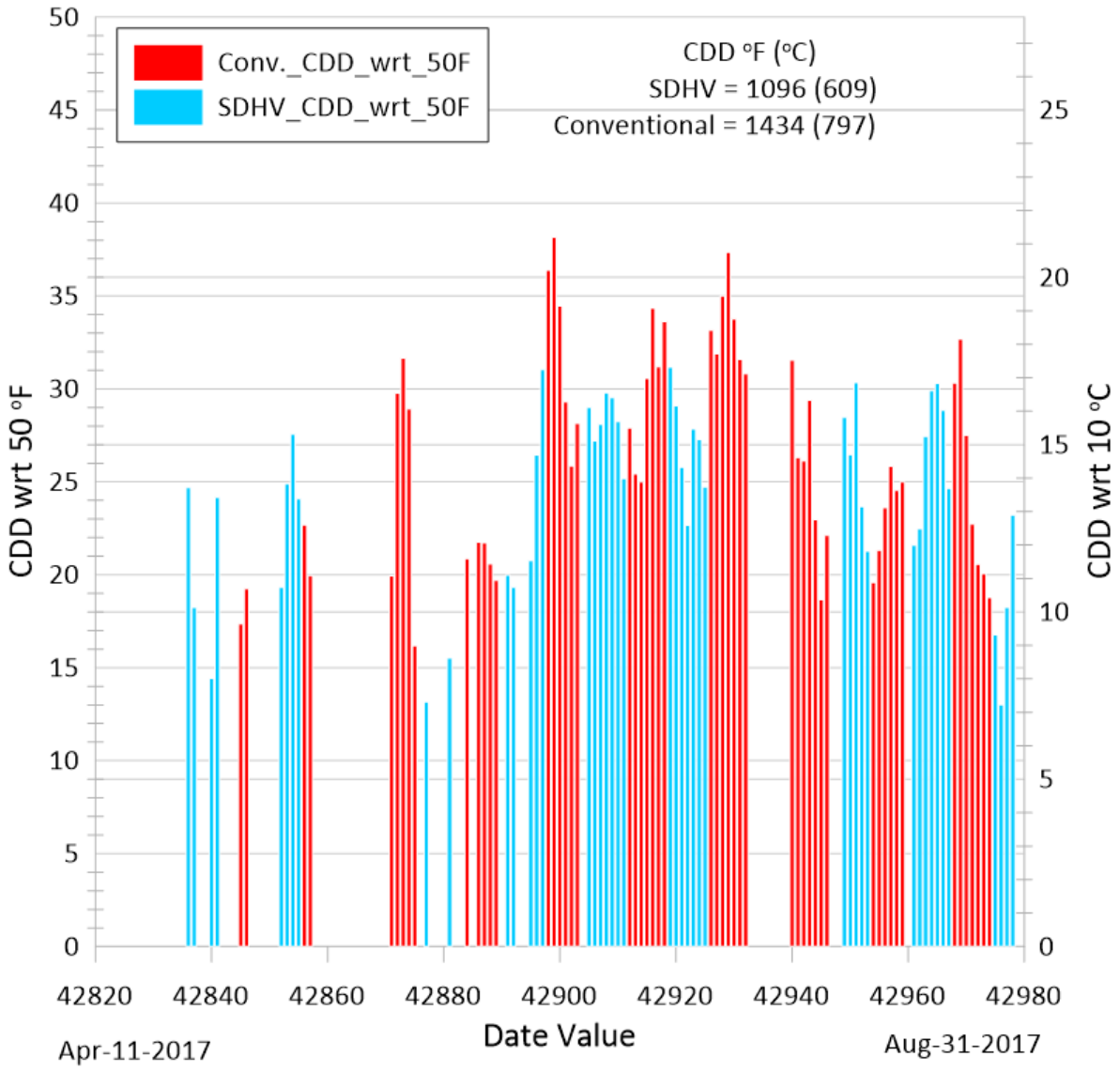

Figure 4.43. CDDs seen by both systems.

4.2.5 Cooling Energy

Figure 4.7 shows the average daily energy usage for the two systems along with the totals for the entire cooling season. Because of the higher number of CDDs seen by the conventional system, its energy usage was 38% greater. Figure 4.8 shows the daily total electrical energy usage with respect to the CDDs of the two systems. There is no statistical difference in their normalized average daily energy use for the cooling season at a 95% confidence level. The daily electrical energy usage per CDD for the CDHP and SDHV were (2.327 ± 0.209) kWh°C^{-1} ([1.293±0.116] kWh°F^{-1}) and (1.916 ± 0.302) kWh°C^{-1} ([1.069±0.168] kWh°F^{-1}), respectively. The difference in the cooling season electrical energy usage per CDD was statistically insignificant; on average, the SDHV system used (282 ± 1,126) Wh less electrical energy per CDD. The daily thermal energy removed per CDD for the CDHP and the SDHV were (1,738 ± 233) Wh°C^{-1} ([3,123 ± 420] Wh°F^{-1}) and (2,282 ± 359) Wh°C^{-1} ([4,107 ± 647] Wh°F^{-1}), respectively (Figure 4.9). The difference in the cooling season thermal energy removed per CDD was statistically insignificant.

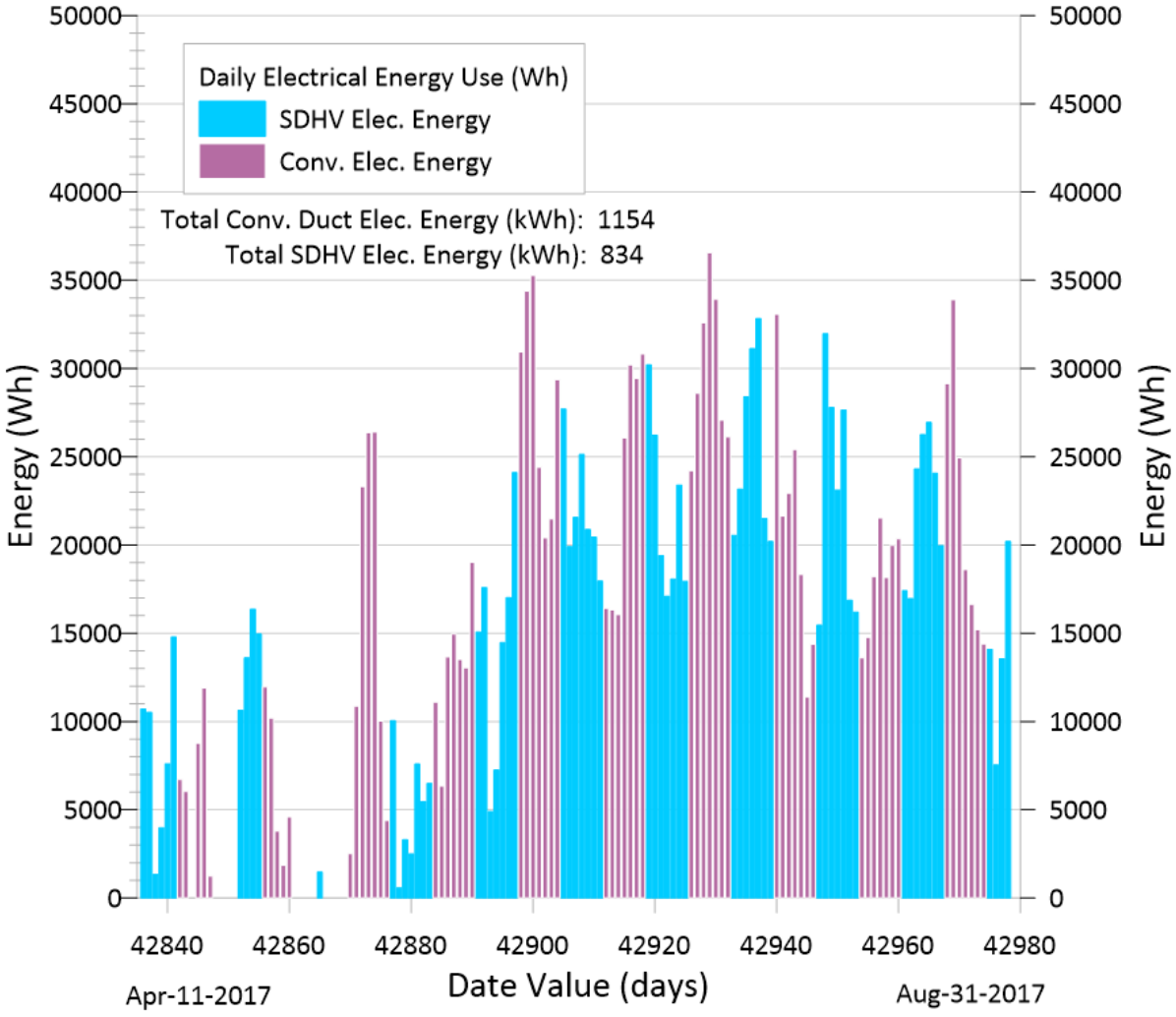

Figure 4.44. Cooling electrical energy use for the entire cooling season.

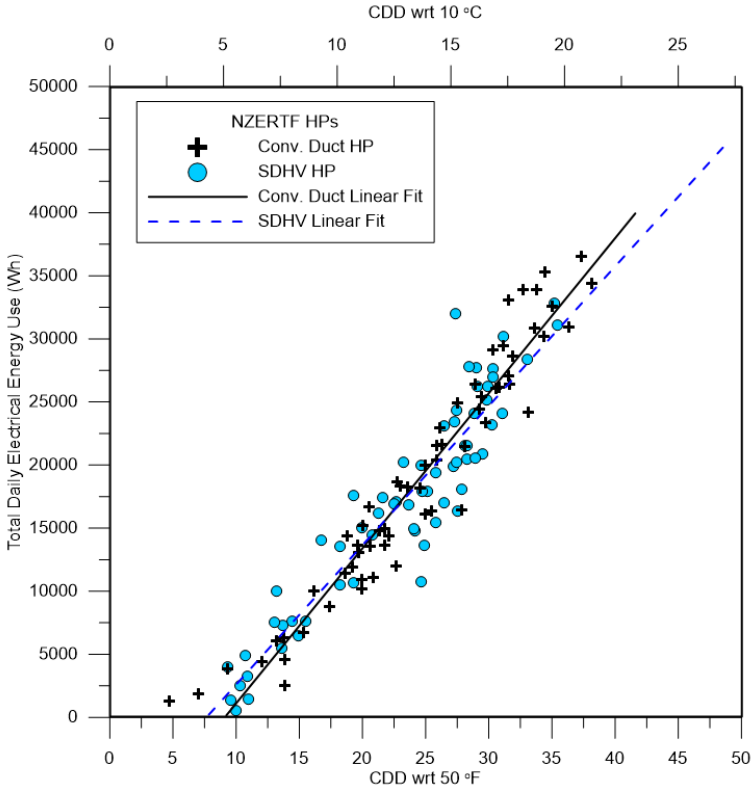

Figure 4.45. Cooling season electrical energy usage.

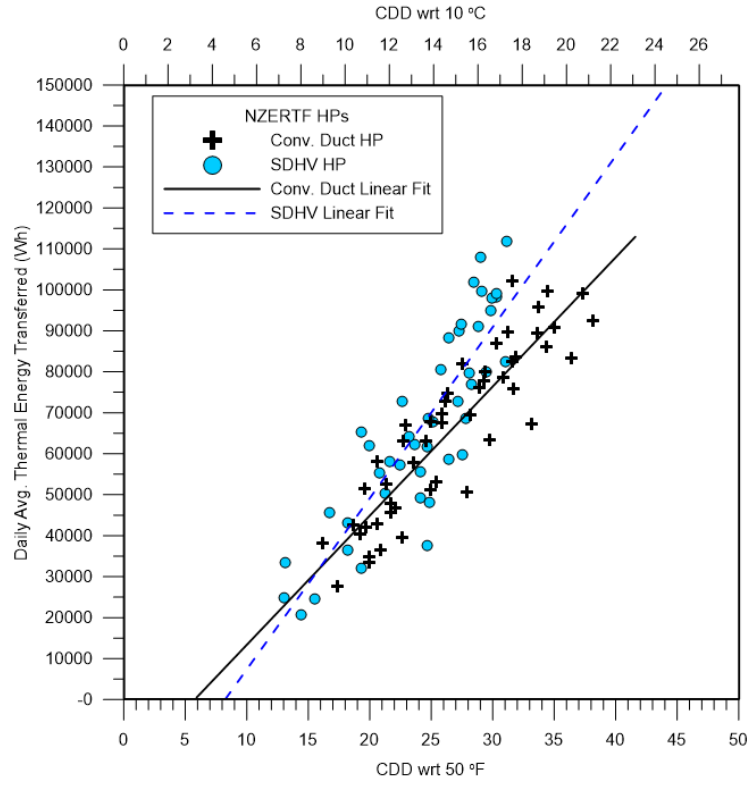

Figure 4.46. Cooling season thermal energy.

Figure 4.10 examines the daily average airflow rates of the two systems. The SDHV system operated at (177 ± 20) cfm lower daily average airflow rates. Figure 4.11 shows the fan efficacy of the two systems as a function of their daily percent run times. The SDHV system clearly

operates at a lower Watt-per-unit airflow rate due to its lower flow rate. Both systems used comparable electronically commutated motors (ECMs). Although the two systems usually operated at different airflow rates, they still circulated the same total volume of air in the house, as shown in Figure 4.12. This figure shows that the total number of house air changes as a function of CDD was statistically equivalent for the two systems. Although the SDHV system operated at lower total airflow rates, it operated for longer periods of time to produce equivalent total air changes. The operating times are shown more clearly in Figure 4.13.

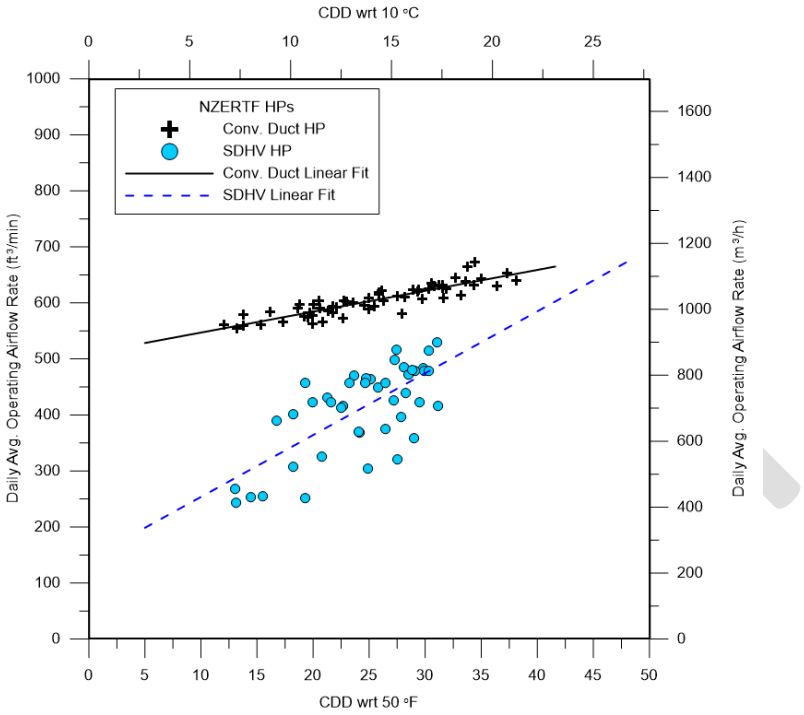

Figure 4.47. Cooling daily average operating airflow rates as a function of CDD.

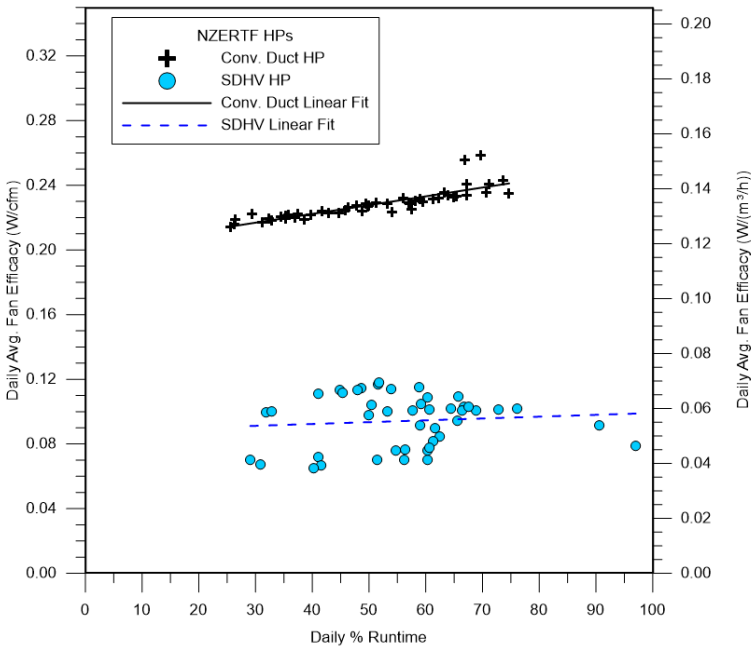

Figure 4.48. Cooling daily average indoor blower efficacy (W/[unit volume flow]).

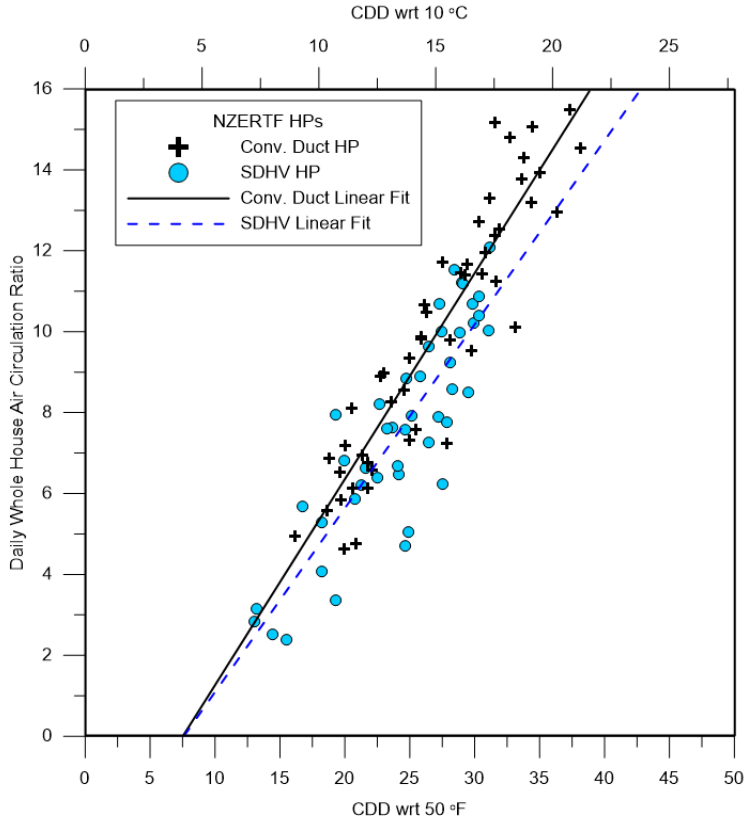

Figure 4.49. Daily cooling air circulation ratio (i.e., number of whole house air volume air changes through the air handler).

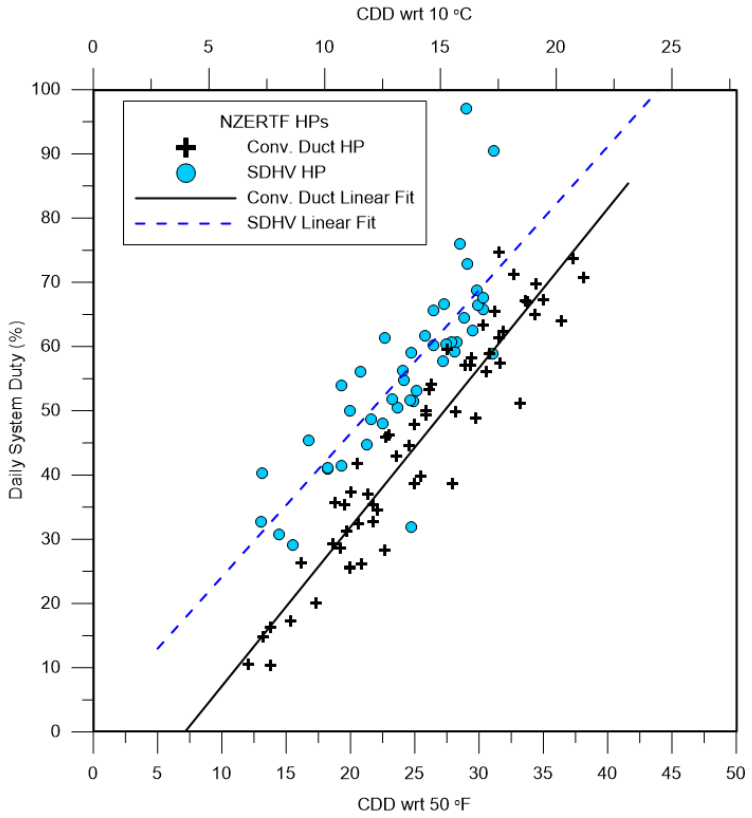

Figure 4.50. Cooling daily system percent duty.

Figure 4.45 showed that the two systems used the same average daily electrical energy per CDD; however, the SDHV system operated at a (4.0 ± 0.2)°C ([7.27 ± 0.44]°F) lower supply air temperature (Figure 4.14) than the CDHP and a 3.70 ± 0.22°C (6.66 ± 0.42°F) greater delta temperature (Figure 4.15) across the air handler than the CDHP. Figure 4.16 shows that the two systems had comparable average return air temperatures with the SDHV averaging slightly lower than the CDHP (-0.33 ± 0.10)°C ([-0.60 ± 0.18°F]).

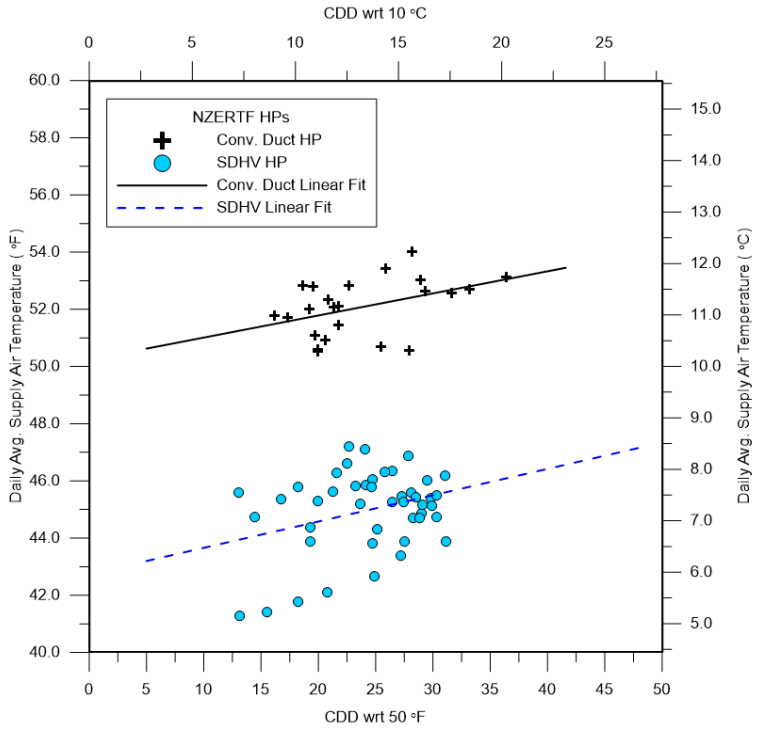

Figure 4.51. Cooling average operating supply air temperatures.

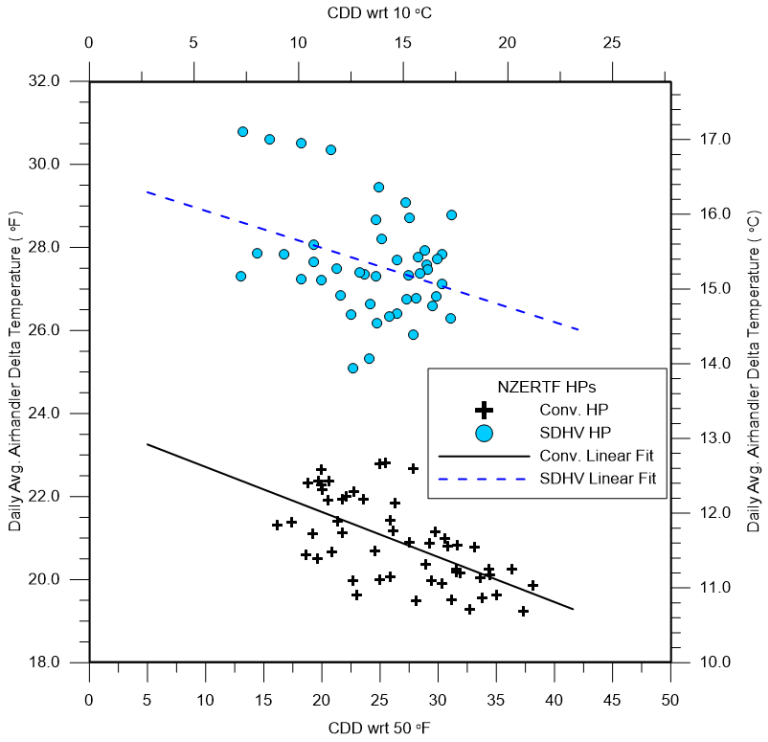

Figure 4.52. Cooling average operating indoor unit air temperature change.

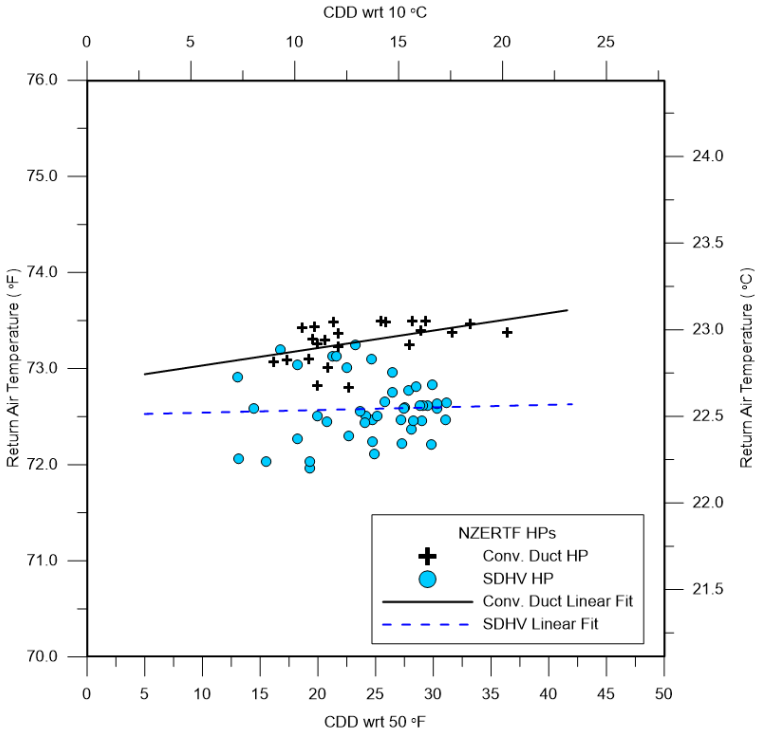

Figure 4.53. Cooling daily average operating return air temperatures.

4.2.6 Cooling Standby Energy Use

Table 4.3 shows the average power demand during standby for the two systems. During standby, the system is not performing any cooling, heating, or ventilation functions. Any electrical energy that is consumed is not being used to condition the space, and it is a waste of energy that reduces overall space-conditioning efficiency. The system is still powered up, and the indoor and outdoor unit controls are consuming energy. The large difference between the power demands is due to the difference in the type of low-voltage transformer used by the two systems; the SDHV uses a toroidal transformer, whereas the CDHP uses an E-core, laminated steel-plate type transformer. Figure 4.17 shows the two different types of transformers installed in the systems. The indoor standby energy use of the SDHV system averaged (113.5 ± 7.0) Wh per day less than the CDHP (Figure 4.18), whereas the outdoor standby averaged (222.3 ± 14.3) Wh less (Figure 4.19). These results combined for the SDHV system to produce a total daily standby energy use that was (335.8 ± 21.3) Wh less than the CDHP (Figure 4.20).

Table 4.9. Cooling standby power demand.

System	Indoor standby (W)	Outdoor standby (W)
CDHP	11.9	23.4
SDHV	3.9	7.7
% difference wrt CDHP	-67%	-67%

(a) (b)

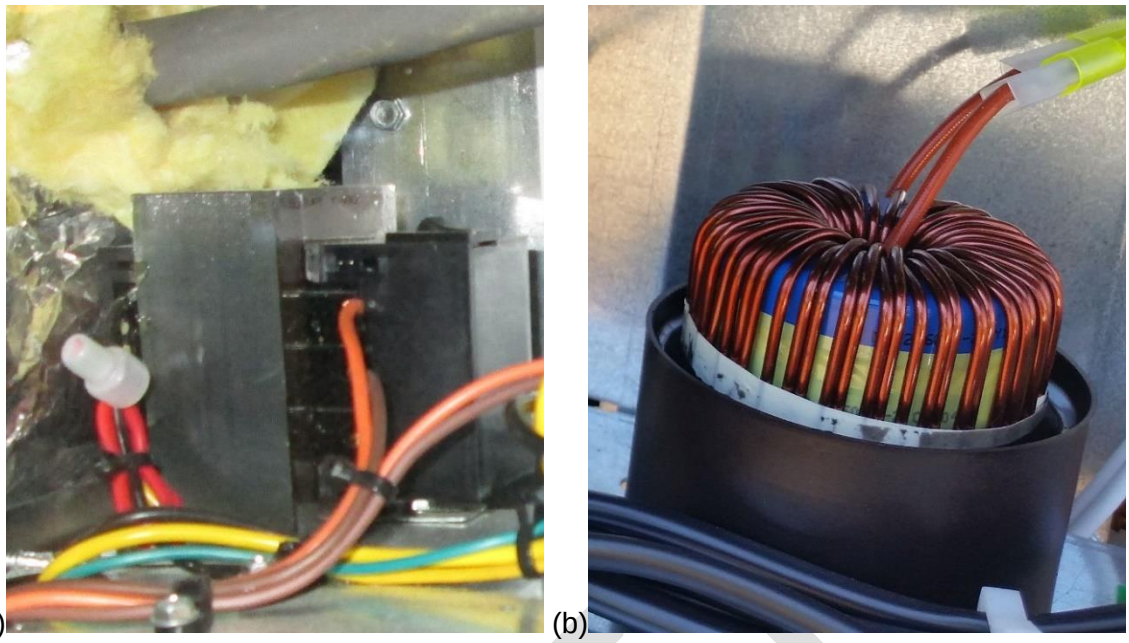

Figure 4.54. Low voltage transformers in the two systems: (a) CDHP E-core laminated plate and (b) SDHV toroidal.

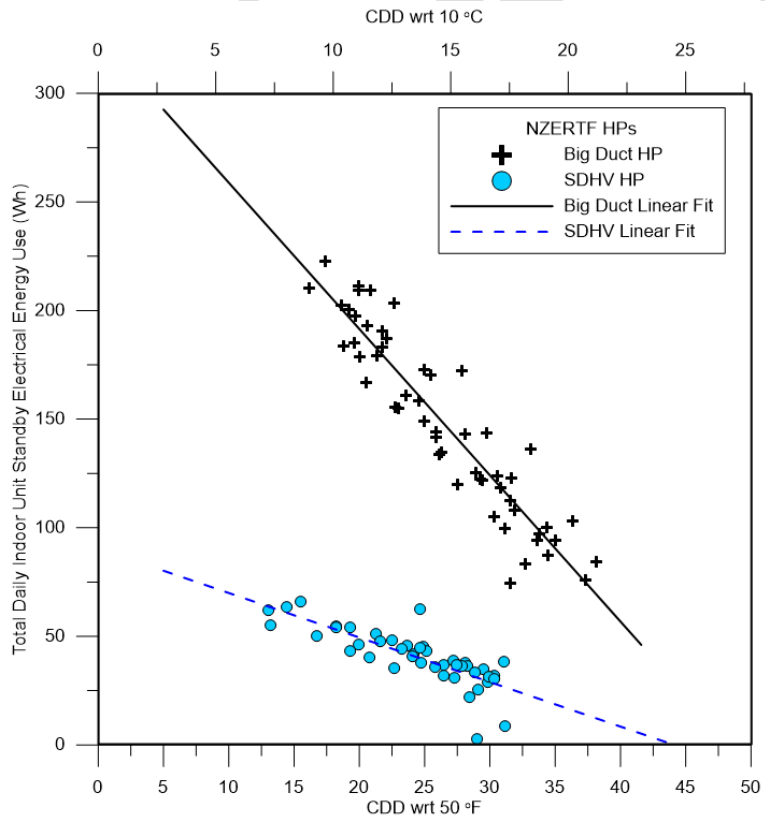

Figure 4.55. Cooling indoor unit daily standby energy use.

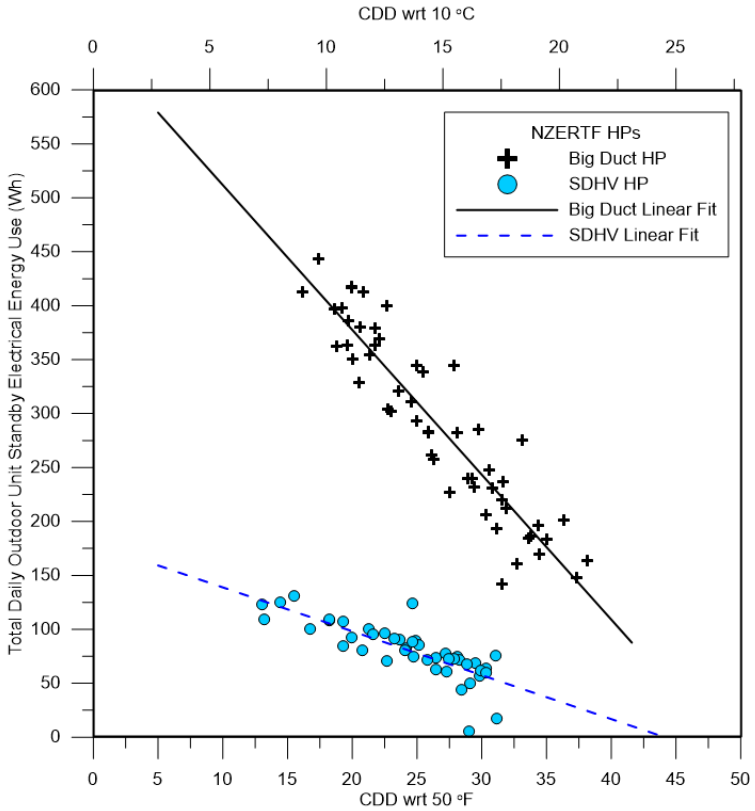

Figure 4.56. Cooling outdoor unit daily standby energy use.

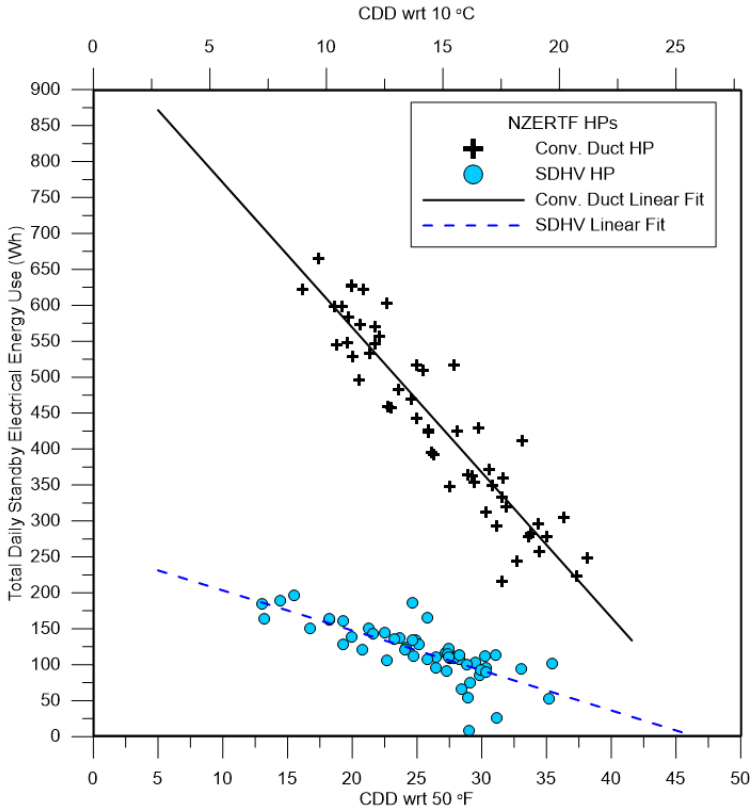

Figure 4.57. Cooling system daily total standby energy use.

4.2.7 Cooling Efficiency

Figure 4.21 shows the cooling COP as a function of CDDs. There is more scatter in the variable speed COP data than for the two-stage HP. The SDHV system averaged a slightly higher COP for the cooling season being (0.396 ± 0.113) higher than the CDHP. Figures 4.22 and 4.23 show the compressor suction and discharge refrigerant saturation temperatures, respectively, for a comparable day for the two systems. In Figure 4.22 the CDHP has an on cycle from approximately 700–2,400 seconds, whereas the SDHV system runs continuously over that same time. Figure 4.23 shows that the evaporator saturation temperature of the CDHP is 5°C (9°F) higher than the SDHV, whereas the discharge saturation temperatures are within 2°C (3.6°F) of each other. This means that the SDHV system was operating at a higher temperature lift than the CDHP. The temperature lift for the two systems is shown in Figure 4.24. If the SDHV system hunting behavior between 1,000 and 2,000 seconds is neglected, then the SDHV operated with approximately 35°C (63°F) lift, and the CDHP operated with 27°C (49°F) lift. If everything else were equal, then the CDHP should have a higher COP because it was operating at a lower lift; however, Figure 4.25 shows that the instantaneous COP was better for the SDHV system. The reasons are shown in Figures 4.26 and 4.27, which show the instantaneous power and capacity, respectively. The capacity is equivalent, but the power demand of the SDHV system is less. The SDHV system showed this behavior consistently, producing higher COP even though it was operating at a higher lift (condenser refrigerant saturation temperature and evaporator saturation temperature difference). This behavior could have been modified in the control system to raise the evaporator saturation temperature when there was less need for dehumidification, thus increasing COP during more of the operating time.

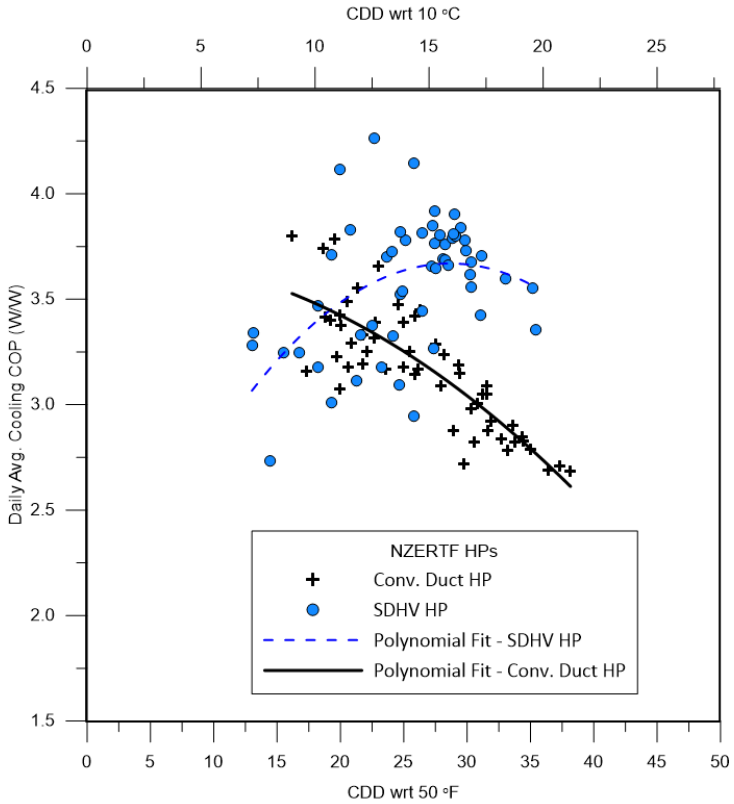

Figure 4.58. Cooling season COP.

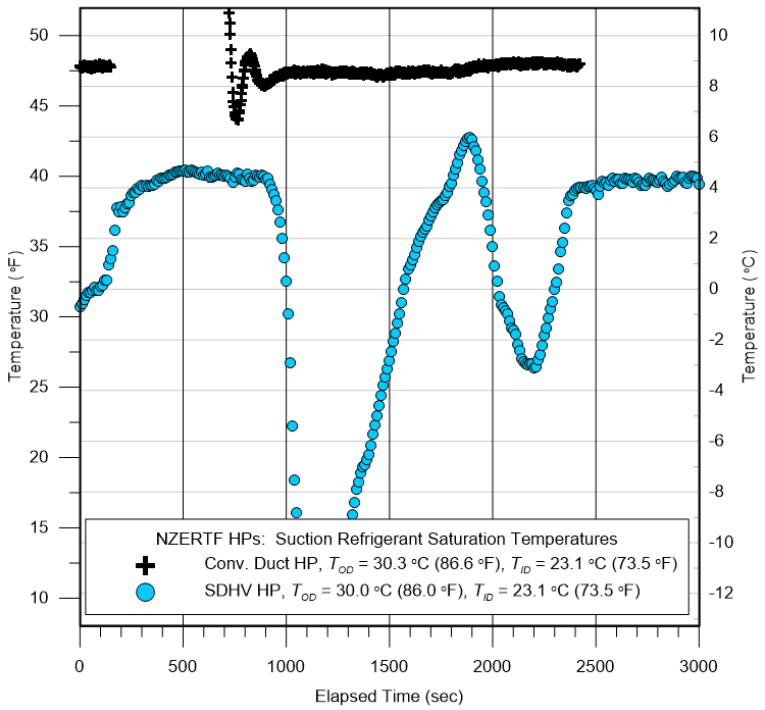

Figure 4.59. Cooling suction refrigerant saturation temperature example.

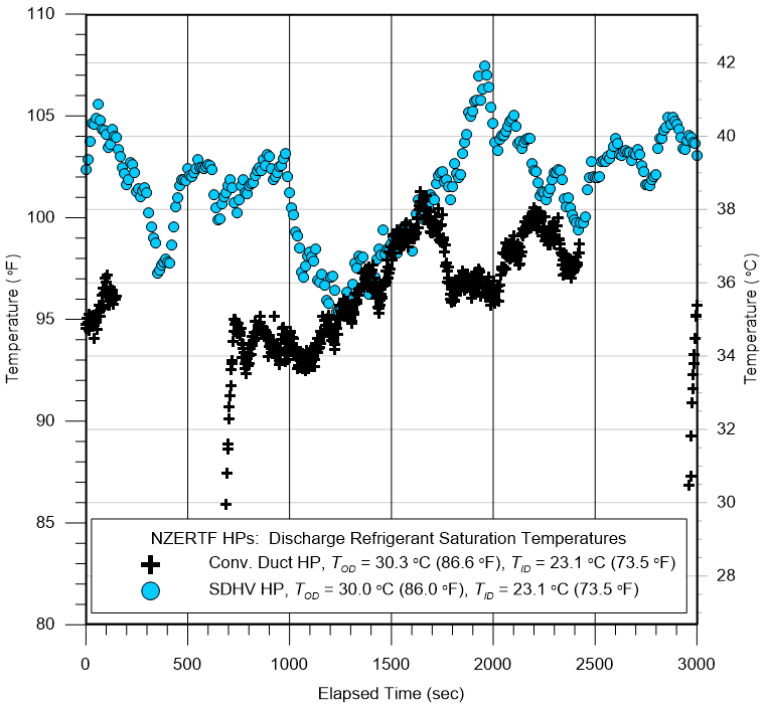

Figure 4.60. Cooling discharge refrigerant saturation temperature example.

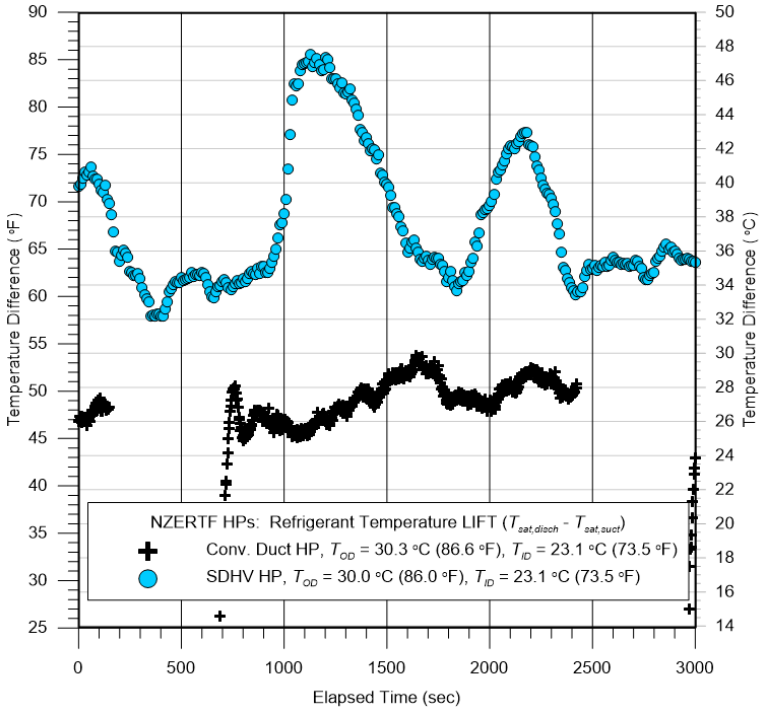

Figure 4.61. Cooling temperature lift example.

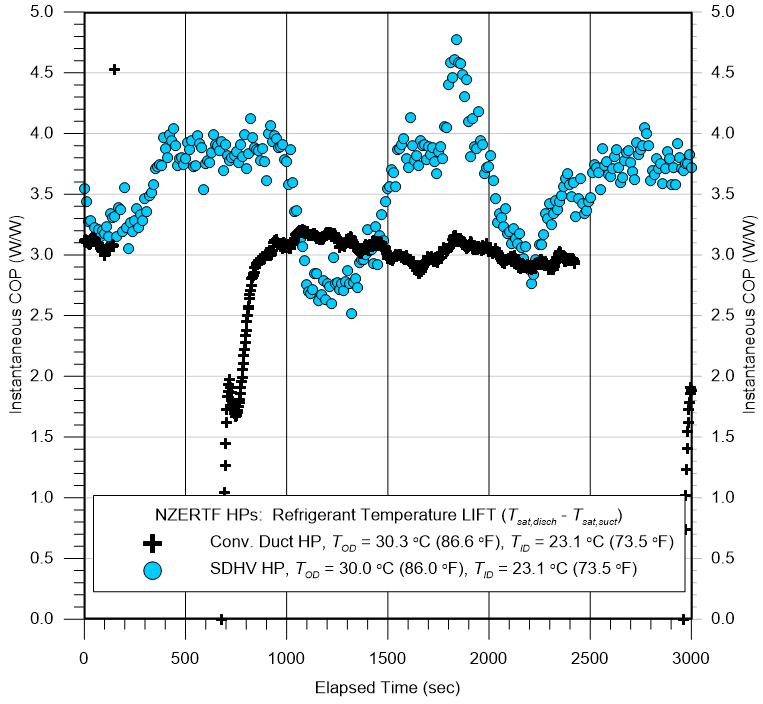

Figure 4.62. Cooling instantaneous COP example.

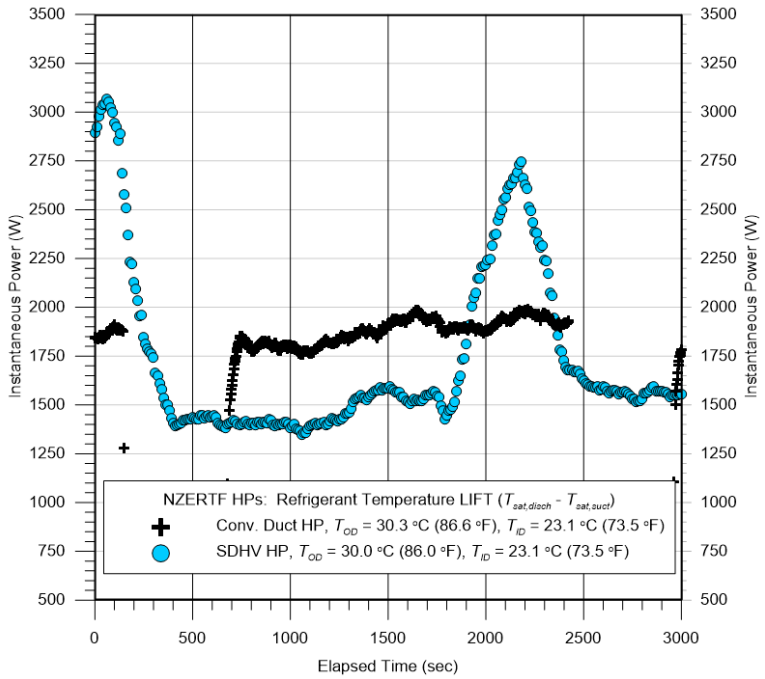

Figure 4.63. Cooling instantaneous power example.

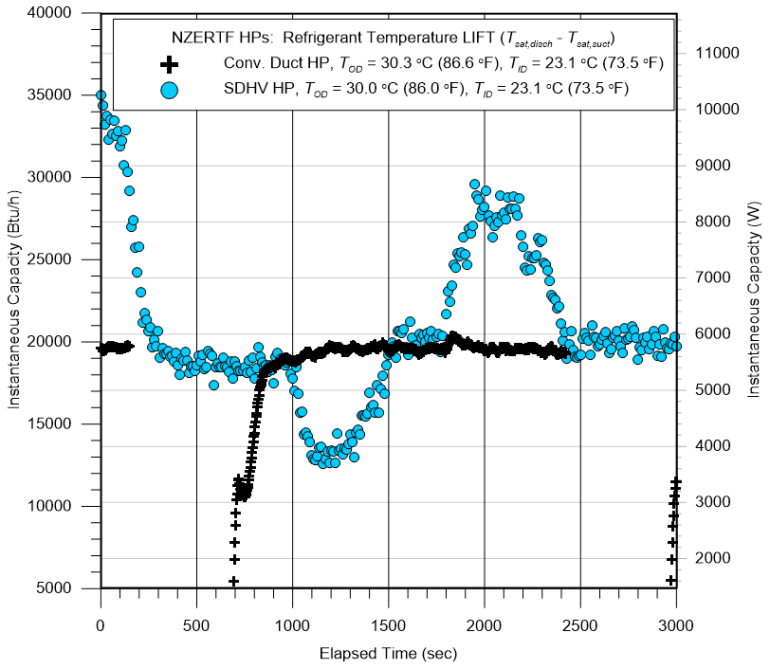

Figure 4.64. Cooling instantaneous capacity example.

Figure 4.28 shows a comparison of the daily average COP as a function of the daily average outdoor dry-bulb temperature. The SDHV, variable-speed system tended to operate at higher COPs for most of the outdoor conditions shown. The CDHP experienced higher temperature degree days but maintained good COP running at its lowest stage. Even on the highest temperature days, the CDHP operated at its low-stage capacity. The higher temperatures experienced by the CDHP lowered its average COP compared with the SDHV.

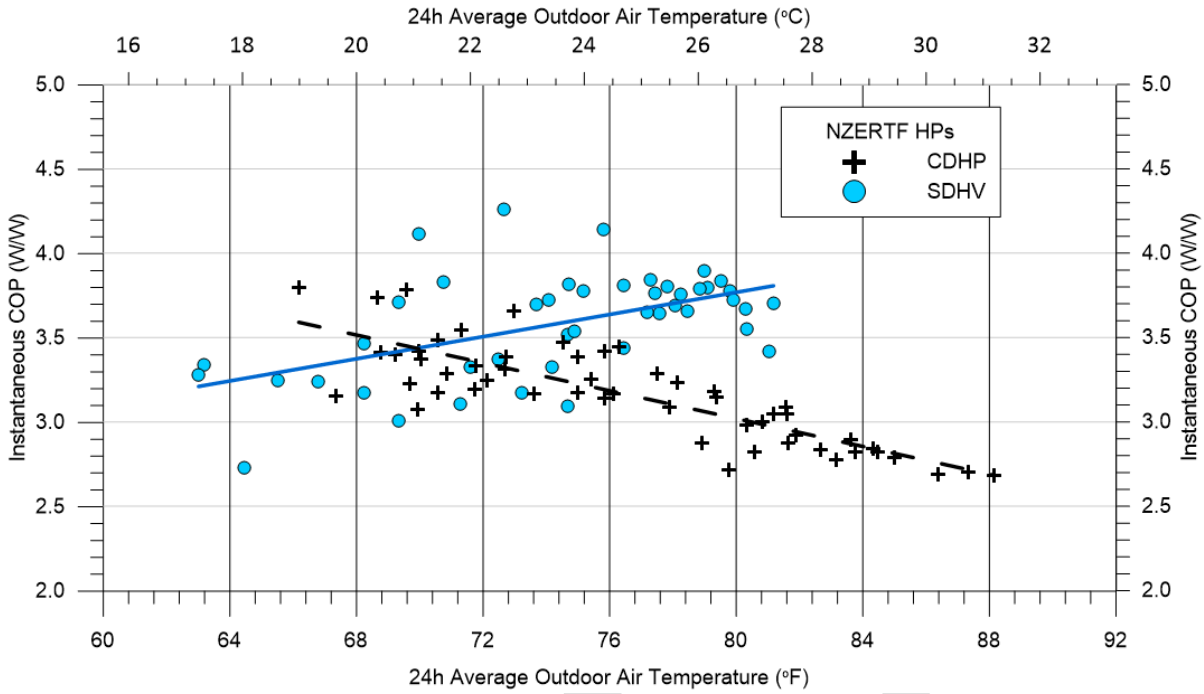

Figure 4.65. Cooling COP as a function of daily average outdoor temperature.

4.2.8 Heating Season

Figure 4.29 compares the HDDs with an 18.3°C (65°F) reference for the two HP systems. The heating season was from November 16, 2016 to April 2, 2017. The SDHV system had 22.4% more HDDs than the CDHP, even though they were operating on a weekly alternating schedule. For the heating season, as in the cooling season, degree days are used in the plots to normalize the results.

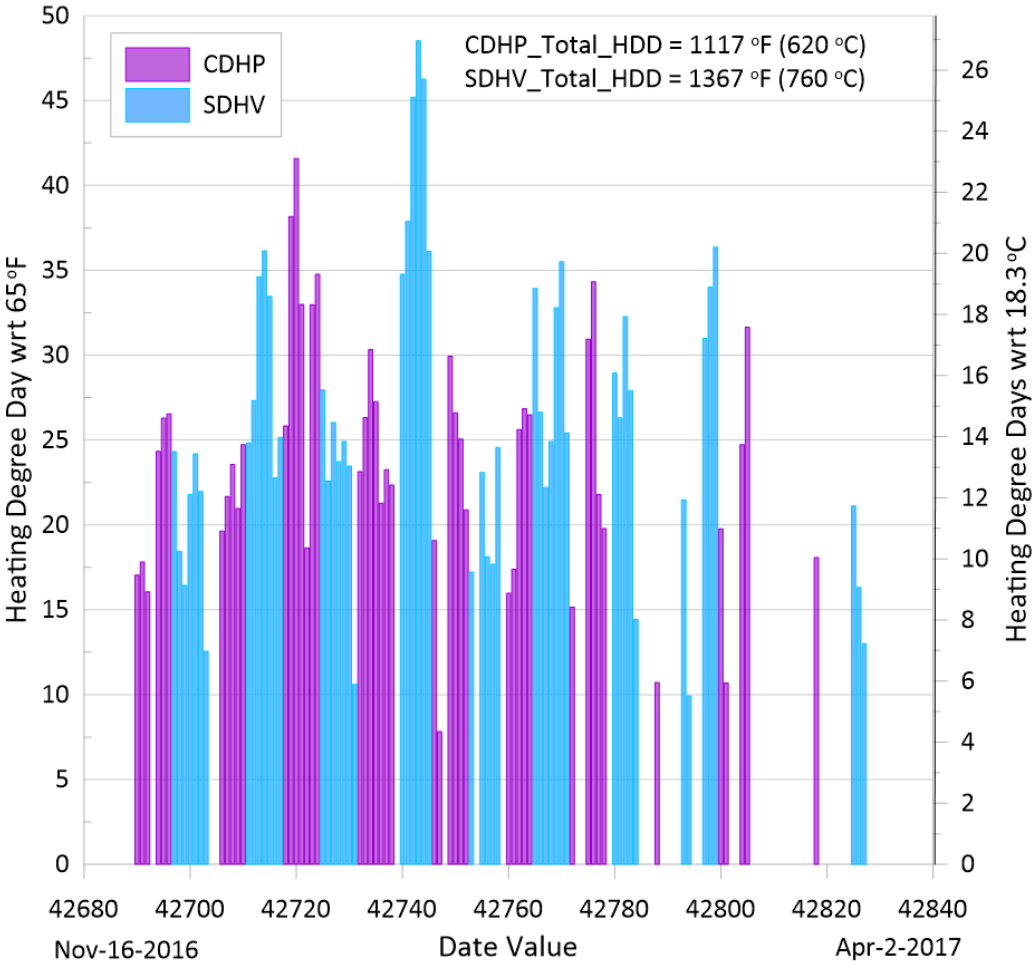

Figure 4.66. HDDs for the CDHP and SDHV.

4.2.8.1 Heating Energy

Figure 4.30 shows the daily average electrical energy consumed by the systems as a function of HDD. Because of the higher number of HDDs, the SDHV consumed 31.4% more electrical energy over the heating season. The daily electrical energy usages per HDD for the CDHP and SDHV (Figure 4.31) were (1,975 ± 355) Wh°C^{-1} ([1,09 7± 197] Wh°F^{-1}) and (1,931 ± 243) Wh°C^{-1} ([1,073 ± 135] Wh°F^{-1}), respectively. The difference in heating season electrical energy usage per HDD was statistically insignificant. The daily thermal energy transferred per HDD (Figure 4.32) for the CDHP and the SDHV were (860 ± 208) Wh°C^{-1} ([1,548 ± 374) Wh°F^{-1}) and (939 ± 173) Wh°C^{-1} ([1,690 ± 311] Wh°F^{-1}), respectively. The difference in the cooling season thermal energy removed per HDD was statistically insignificant.

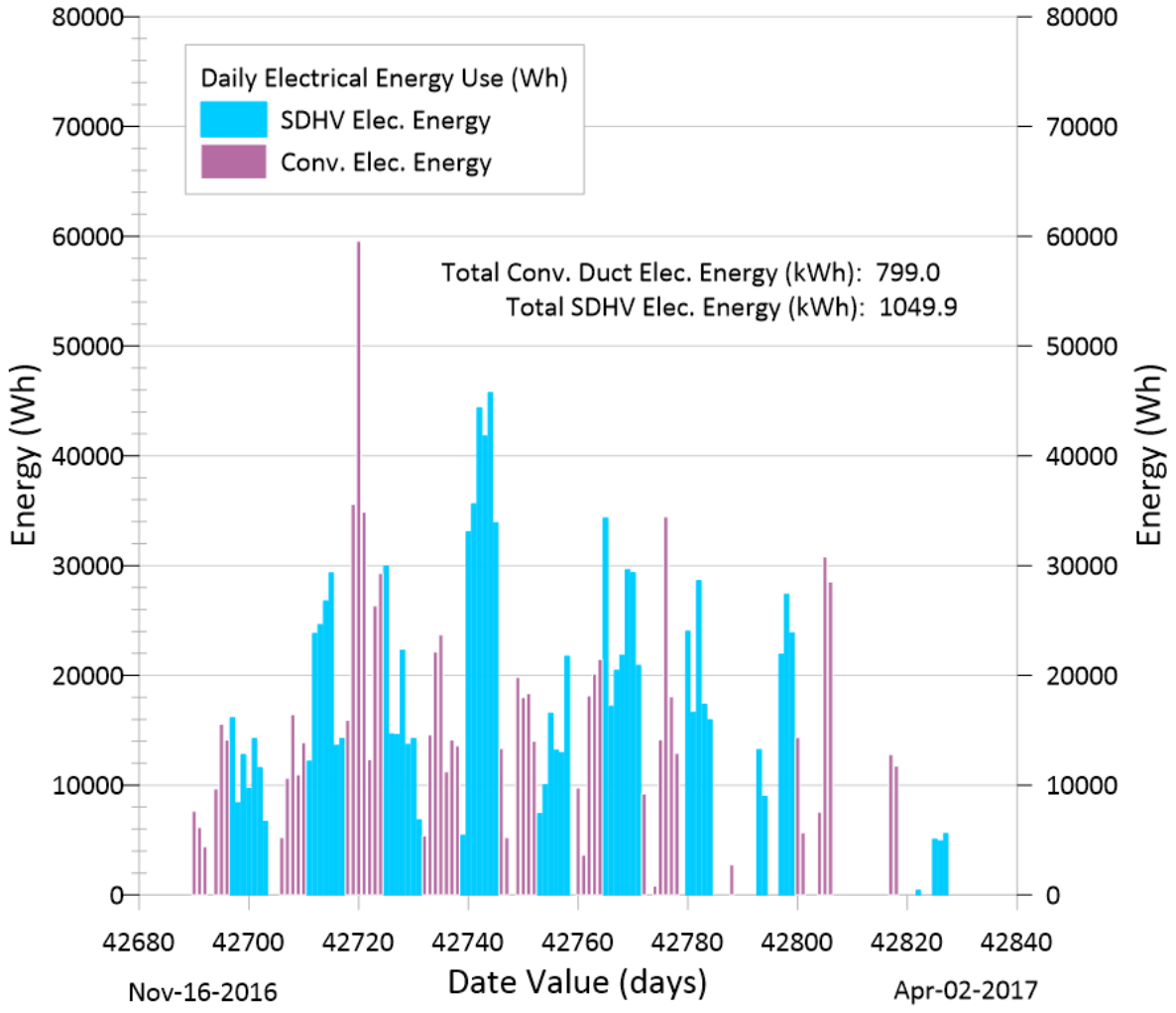

Figure 4.67. Heating season daily and total electrical energy use.

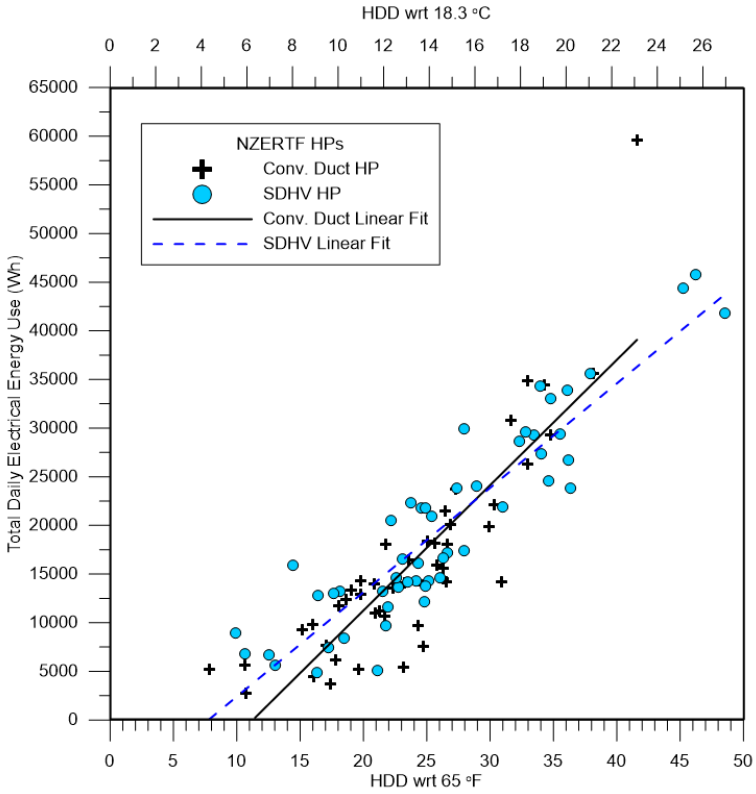

Figure 4.68. Heating season electrical energy use as a function of HDDs.

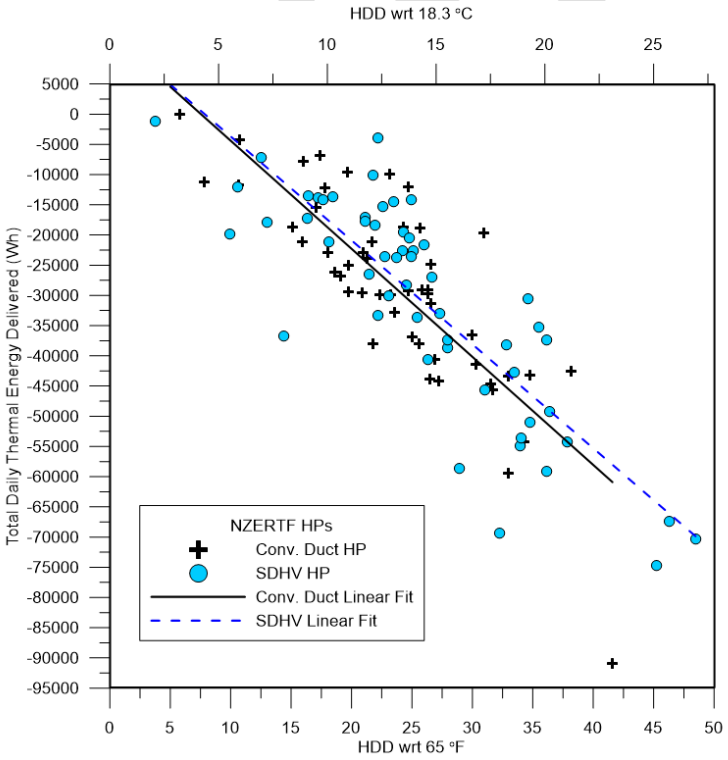

Figure 4.69. Heating season thermal energy delivered.

Figure 4.33 shows that the SDHV system operated at a lower average daily airflow rate than the CDHP. The SDHV operated at (625 ± 53.2) m^3h^{-1} ([368 ± 31.3] cfm) lower average airflow than the CDHP. Similar to the cooling mode, the SDHV indoor blower operated in a more efficient range (Figure 4.34). Unlike the cooling mode, the SDHV circulated an average of

(3.6 ± 0.8) fewer air changes (Figure 4.35) while operating for about the same number of hours per day (Figure 4.36). The SDHV had a higher supply of air delivery temperature (Figure 4.37) and a higher average temperature change across the air handler ([13.9 ± 1.6]°C [(25 ± 2.8)°F] higher, Figure 4.38). House average return air temperatures were equivalent (Figure 4.39). The SDHV system was delivering higher energy supply air to meet the load at a lower airflow rate.

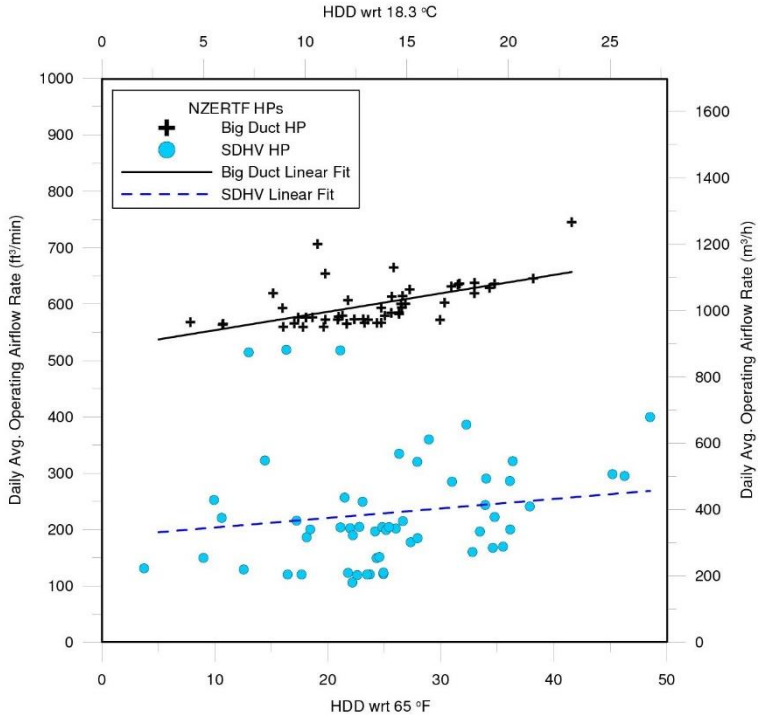

Figure 4.70. Heating daily average operating airflow rates.

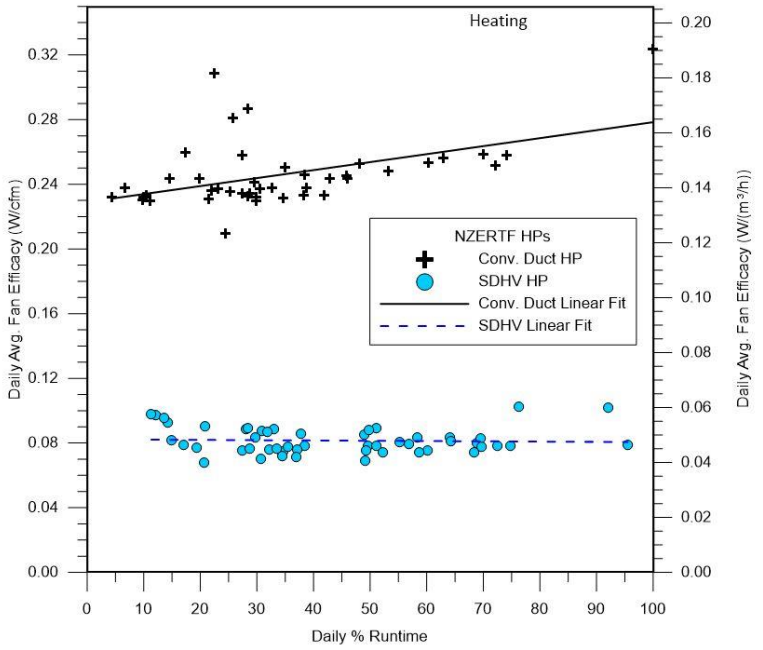

Figure 4.71. Heating average indoor blower efficacy (W/[unit volume flow]).

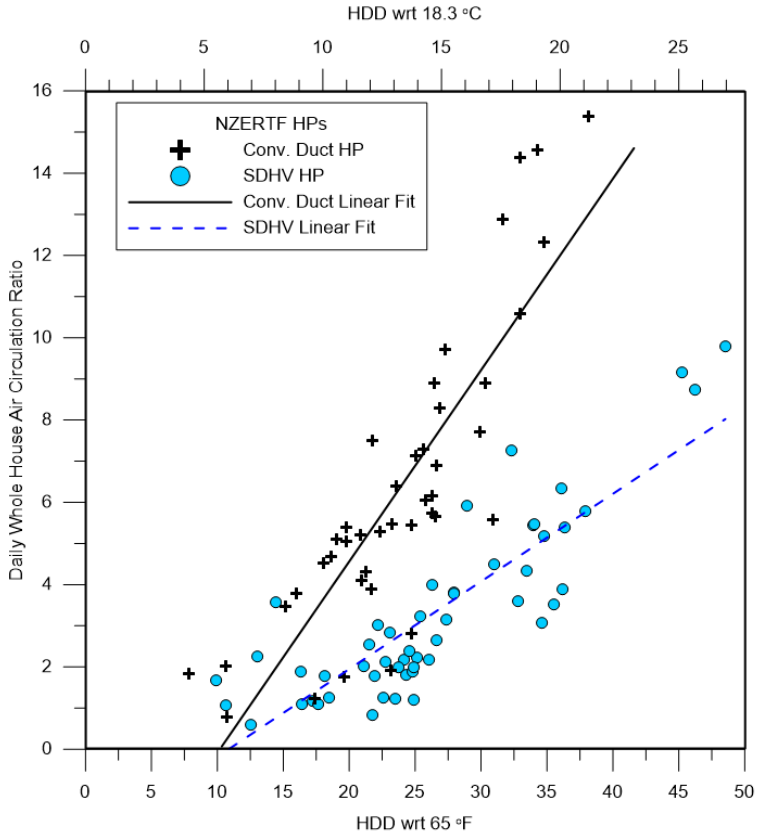

Figure 4.72. Daily heating air circulation ratio.

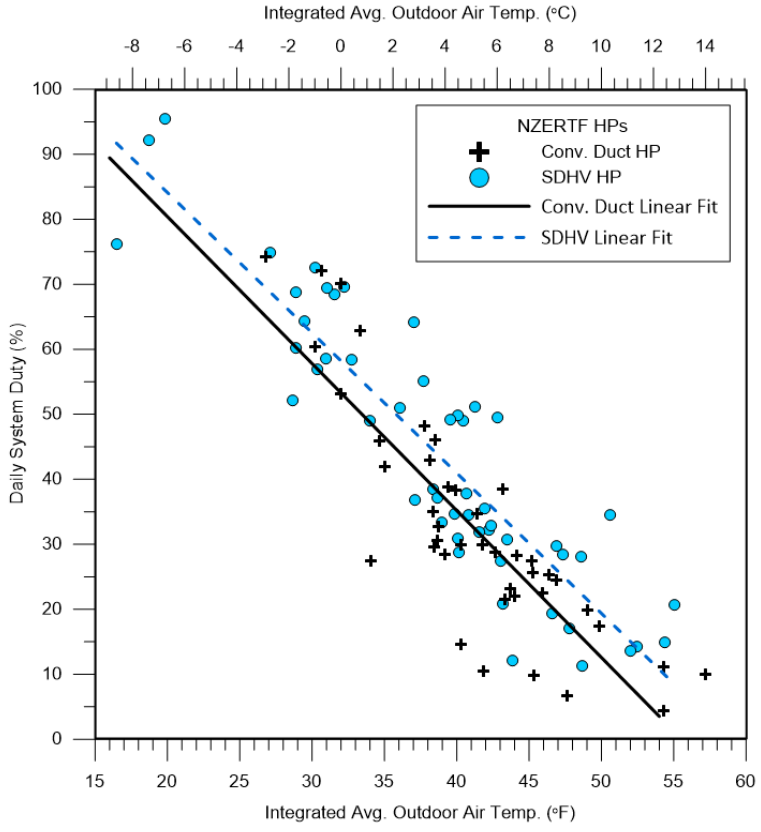

Figure 4.73. Heating daily system percent duty.

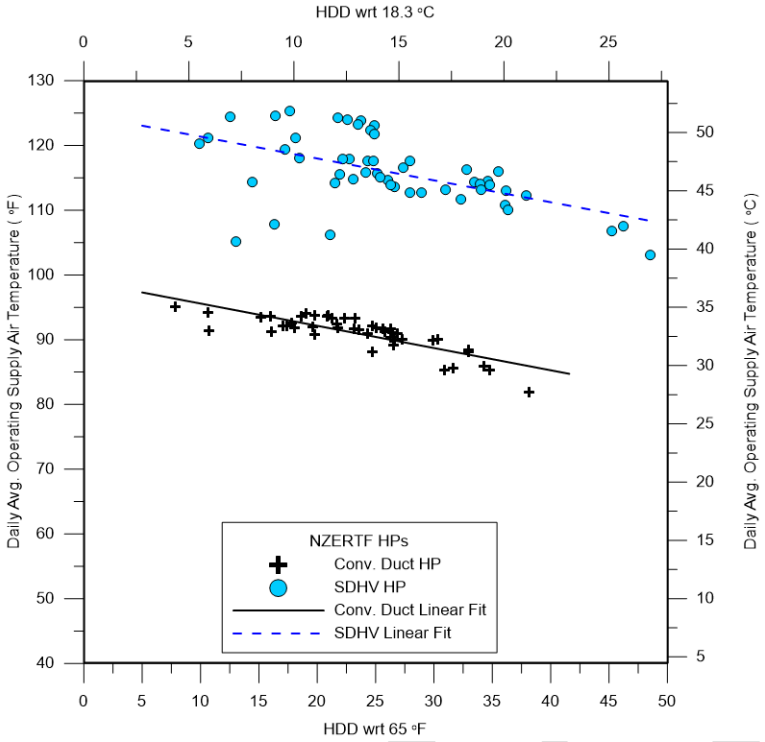

Figure 4.74. Heating average operating supply air temperatures.

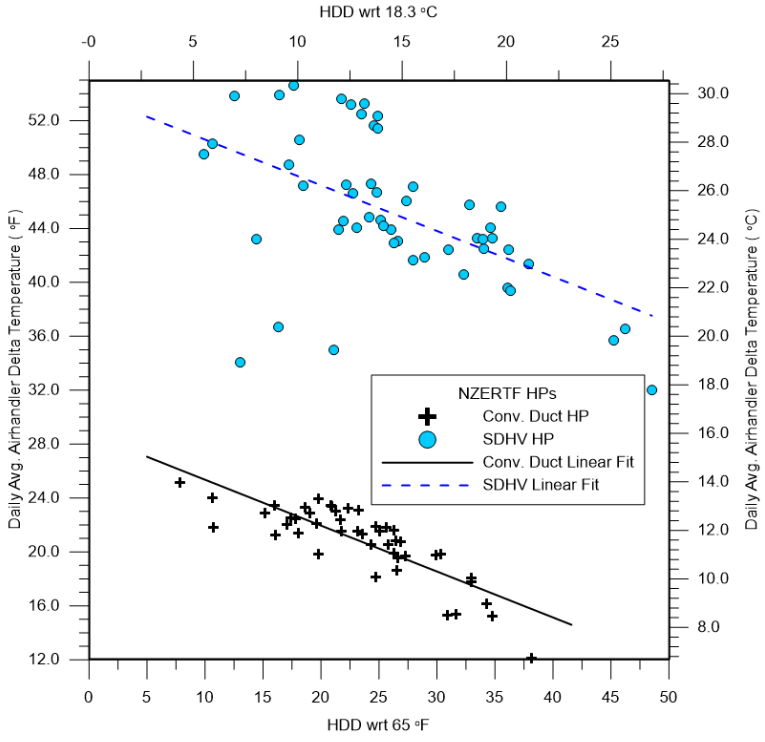

Figure 4.75. Heating average operating indoor unit air temperature change.

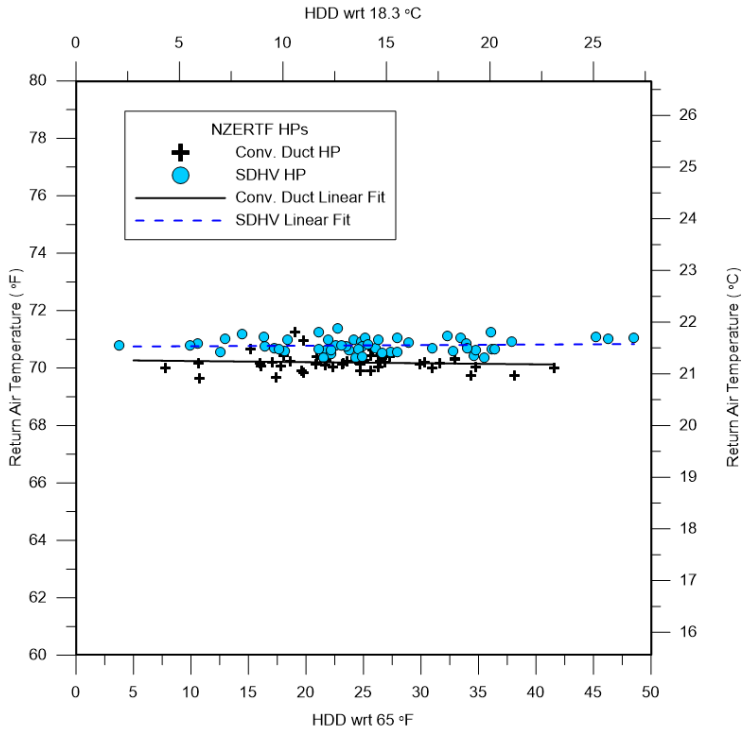

Figure 4.76. Heating daily average operating return air temperature.

4.2.9 Heating Standby Energy Use

Heating standby energy use for the indoor unit is shown in Figure 4.40. The SDHV indoor air handler averaged (123.0 ± 9.4) Wh less daily standby energy than the CDHP with an almost constant demand of 4 and 11 W for the SDHV and CDHP, respectively (Figure 4.41). The SDHV outdoor unit standby energy use (Figure 4.42) did not have a constant demand with HDD but increased at the colder outdoor temperatures (Figure 4.43) due to electric resistance compressor sump heating. The decrease in CDHP energy use at high HDD was due to less standby time. The CDHP has an external electric resistance sump heater, but it was never energized during the heating season. The overall result for total standby energy use is shown in Figure 4.44. The SDHV system consumed an average of (255.5 ± 46.0) Wh less standby energy daily than the CDHP.

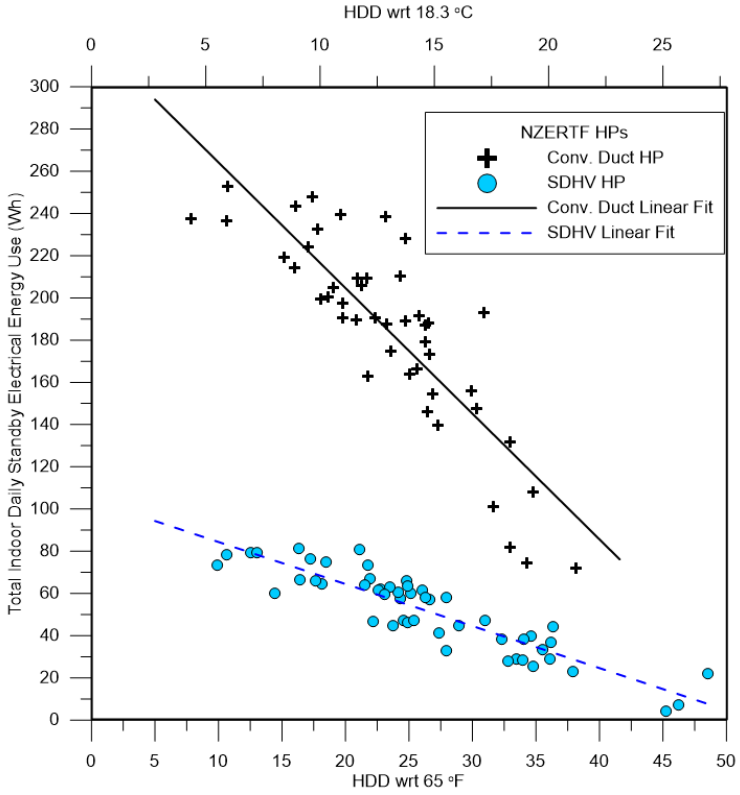

Figure 4.77. Heating ID unit standby energy use.

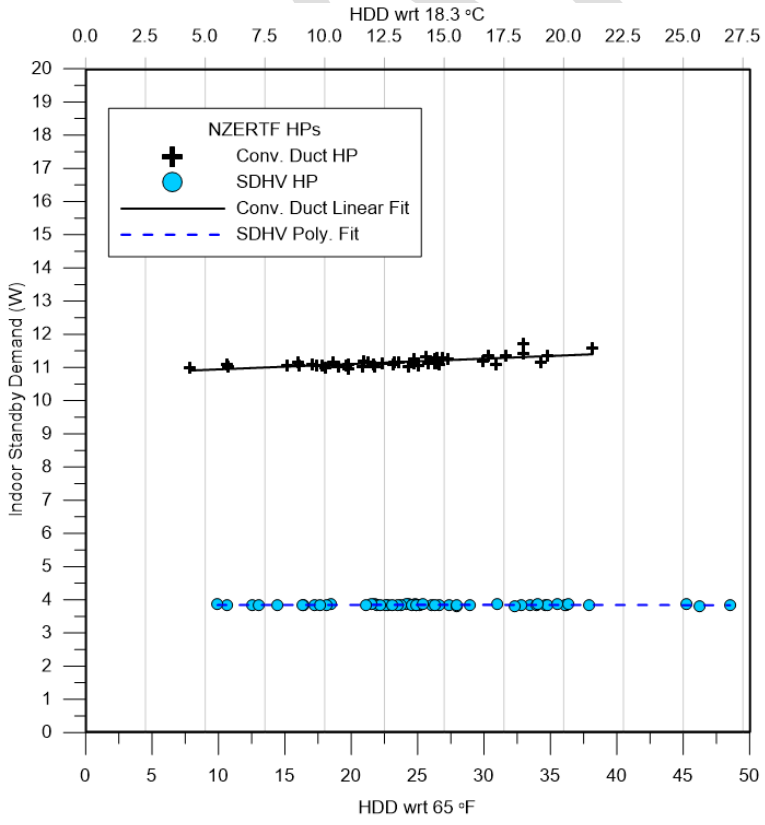

Figure 4.78. Heating ID unit standby power demand.

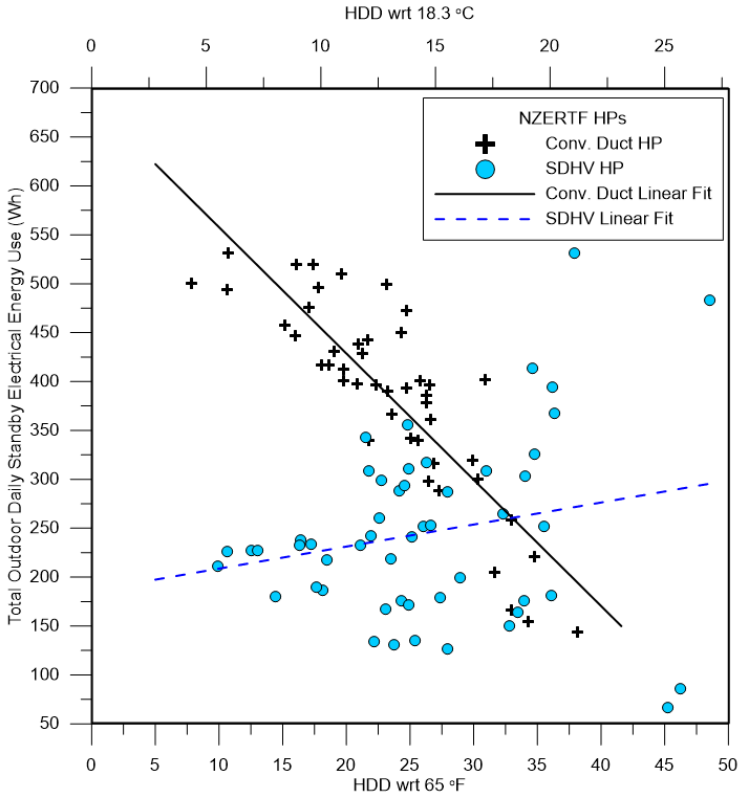

Figure 4.79. Heating OD unit standby energy use.

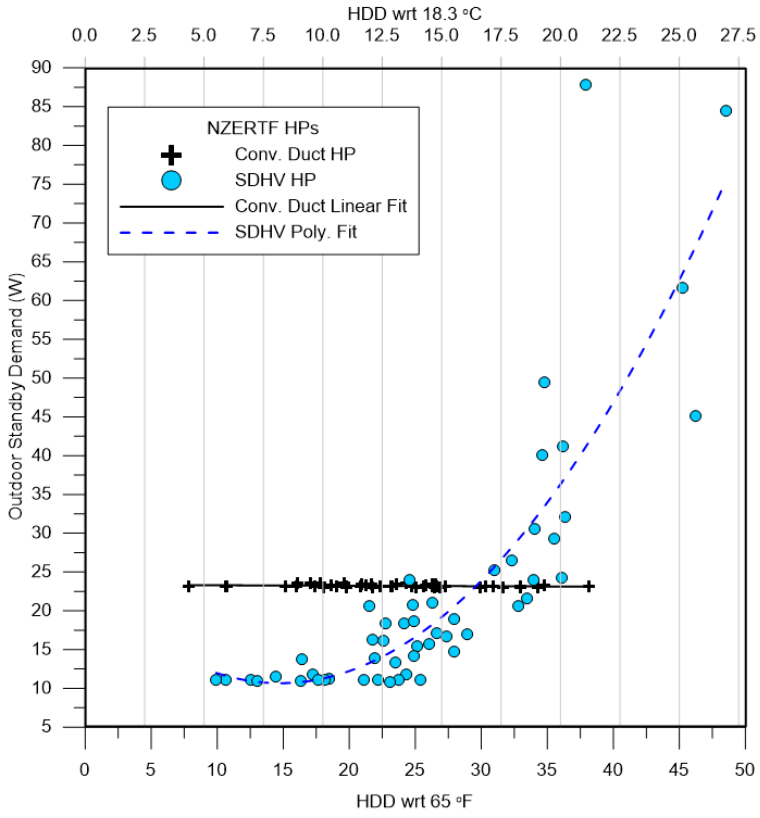

Figure 4.80. Heating OD unit standby power demand.

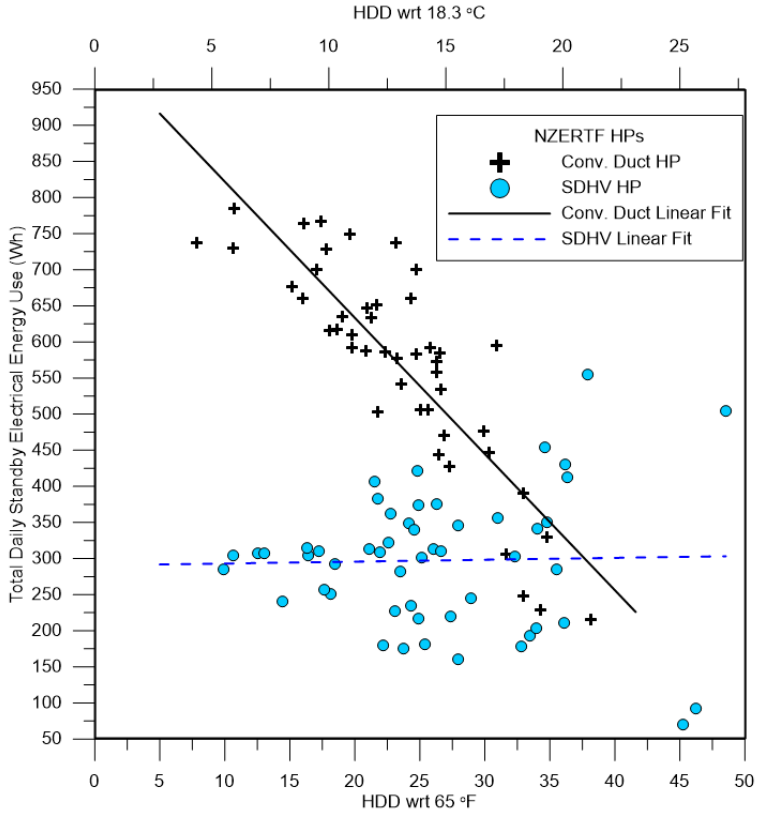

Figure 4.81. Heating system standby total energy use.

4.2.10 Heating Efficiency

Figure 4.45 shows the daily average heating COP as a function of the HDD. High-supply air temperatures were produced by the SDHV system, which reduce the “cold blow” effect that many people complain about when a new HP is retrofitted to a hot air furnace system [59]. These high temperatures were meant to reduce the cold blow effect, but instead they directly affected the heating COP. As a remedy to the excessively high supply air temperatures, new firmware was uploaded to the SDHV system controller, which produced significant changes in heating efficiency and supply air temperature (Figure 4.46). The CDHP had an average daily heating COP of (1.9 ± 0.4) compared with (1.8 ± 0.9) for the SDHV with original firmware. The CDHP average heating COP was statistically equal to that of the SDHV that runs the original firmware. The SDHV system with the new firmware averaged a heating COP of (2.5 ± 1.1). The heating COP of the new firmware SDHV was (0.6 ± 0.18) higher than the CDHP over comparable temperature conditions. Further testing of the new firmware is needed to reduce its standard error and improve the comparison with the CDHP. Figure 4.47 shows the daily average heating COP of the two systems as a function of outdoor air dry-bulb temperature. This figure illustrates the large improvement in heating COP due to a change in the SDHV firmware. This figure also shows that the SDHV system experienced the coldest heating days during the test period, but this did not reduce its COP as compared with the CDHP.

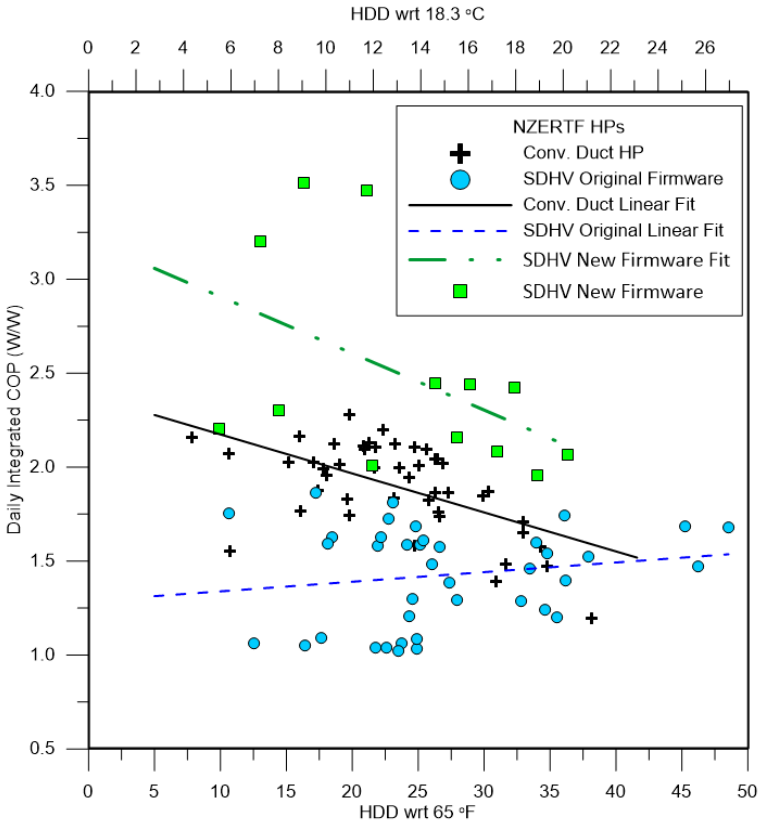

Figure 4.82. Heating COP vs. HDD with original and new firmware.

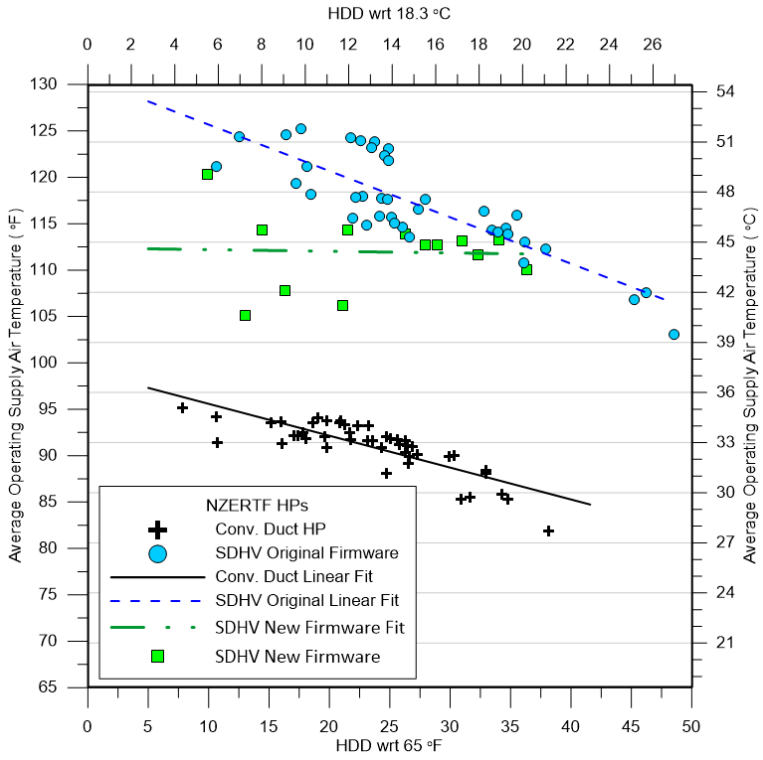

Figure 4.83. Heating supply air temperatures with original and new firmware.

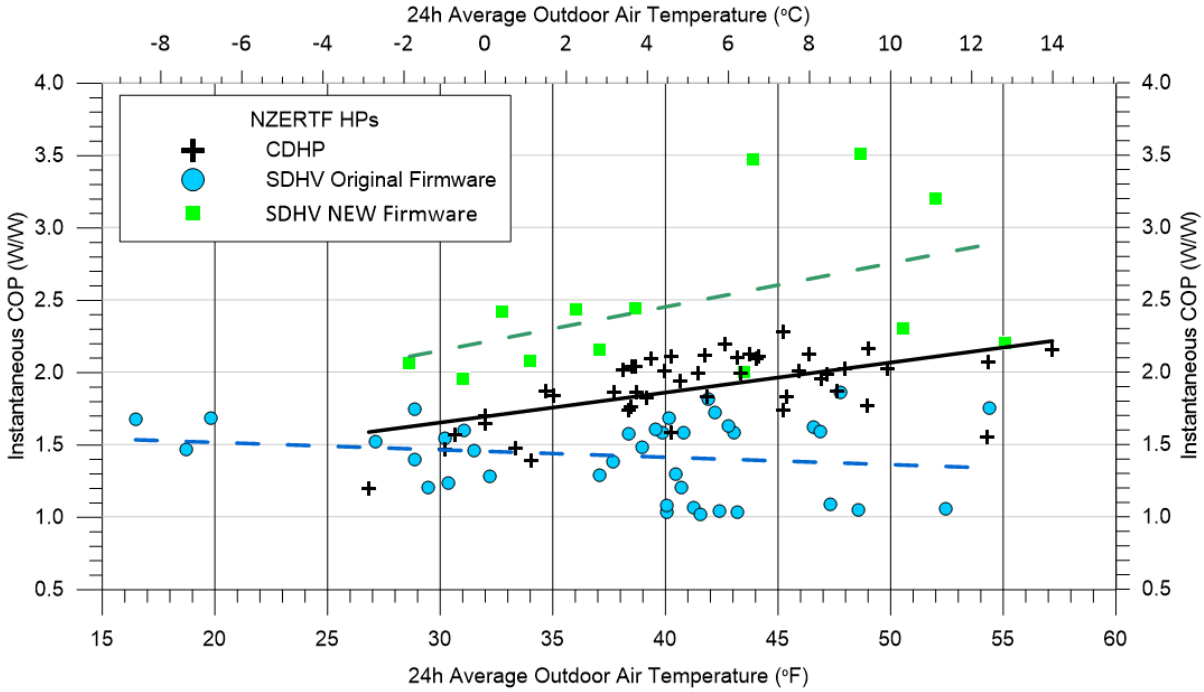

Figure 4.84. Heating COP as a function of daily average outdoor air temperature.

4.2.11 Defrost Performance

The conventional system and the SDHV system performed defrost operations to remove the buildup of frost on the outdoor heat exchangers. The CDHP defrost control was set to defrost every 90 minutes, as needed. Observations of the CDHP defrost showed that the defrost operation would occur every 90 minutes of accumulated compressor run time when the outdoor temperature was below 35°F.

The SDHV system takes a different approach to the traditional reverse cycle defrost. When it senses frosting conditions, the unit employs hot-gas bypass to the outdoor heat exchanger while allowing the indoor unit to remain operating. If the control detects that the defrost parameter is not resolved by hot-gas bypass, then the system resorts to a full reverse-cycle defrost. The SDHV system uses no auxiliary electrical resistive heating elements in the air stream.

The SDHV system used an average of (624 ± 254) Wh less defrost energy per day than the CDHP (Figure 4.48). To demonstrate how the two systems perform defrosts, Figure 4.49 shows a heating capacity plot that begins at the start of a defrost and ends at the end of a second defrost. The two systems perform a defrost, run at a steady state for a while, then defrost again. The timescales are not equivalent because the steady state run time between defrosts is very different for these examples. The top axis is the timescale for the CDHP, about 7,000 seconds (1 hour, 57 minutes), and the bottom axis is the timescale for the SDHV HP, about 22,000 seconds (6 hours, 6 minutes).

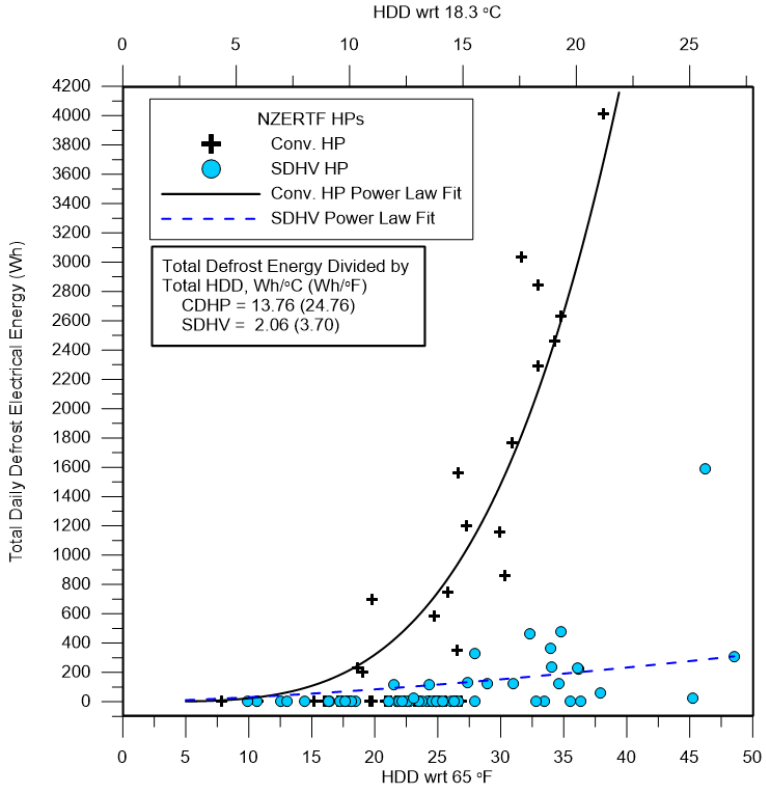

Figure 4.85. Heating daily defrost energy use.

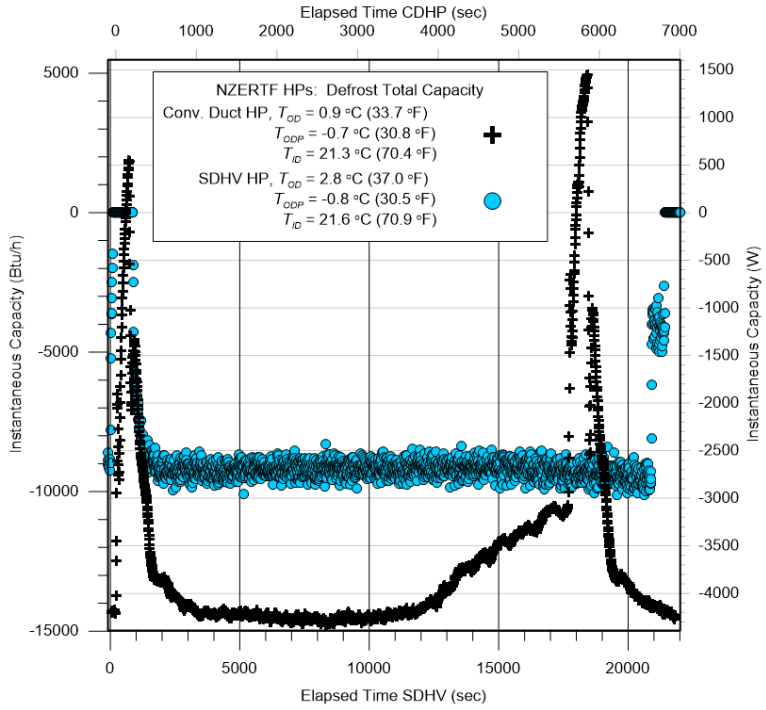

Figure 4.86. Example defrost heating capacity.

The CDHP defrost begins when the heating capacity before defrosting is 4,195 W (14,314 Btu h^{-1}). Figure 4.50 shows a combined plot of heating capacity, resistive heat power, indoor (ID) blower power, and outdoor (OD) coil temperature during the CDHP defrost from 0

to 195 seconds. Heating capacity is shown as a negative value to differentiate it from cooling capacity. At the initiation of defrost, the outdoor fan is turned off as the refrigerant reversing valve is energized, like in cooling mode operation. About 15 seconds pass before electric resistive heat engages (5,000 W), and the indoor blower ramps up airflow rate; thus, the blower power demand moves up to approximately 400 W. A few seconds after the resistive heat turns on and the indoor blower ramps up, the outdoor coil temperature starts to increase. The outdoor coil temperature reaches a peak of 26.8°C (80.2°F) before the reversing valve switches back to heating mode (170 seconds). Resistive heat remains energized after the reversing valve switches to heating mode until turning off at 195 seconds as normal heating resumes. The 5 kW nominal supplementary resistive heat is not enough to prevent cold blow during defrost; the heating capacity goes positive, indicating a cooling effect upon the house, from 105 to 175 seconds. This defrost consumed 278 Wh of electrical energy.

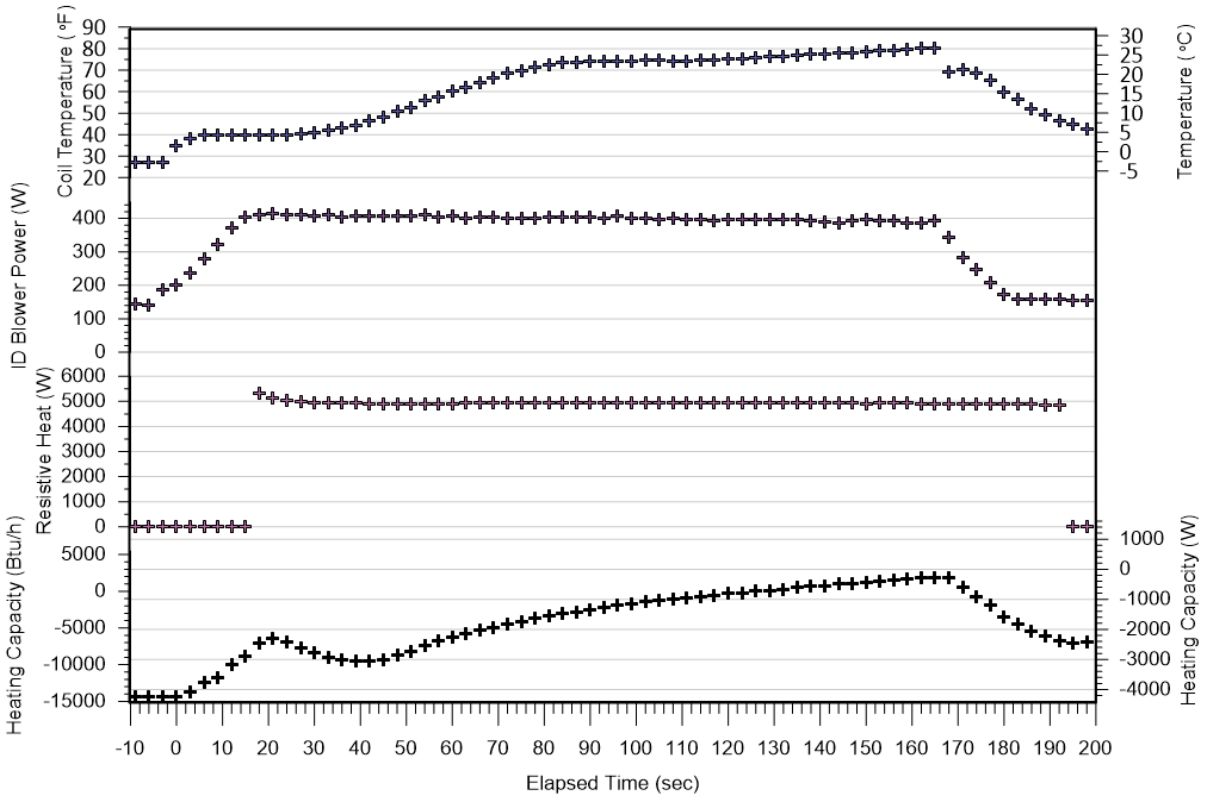

Figure 4.87. CDHP defrost characteristics.

The SDHV defrost begins when the heating capacity before defrosting is 2,696 W (9,200 Btu h^{-1}). Figure 4.51 shows a combined plot of heating capacity, resistive heat power, ID blower power, and OD coil temperature during the SDHV defrost from 0 to 760 seconds. Heating capacity is shown as a negative value to differentiate it from cooling capacity. At the initiation of defrost, the outdoor fan is turned off as the refrigerant reversing valve is energized, like in cooling mode operation. After about 100 seconds, the indoor blower ramps all the way off, and the outdoor coil temperature starts to increase. The outdoor coil temperature reaches a peak of 29.7°C (85.5°F) before the reversing valve switches back to heating mode (760 seconds). The cold blow effect seen for the CDHP during defrost is absent here. The heating capacity never goes positive since the indoor blower energizes at 860 seconds to resume normal heating operation. This defrost consumed 265 Wh of electrical energy.

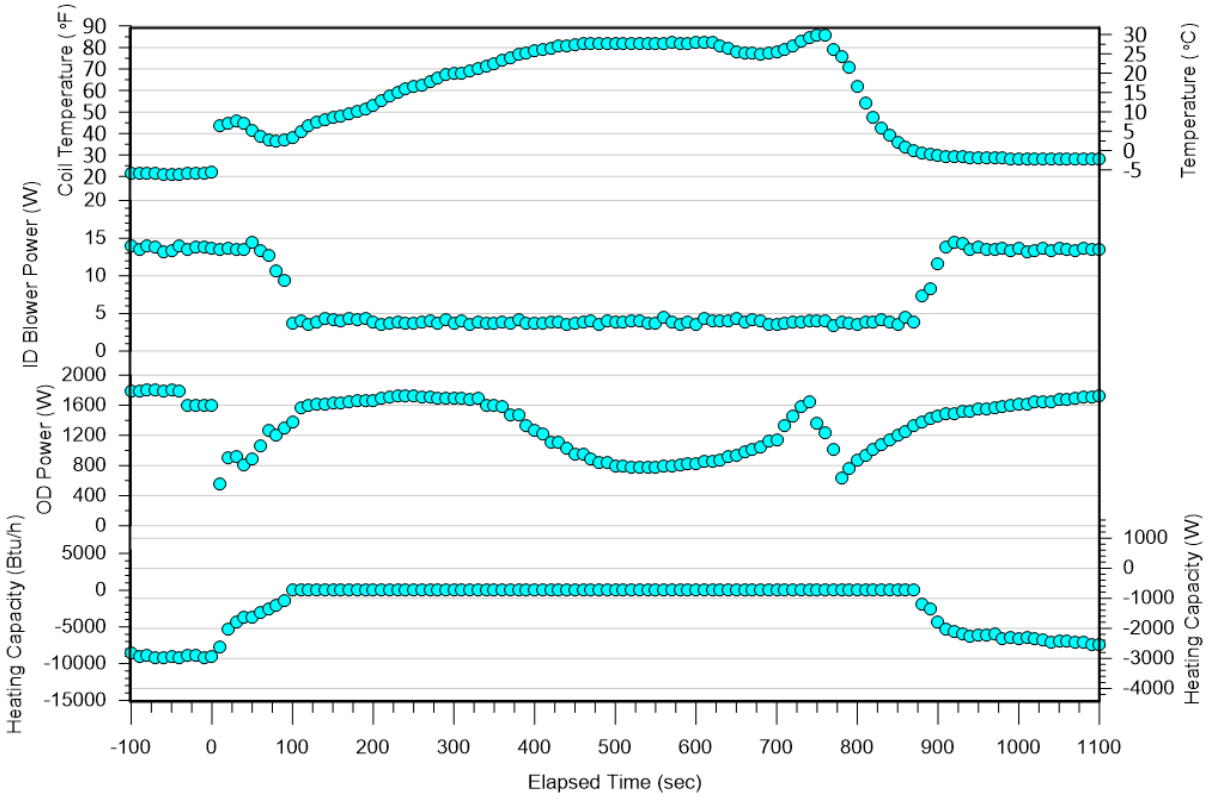

Figure 4.88. SDHV defrost characteristics.

Figure 4.52 looks at the frosting interval for both systems in more detail; heating capacities are shown as negative numbers. Before the previous defrost (not shown in the figure), the SDHV had a heating capacity of (2,700 ± 166) W ([9,215 ± 568] Btu h^{-1}) and total power demand of (1,766 ± 70) W. After defrost and once at a steady state again (Figure 4.52), the heating capacity was (2,709 ± 145) W ([9,244 ± 496] Btu h^{-1}) as power dropped to (1,695 ± 86) W while maintaining capacity. During frosting (i.e., the end of defrost to the start of the next defrost), the capacity was maintained at (2,703 ± 148) W ([9,222 ± 504] Btu h^{-1}), and the power demand averaged (1,672 ± 88) W. One minute before the initiation of the next defrost, the heating capacity averaged (2,684 ± 156) W ([9,159 ± 532] Btu h^{-1}) with the total power demand averaging (1,636 ± 8) W. During frosting, the average heating capacity decreased by less than 1%, and the average total power demand decreased by 3.5%.

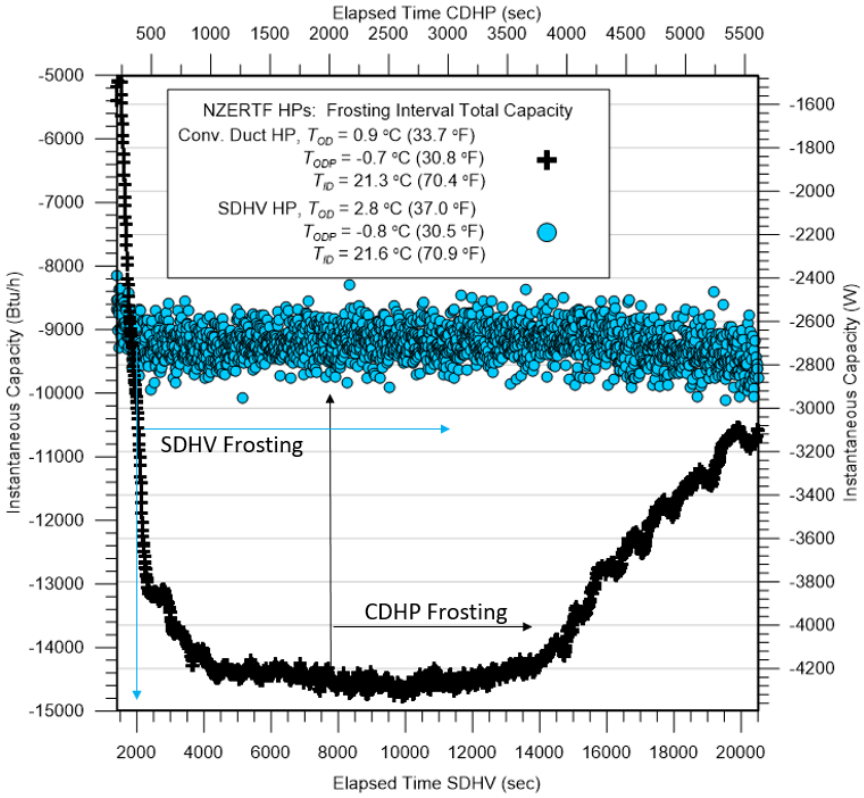

Figure 4.89. Frosting interval heating capacity.

Before the previous defrost, the CDHP had a heating capacity of (4,194 ± 19) W ([14,310 ± 64] Btu h^{-1}) and a total power demand of (2,003 ± 424) W (Figure 52). After defrost and once at a steady state again (1,100–3,750 seconds), the heating capacity was (4,244 ± 69) W ([14,480 ± 234] Btu h^{-1}) and power demand was (2,011 ± 52) W. One minute before the initiation of the next defrost, the heating capacity averaged (3,144 ± 47) W ([10,729 ± 162] Btu h^{-1}) with the total power demand averaging (1,925 ± 10) W. During the last part of the frosting interval (3,750–5,610 seconds), the capacity dropped at an average of 36.2 W (123.4 Btu h^{-1}) each minute. The average heating capacity dropped by 26% during the frosting interval and before the next defrost began.

4.3 Conclusions of the NZERTF Field Experience

The objective of this study was to determine whether the high-velocity system could provide comparable energy use efficiency to the conventional system. The results of this study showed that the SDHV system meets the required loads and has slightly greater efficiency; the average cooling COP was (0.396 ± 0.113) higher, and the average heating COP was statistically equal. This near-equal performance was realized despite the fact that the SEER and HSPF ratings of the SDHV were 11 and 8% lower than the CDHP, respectively. New firmware was provided to improve the heating performance at the end of the heating season; this greatly improved the heating performance of the high-velocity system. The improvement was produced due to lowered condensing temperatures, which produced lower compressor power demand. Its average heating COP went from (1.8 ± 0.9) to (2.5 ± 1.1) at a 95% confidence level. The new firmware heating COP averaged (1.05 ± 0.23) higher than the old firmware over comparable temperature conditions.

The frosting and defrosting characteristics of these two systems were totally different. The SDHV avoided rapid capacity losses due to frosting by using the hot-gas bypass to reduce the frosting effect on capacity. The SDHV used no electric resistance backup heat, yet it provided comfortable conditions without cold blow during defrost. The CDHP showed a steady decrease in heating capacity during frosting with comparable drops in supply air temperature. The CDHP defrosted with a full reverse cycle while applying electric resistance heat to prevent cold blow. Although the two systems used comparable amounts of energy during the heating season to remove frost from the outdoor heat exchanger, the SDHV frosting/defrosting controls provided a more consistent supply of air temperatures and avoided electric resistance heat installation. The better frosting defrost temperatures of the SDHV were produced at the cost of more system complexity due to the added hot-gas bypass valving.

The SDHV generally operated at very low airflow rates with total external static pressures (ESP) ranging from 37 to 63 Pa (0.15 to 0.25 in. WG). Although this ductwork was a high-pressure system designed for 2,039 m^3h^{-1} (1,200 cfm), due to its variable capacity and low airflows at low load, the system operated in the static pressure range of a well-designed conventional duct system. The CDHP operated most of the time at low compressor speeds with ESP in ranging from 50 to 125 Pa (0.2 to 0.5 in. WG). These results raise the question of whether a conventional, multispeed, or variable-speed HP with an ECM blower could work well with this kind of high-velocity duct system. Potential future work will include the investigation of a hybrid system that uses round duct trunk lines with an optimized version of the SDHV flexible take-offs and supplies. The round duct is much easier to join and seal than rectangular ducting, and less raw material is used to produce a given flow area with round duct.

5 Conclusions and Outlook

5.1 Personal Cooling System

An assessment was performed on RoCo energy saving potentials for office buildings in the United States. For seven cities representing various climates, RoCo can provide up to 49% energy savings in mild climate, such as San Francisco, California, and 9% energy savings in hot climate, such as Phoenix, Arizona.

PCM development is another focus of the project. Before starting the project, the team expected the primary challenge to be obtaining a material with both good latent heat capacity and thermal conductivity. The two issues were solved by having a compressed graphite-assisted PCM. The targeted latent heat capacity and thermal conductivity were successfully achieved. However, the PCM research then shifted to lowering costs and VCC integration. To lower the cost, a compressed graphite disc manufacturing process and alternative PCM materials were investigated. To better integrate the PCM with the VCC, the refrigerant piping and header design of the PCM condenser were investigated.

RoCo also provides good thermal comfort. Field testing showed that RoCo can provide 10 W effective cooling, reducing body temperature by 1 K and heart rate by 9 BPM. Most people expressed a better thermal sensation with RoCo.

5.2 IHP Systems

Key Observations and Future Potential

- Electric-driven GS-IHP.
  - This commercial product was introduced to the US market in late 2012 by CM, its Trilogy Q-Mode system.[13] The product remains on the market as of this report's preparation date.
  - Field demonstration results for two systems in commercial/institutional applications showed annual energy and energy cost savings of ~60% vs. a baseline AS HP with electric resistance WH.
  - Payback vs. the baseline system.
    - Estimated at ~8 years under favourable ground-loop HX installation conditions
    - Can exceed 20 years if loop install costs are high
    - Payback can be almost immediate with third-party ground loop installation and cost recovery on monthly electric bills
- AS-IHP: Prototypes of two different AS-IHP system arrangements were field tested in Knoxville, Tennessee.
  - System 1: Single compressor or combined system.
    - Features a VS compressor and fans, as well as a multispeed pump for DHW circulation.
    - Field test results showed 38% energy savings vs. baseline ASHP for HVAC and electric WH system.
  - System 2: Two-compressor system.

[13] https://www.climatemaster.com/Homeowner/side-links/products/product-details/trilogy.

        - The system consists of a high-efficiency ASHP for SH/SC coupled with a separate HP WH/DH unit. The two systems can be coupled via the air-circulation duct system or can be separate.
        - Field-test results showed 38% energy savings vs. baseline ASHP for HVAC and electric WH system.
        - The separate WH-DH unit includes a demand DH mode for indoor-space air and V air, which is especially useful during spring and fall months when SH and SC loads are small.
        - This IHP concept is also the most adaptable for retrofit applications.
    - Both systems showed much better cooling and water-heating performance than SH, which suffered from reliance on electric resistance backup heating requirements.
    - Small commercial applications with annual loads dominated by SC and water-heating demand are deemed to be most ideal applications for these systems.
- Gas engine-driven AS-IHP.
    - This IHP concept features a natural gas-driven VS engine and scroll compressor and VS fans.
    - Commercial-size system (~40 kW cooling capacity) on the US market since 2012.
        - Field demonstration in Las Vegas, Nevada showed simple payback vs. electric ASHP + WH of under 4 years.
    - Residential size prototype (~17.6 kW cooling capacity) developed.
        - Production cost of prototype ~$15,000; too high for market.
        - Value engineering project demonstrated that a potential cost reduction of ~44% is achievable; this could attract energy or “green” conscious buyers but is still too high for most of market.
        - Market study recommended including an electric generation capability to enable the unit to start and run during grid outages and run critical appliances (e.g., refrigerator); key value-added benefit.

5.3 NIST NZERTF Future Research and Investigations

The net-zero home on the NIST campus provides a unique opportunity to test new appliances, HVAC systems, and all associated controls/strategies. Several different aspects of low-energy homes will be investigated in the coming years. Some of these studies will include:

- air-distribution and HVAC zoning for low energy homes,
- a collaboration with ORNL to verify aspects of the Energy Plus software using NZERTF;
- performance testing of a ground-source CO_2-based air-conditioning system;
- performance testing of a combined HP and water-heating appliance;
- an indoor air quality collaboration and study with Boston University and NTNU/SINTEF to develop and exercise coupled residential building models;
- performance testing of a residential CO_2 HP-based water heating system; and
- CONTAM on a Chip, which is hardware implementation, integration into HVAC system.

6 References

[1] Baxter, V., T. Grubbs, R. Campbell, W. V. Payne, and R. Radermacher, 2018. "State-of-the-Art Analysis of Nearly Zero Energy Buildings: Country report IEA HPT Annex 49 Task 1 USA," ORNL/TM-2018/981, October.

[2] The National Institute of Building Sciences, *A Common Definition for Zero Energy Buildings*, U.S. Department of Energy, DOE/EE-1247, September 2015.

[3] New Buildings Institute, "2016 List of Zero Net Energy Buildings," 2016. [Online]. Available: https://newbuildings.org/wp-content/uploads/2016/10/GTZ_2016_List.pdf.

[4] United States Environmental Protection Agency, "ENERGY STAR," [Online]. Available: http://www.energystar.gov. [Accessed December 2017].

[5] U.S. Energy Star Homes Program, "ENERGY STAR Qualified Homes, Version 3 Savings & Cost Estimate summary," June 2013. [Online]. Available: http://energystar.gov/ia/partners/bldrs_lenders_raters/downloads/EstimatedCostandSavings.pdf?1665-0032. [Accessed December 2017].

[6] U.S. ENERGY STAR Program, "About ENERGY STAR," [Online]. Available: https://www.energystar.gov/about/origins_mission/energy_star_overview/about_energy_star_residential_sector. [Accessed December 2017].

[7] U.S. ENERGY STAR Program, "2016 ENERGY STAR Certified New Homes Market Share," [Online]. Available: https://www.energystar.gov/newhomes/2016_energy_star_certified_new_homes_market_share. [Accessed December 2017].

[8] California Public Utilities Commission, "Zero Net Energy - Action Plan: Commercial Building Sector 2010-2012".

[9] Du, Y., Battery powered portable vapor compression cycle system with PCM condenser, Mechanical Engineering, University of Maryland, 2016.

[10] Deru, M., K. Field, D. Studer, K. Benne, B. Griffith, P. Torcellini, B. Liu, M. Halverson, D. Winiarski, M. Yazdanian, J. Huang, D. Crawley. U.S. Department of Energy Commercial Reference Building Models of the National Building Stock. NREL; 2011.

[11] ASHRAE Standard 90.1-2019: Energy Standard for Buildings except Low-Rise Residential Buildings, American Society of Heating, Refrigeration Air Conditioning Engineers, Inc., Atlanta, GA, 2019.

[12] ASHRAE Standard 169-2006: Weather Data for Building Design Standards, American Society of Heating, Refrigerating, and air-conditioning Engineers, Inc., Atlanta, GA, 2006.

[13] Heidarinejad, M., D. Alejandro Dalgo, N. W. Mattise, and J. Srebric, Personalized cooling as an energy efficiency technology for city energy footprint reduction, Journal of Cleaner Production, Volume 171, 2018, Pages 491-505, ISSN 0959-6526

[14] Heidarinejad, M., M. Dahlhausen, S. McMahon, C. Pyke, and J. Srebric, Cluster analysis of simulated energy use for LEED certified U.S. office buildings, Energ Buildings, 85 (0) (2014) 86-97.

[15] Zhu, S., Dalgo, D., Srebric, J., and Kato, S. 2017. “Cooling Efficiency of a Spot-type Personalized Ventilation,” Building and Environment, 121(2017): 35-48.

[16] Wemhoener, C. (Ed.). 2016. IEA HPT Annex 40 – Heat pump concepts for nearly Zero Energy Buildings, Final report Part 3, Report no. HPP-AN40-3, IEA Heat Pumping Technologies TCP, Borås.

[17] Murphy, R.W., V. D. Baxter, C. K. Rice, and W. G. Craddick. 2007a. "Ground-Source Integrated Heat Pump for Near Zero Energy Houses: Technology Status Report." ORNL/TM-2007/177, December.

[18] Murphy, R.W., V. D. Baxter, C. K. Rice, and W. G. Craddick. 2007b. "Air-Source Integrated Heat Pump for Near Zero Energy Houses: Technology Status Report." ORNL/TM-2007/112, July.

[19] Baxter, V., J. Munk, and A. Gehl, 2016. "Field Demonstration of Ground-Source Integrated Heat Pump - Final Report. ORNL/TM-2016/474, September.

[20] Air-conditioning, Heating, and Refrigeration Institute, 1998, ANSI/AHRI/ASHRAE/ISO Standard 13256-1, “Water-to-Air and Brine-to-Air Heat Pumps — Testing and Rating for Performance.”

[21] ClimateMaster, 2019, Trilogy Q-mode (QE) Series IOM; Installation, Operation, and Maintenance Instructions, October.

[22] AHRI, Performance Rating of Unitary Air-Conditioning and Air-Source Heat Pump Equipment, 2017, Air-Conditioning Heating and Refrigeration Institute, 2111 Wilson Blvd., Suite 500,Arlington, VA 22201 USA. http://www.ahrinet.org/App_Content/ahri/files/STANDARDS/AHRI/AHRI_Standard_210-240_2017_add1.pdf

[23] Battocletti, E. C. and W. E. Glassley, 2013. “Measuring the Costs and Benefits of Nationwide Geothermal Heat Pump Deployment,” prepared for the USDOE Geothermal Technologies Program, February.

[24] Ingram website: http://ingramswaterandair.com/commercial-units-commercial-package-heat-pump-c-45_170_173.html, accessed August 29, 2016

[25] Vineyard, E., R. Wetherington, M. Bhandari, and J. Munk, 2015. "Field Demonstration of Gas Heat Pump Rooftop Unit with Waste Heat Recovery for Water Heating." Oak Ridge National Laboratory, September.

[26] Cunningham, R., 2015. “In the Loop,” Rural Electric Magazine October 5 web edition, http://remagazine.coop/in-the-loop/, accessed August 31, 2016.

[27] Baxter, V., V. Payne, J. Ling, and R. Radermacher, 2015. "Heat Pump Concepts for nZEB - Technology developments, design tools, and testing of heat pump systems for

nZEB in the USA: Country report IEA HPT Annex 40 Task 2, Task 3 and Task 4 of the USA," ORNL/TM-2015/560, December.

[28] Baxter, V., C. K. Rice, J. Munk, M. Ally, and B. Shen, 2015. "Advanced Variable Speed Air Source Integrated Heat Pump (AS-IHP) Development– Final Report," ORNL/TM-215/525, September.

[29] Baxter, V., C. K. Rice, J. Munk, M. Ally, B. Shen, and R. B. Uselton, 2017. "Air-Source Integrated Heat Pump System Development – Final Report," ORNL/TM-2017/305, July.

[30] DOE/BTO Building America Program 2013. "Website for Building America Analysis Spreadsheets: DHW Event Schedule Generator," http://energy.gov/eere/buildings/building-america-analysis-spreadsheets (last accessed on September 24, 2015).

[31] Hendron, R. and C. Engebrecht 2010. "Building America House Simulation Protocols," NREL REPORT: TP-550-49426, October.

[32] Munk, J. D., C. Halford, and R. Jackson, 2013. "Component and System Level Research of Variable-Capacity Heat Pumps," ORNL/TM-2013/36, June.

[33] ASHRAE, 2013. ASHRAE Handbook: Fundamentals.

[34] National Oceanic and Atmospheric Administration (NOAA) *NOAA Online Weather Data*. Accessed August 3, 2015, and August 14, 2015. http://w2.weather.gov/climate/xmacis.php?wfo=mrx.

[35] Uselton, R., 2014. Dedicated Dehumidifier and Water Heater, United States Patent 8,689,574 B2, April 1.

[36] Lennox Industries Inc., 2014. “Lennox XP-25 2 to 5 Ton Heat Pump Product Specifications,” Bulletin 210659, May.

[37] Munk, J. D., V. D. Baxter, A. C. Gehl, M. R. Ally, B. Shen, C. K. Rice, and R. B. Uselton, 2017. “Prototype Air-Source Integrated Heat Pump Field Evaluation Results.” Paper O.1.4.1 in Proceedings of the 12th IEA Heat Pump Conference, Rotterdam, The Netherlands, May 15–18, 2017.

[38] NOAA. NOAA Online Weather Data. Accessed December 22, 2016. http://w2.weather.gov/climate/xmacis.php?wfo=mrx.

[39] Zaltash, A., Vineyard, E.A., Linkous, R.L., Geoghegan. P., Wetherington, R., Mahderekal, I., 2008. “Laboratory evaluation: Performance of a 10 RT gas engine-driven heat pump (GHP)”, ASHRAE Transactions, Vol 213.

[40] Nextaire, no date. Multi-zone gas heat pump technical specifications Model 132.6.00.P.H.A.

[41] Momen, A., A. Abu-Heiba, and E. A. Vineyard, 2015. "Multi-Function Gas Fired Heat Pump," ORNL/TM-2015/701, November.

[42] US Department of Energy, 2019. "Technology Commercialization Fund." https://www.energy.gov/technologytransitions/services/technology-commercialization-fund (accessed 8-November.

[43] Kim, H., K. Nguyen, A. McGuinness, and T.V. Dai, 2019, Characterization of residential air distribution system performance for thermal comfort, NIST GCR 19-021, National Institute of Standards and Technology. https://doi.org/10.6028/NIST.GCR.19-021

[44] Fanney, A. H., W. V. Payne, T. Ullah, L. Ng, M. Boyd, F. Omar, M. Davis, H. Skye, B. Dougherty, B. Polidoro, W. Healy, and E. Pettit, 2015, Net-Zero and Beyond! Design and Performance of NIST's Net-Zero Energy Residential Test Facility, Energy and Buildings, 101, 95-109. https://www.sciencedirect.com/science/article/pii/S0378778815003655

[45] ASHRAE Std. 62.2-2010, Ventilation and Acceptable Indoor Air Quality in Residential Buildings- (ANSI Approved), American Society of Heating, Refrigerating and Air-Conditioning Engineers, 1791 Tullie Circle, N.E., Atlanta, GA 30329.

[46] Building America Program, 2019, Building America Publication and Product Library, https://www1.eere.energy.gov/library/default.aspx?page=2&spid=2.

[47] Poerschke, A. and A. Rudd, 2016, Performance analysis of a modular small-diameter air distribution system. https://www.osti.gov/biblio/1240364

[48] Besant, R. W. and Y. Asiedu, 2000, Sizing and balancing air duct systems, ASHRAE Journal. https://www.semanticscholar.org/paper/Sizing-and-balancing-air-duct-systems-Besant-Asiedu/56fe8e48450bb084dd00518246bf09d7d7d1586c.

[49] Tsal, R. J., H.F. Behls, and R. Mangel, 1988, T-Method duct design, part I: optimization theory, ASHRAE Transactions, Vol. 94-2, Ottawa.

[50] Caldas, L. G. and L.K. Norford, 2003, Genetic algorithms for optimization of building envelopes and the design and control of HVAC systems, ASME Transactions, Vol. 125, 343-51. https://doi.org/10.1115/1.1591803

[51] Jorens, S., I. Verhaert, and K. Sorensen, 2018, Design optimization of air distribution systems in non-residential buildings, Energy & Bldgs., 175, 48-56. https://doi.org/10.1016/j.enbuild.2018.07.018

[52] Martin, E., Withers, C., McIlvaine, J., Chasar, D., and Beal, D. 2018, Evaluating Moisture Control of Variable Capacity Heat Pumps in Mechanically Ventilated, Low-Load Homes in Climate Zone 2A, Cocoa, FL; Florida Solar Energy Center (FSEC). DOE/EE-1702. https://www.osti.gov/biblio/1421385-evaluating-moisture-control-variable-capacity-heat-pumps-mechanically-ventilated-low-load-homes-climate-zone .

[53] Balke, Elizabeth, Gregory Nellis, Sanford Klein, Harrison Skye, Vance Payne and Tania Ullah, 2018 Detailed energy model of the National Institute of Standards and Technology Net-Zero Energy Residential Test Facility: Development, modification, and validation, Science and Technology for the Built Environment, 24:7, 700-713. https://doi.org/10.1080/23744731.2017.1381828

[54] ACCA, 2012a, Manual J: Residential Load Calculation, 8th Edition, Version 2, Air Conditioning Contractors of America, 2800 Shirlington Rd, Suite 300, Arlington, VA USA 22206.

[55] ACCA, 2012b, Manual D: Residential Duct Systems, 2nd Edition, Air Conditioning Contractors of America, 2800 Shirlington Rd, Suite 300, Arlington, VA USA 22206.

[56] Cummings, J. B., and C. R. Withers Jr., 2014, Making the Case for Oversizing Variable-Capacity Heat Pumps, Florida Solar Energy Center, FSEC-PF-459-14, presented at 2014 ACEEE Summer Study on Energy Efficiency in Buildings. http://fsec.ucf.edu/en/publications/pdf/FSEC-PF-459-14.pdf.

[57] Shirey III, D. B., H.I. Henderson, and R.A. Raustad, 2006, Understanding the dehumidification performance of air-conditioning equipment at part-load conditions, FSEC-CR-1537-05, Florida Solar Energy Center, DOE/NETL Proj. No. DE-FC26-01NT41253. https://doi.org/10.2172/881342

[58] Davis, M., W.M. Healy, M. Boyd, L.C. Ng, W.V. Payne, H.M. Skye, and T. Ullah, 2014, Monitoring Techniques for the Net-Zero Energy Residential Test Facility, NIST Technical Note 1854. https://doi.org/10.6028/NIST.TN.1854.

[59] Bouchelle, M. P., D.S. Parker, M.T. Anello, and K.M. Richardson, 2000, Factors influencing space heat and heat pump efficiency from a large-scale residential monitoring study, Proceedings of 2000 summer study on energy efficiency in buildings, ACEEE. http://www.fsec.ucf.edu/en/publications/html/FSEC-PF-362-01/

Acknowledgments

The authors gratefully acknowledge the substantial contributions provided for this report from others, including, but not limited to, the following individuals.

- For the IHP section: Jeff Munk, Anthony Gehl, Ayyoub Momen, Bo Shen, Moonis Ally, Keith Rice (ret.), and Ed Vineyard (ret.) of ORNL; and Isaac Mahderekal of Intellichoice Energy.
- For the Personal Cooling system section: Mohammad Heidarinejad, Daniel Alejandro Dalgo, Nicholas W. Mattise, Shengwei Zhu, Daniel Dalgo, and Shinsuke Kato of University of Maryland. We also gratefully acknowledge the support from the sponsors of the Center for Environmental Energy Engineering (CEEE) and Center for Sustainability in the Built Environment (City@UMD) at the University of Maryland.
- For the NZERTF section: We would like to acknowledge the support and hard work of our Engineering Technician staff at the National Institute of Standards and Technology in Gaithersburg, Maryland, who were invaluable in obtaining the data used in this report. We thank Mr. Arthur Ellison, Mr. John Wamsley, and Mr. Luis Luyo.

Finally, the authors gratefully acknowledge Antonio Bouza of DOE BTO for his support of the US participation in IEA HPT Annex 49, the assembly of this report, and the ORNL technical activities summarized herein under Contract No. DE-AC05-00OR22725 with UT-Battelle LLC.